AFM Surface Force Measurements between Hydrophobized Gold Surfaces

Jialin Wang

Dissertation submitted to the faculty of Virginia Polytechnic Institute and State University in partial fulfillment of the requirements for the degree of

Doctor of Philosophy
in
Materials Science and Engineering

Submitted to:

Dr. Roe-Hoan Yoon, Committee Chair
Dr. David E Clark
Dr. John Y Walz
Dr. Michael F Hochella
Dr. Richard D Gandour

September 8, 2008
Blacksburg, Virginia Tech

Keywords: AFM, DLVO, surface force, hydrophobic force, gold, long-range attraction, thin film, temperature effect, water structure

AFM Surface Force Measurements between Hydrophobized Gold Surfaces

Jialin Wang

Abstract

In 1982, Israelachvili and Pashley reported the first measurements of a hitherto unknown attractive force between two mica surfaces hydrophobized in cetyltrimethylammonium bromide (CTAB) solutions. Follow-up experiments conducted by many investigators confirmed their results, while others suggested that the "hydrophobic force" is an artifact due to nanobubbles (or cavitation). Evidences for the latter included the discontinuities (or steps) in the force *versus* distance curves and the pancake-shaped nano-bubbles seen in atomic force microscopic (AFM) images. Recent measurements conducted in degassed water showed, however, smooth force *versus* distance curves, indicating that the hydrophobic force is not an artifact due to nanobubbles.[1, 2]

Still other investigators[3, 4] suggested that the long-range attraction observed between hydrophobic surfaces is due to the correlation between the patches of adsorbed ionic surfactant and the patches of unoccupied surface. For this theory to work, it is necessary that the charged patches be laterally mobile to account for the strong attractive forces observed in experiment. In an effort to test this theory, AFM force measurements were conducted with gold substrates hydrophobized by self-assembly of alkanethiols and xanthates of different chain lengths. The results showed long-range attractions despite the fact that the hydrophobizing agents chemisorb on gold and, hence, the adsorption layer is immobile.

When the gold surfaces were hydrophobized in a 1×10^{-3} M thiol-in-ethanol solution for an extended period of time, the force curves exhibited steps. These results indicate that the long-range attractions are caused by the coalescence of bubbles, as was also reported by Ederth.[5] The steps disappeared, however, when the species adsorbed on top of the chemisorbed monolayer were removed by solvent washing, or when the gold substrates were hydrophobized in a 1×10^{-5} M solution for a relatively short period of time.

AFM force measurements were also conducted between gold substrates coated with short-chain thiols and xanthates to obtain hydrophobic surfaces with water contact angles (θ) of less than 90^{o}. Long-range attractions were still observed despite the fact that cavitation is thermodynamically not possible.

Having shown that hydrophobic force is not due to coalescence of pre-existing bubbles, cavitation, or correlation of charged patches, the next set of force measurements was conducted in ethanol-water mixtures. The attractive forces became weaker and shorter-ranged than in pure water and pure ethanol. According to the Derjaguin's approximation[6], an attractive force arises from the decrease in the excess free energy (γ^{f}) of the thin film between two hydrophobic surfaces.[7] Thus, the stronger hydrophobic forces observed in pure water and pure ethanol can be attributed to the stronger cohesive energy of the liquid due to stronger H-bonding. Further, the increase in hydrophobic force with decreasing separation between

two hydrophobic surfaces indicates that the H-bonded structure becomes stronger in the vicinity of hydrophobic surfaces.

The force measurements conducted at different temperatures in the range of 10-40ºC showed that the hydrophobic attraction between macroscopic surfaces causes a decrease in film entropy (S^f), which confirms that the hydrophobic force is due to the structuring of water in the thin film between two hydrophobic surfaces. The results showed also that the hydrophobic interaction entails a reduction in the excess film enthalpy (H^f), which may be associated with the formation of partial (or full) clathrates formed in the vicinity of hydrophobic surfaces. The presence of the clathrates is supported by the recent finding that the density of water in the vicinity of hydrophobic surfaces is lower than in the bulk.[8]

References

1. Meyer, E. E.; Lin, Q.; Israelachvili, J. N., *Langmuir* **2005,** 21, 256-259.
2. Zhang, J.; Yoon, R.-H.; Mao, M.; Ducker, W. A., *Langmuir* **2005,** 21, 5831-5841.
3. Miklavic, S. J.; Chan, D. Y. C.; White, L. R.; Healy, T. W., *J. Phys. Chem.* **1994,** 98, 9022-9032.
4. Meyer, E. E.; Lin, Q.; Hassenkam, T.; Oroudjev, E.; Israelachvili, J. N., *Proc. Nat. Acad. Sci. U.S.A* **2005,** 102, 6839-6842.
5. Ederth, T.; Claesson, P.; Liedberg, B., *Langmuir* **1998,** 14, 4782-4789.
6. Derjaguin, B. V., *Kolloid Zeits* **1934,** 69, 155-164.
7. Eriksson, J. C.; Ljunggren, S.; Claesson, P. M., *J. Chem. Soc., Faraday Trans. 2* **1989,** 85, (3), 163-176.
8. Doshi, D. A.; Watkins, E. B.; Israelachvili, J. N.; Majewski, J., *Proc. Nat. Acad. Sci. U.S.A* **2005,** 102, 9458-9462.

Acknowledgements

After all those years, I have got quite a list of people. Without their help, it would not have been possible for me to complete my Ph. D program at Virginia Tech. I would like to take this opportunity to express my sincere gratitude to all of them.

Firstly, I owe my most sincere gratitude to my advisor Dr. Roe-Hoan Yoon, Director of the Center for Advanced Separation Technologies (CAST), Virginia Tech, for his support, guidance, and encouragement during my study program. He set up a good example for me. I will always be thankful for his enthusiasm, wisdom and knowledge as well as the motivation and challenge he gave me. My thanks also go to Dr. David Clark, Dr. John Walz, Dr. Michael Hochella and Dr. Richard Gandour for serving on my committee. They are greatly appreciated for their criticisms and suggestions for my work. Dr. Richard Gandour was especially acknowledged for kindly training me in the chemical synthesis in his lab.

My research work at Virginia Tech has been strengthened through collaboration with Dr. Jan Christer. Eriksson of the Department of Chemistry, Royal Institute of Technology, Sweden. Special thank goes to him for his advices, inspirations and illuminating discussions on hydrophobic force during his visits at Virginia Tech.

I would also like to thank Dr. Jinhong Zhang for teaching me to conduct surface force measurement with Atomic Force Microscope (AFM). I thank Stephen McCartney for assistance and helpful discussion in AFM force measurement. Sincere gratitude is expressed to Dr. Jinming Zhang, Dr. Liguang Wang for their assistance, discussion and suggestion on my work during the past few years. I would like to thank my fellow graduate students and the

staffs at CAST center, particularly, Ruijia Wang, Monica Ma, Hyunsun Do, Chris Hull and Kathy Flint for their support and friendship. Many thanks go to my officemate Charles Schlosser for reading the manuscript and discussion. I would like to extend my gratitude to several friends, especially, Li Yan, Zaijing Sun, Kai Zhang and Xiaojing Zhu, who made my life in Blacksburg memorable.

I am very grateful to my caring parents, my old sister and my old brother for their unconditional love and encouragement. Finally, I would like to express my deepest appreciation to my dear wife Ru Li for her understanding, patient, selfless support and love. I would be lost without her because she love and support me greatly in everything I do.

Table of Contents

List of Figures

List of Tables

Chapter 1

Introduction

1.1 General

Froth flotation is the most widely used solid-solid separation process employed in the mining industry. The process is designed to separate hydrophobic particles from hydrophilic ones. Therefore, control of particle hydrophobicity is most important in flotation. For this reason, the early days of flotation research was focused on developing various reagents (collectors) that can be used to hydrophobize different minerals. During these early days of research, contact angle was used as the measure of hydrophobicity. However, it is a thermodynamic property and, hence, doses not give kinetic information. On the other hand, flotation is a kinetic process, and the industry strives to improve flotation rate and, thereby, to maximize recovery and throughput.

In colloid chemistry, the kinetics of coagulation can be predicted by the classical DLVO theory[1, 2], which considers two surface forces, namely, repulsive electrical double-layer force (F_e) and attractive van der Waals dispersion force (F_d). These two surface forces are considered additive. Thus, the total interaction force (F_t) between two particles can be given as follows:

$$F_t = F_e + F_d \qquad (1.1)$$

Typically, a plot (Figure 1.1) of Equation 1.1 shows a maximum repulsive force (F_{max}) at a critical separation distance (H_{cr}) between two colloidal particles. If F_{max} is large, coagulation of the particles are slow; and if F_{max} is small, the coagulation is fast. As such, the

DLVO theory is useful for describing the interactions between small mineral particles with limited degree of hydrophilicity[3] in water (*e.g.*, coagulation and dispersion), but not for the interactions between hydrophobic air bubbles and hydrophobic particles (*i.e.*, flotation). In the latter, both F_e and F_d are repulsive under most conditions where flotation is carried out[4]. Thus, the DLVO theory cannot be used to describe flotation processes that are spontaneous and fast in most cases.

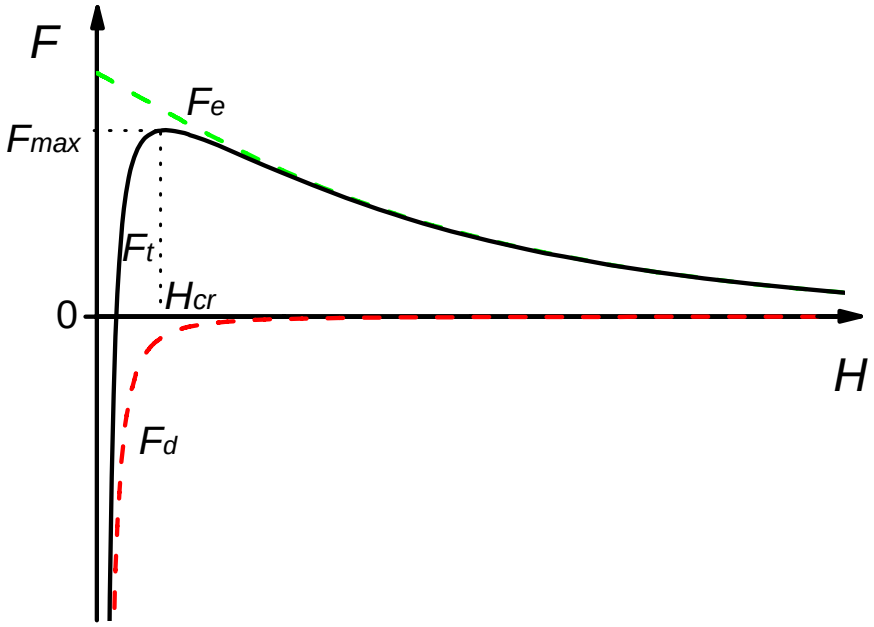

Figure 1.1 Surface interaction (F) *versus* distance (H) diagram for particle-particle interaction, with F_{max} representing the energy barrier.

The DLVO theory is a theoretical model, which was verified in direct surface force measurements conducted between microscopic surfaces[5]. However, the force measurements conducted between two hydrophobic surfaces exhibited an additional attractive force, which is naturally referred to as "hydrophobic force"[6]. Many investigators showed subsequently that the hydrophobic forces were 10 to 100 times larger than the van der Waals force[7]. It was

shown also that coagulation of hydrophobic particles can be modeled much better by recognizing the existence of the hydrophobic forces as follows[8, 9]:

$$F_t = F_e + F_d + F_h \qquad (1.2)$$

where F_h represents the hydrophobic force term. It was shown that Equation 1.2, which is referred to as extended DLVO theory, can also be used for modeling the bubble-particle interactions in flotation[10-12]. Under most flotation conditions, both F_e and F_d are repulsive, as has already been noted. In such cases, F_h is the only driving force for bubble-particle attachment, as shown in Figure 1.2, and it is not possible to model flotation without recognizing the existence of the hydrophobic force.

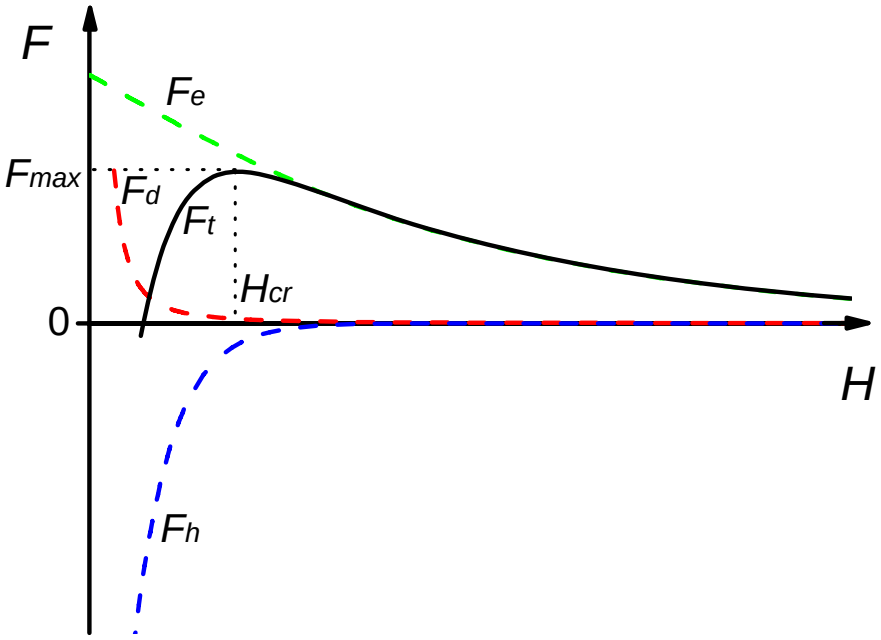

Figure 1.2 Surface interaction (F) *versus* distance (H) diagram for bubble-particle interaction, with F_h representing the hydrophobic force and F_{max} the energy barrier.

However, there has been a great deal of controversy regarding the existence and the origin of the hydrophobic force. Some investigators suggested that it is due to nano-size

bubbles nucleating on hydrophobic surfaces[13] or cavities[14], while others believe that the so-called hydrophobic force is actually an electrostatic attraction[15-18]. It is, thus, the objective of the present work to conduct surface force measurements between hydrophobic surfaces and determine the possible origin(s) of the long-range attractions observed.

1.2 Literature Review

1.2.1 Direct Measurement of Hydrophobic Force

Initially, most of the force measurements were conducted using surface force apparatus (SFA), which was limited to measurements between two curved semitransparent mica sheets. In the SFA technique, surface force was measured between two crossed cylinders of radius of R_1 and R_2 as a function of separation distance H. The surfaces force was obtained by measuring the deflection of a spring, and the separation distance was accurately determined using an interferometer. One can relate the measured force $F(H)$ to the free energy of interaction per unit area $W(H)$ between surface **1** and **2**, as follows:

$$F(H) = 2\pi\left(\frac{R_1 R_2}{R_1 + R_2}\right)W(H) \qquad (1.3)$$

which is know as Derjaguin's approximation[19].

Rabinovich and Yoon[20, 21] used atomic force microscope (AFM) to measure the hydrophobic forces between a glass sphere with a radius of R and a flat silica plate (with $R = \infty$), which made it easier to measure the hydrophobic forces between a varieties of macroscopic solids, *e.g.*, polypropylene[22], polystyrene[23], ZnS[24], gold[25], *etc*. The AFM uses a photodetector to detect the deflection of a cantilever spring resulting from the interaction of a

colloidal particle attached to the apex of the cantilever with a flat substrate which sits on a piezoelectric scanner. The surface interaction can be calculated from the deflection of the cantilever using Hooke's law and the known spring constant of the cantilever. The movement of the surfaces relative to one another is accurately controlled by the piezoelectric scanner. The force *versus* distance data obtained using AFM were presented by normalizing the measured forces by the radius *R* of the sphere (glass) used for the measurement. According to the Derjaguin approximation (Equation 1.3), the normalized force *F(H)/R* could be related to the free energy of interaction *W(H)* per unit area between the sphere and flat surfaces. For the sphere-plate geometry, Equation (1.3) is reduced to:

$$F(H)/R = 2\pi W(H) \qquad (1.4)$$

The results should be independent of the force-measuring technique, and one can directly compare the results obtained using different methods. However, surface force measurements are difficult when one or both surfaces are deformable.

Since no theory is able to explain all the experimental results, the measured hydrophobic forces were usually represented by an empirical force law[26, 27]:

$$F/R = C\exp(-H/D) \qquad (1.5)$$

where *h* is the closest separation distance between two surfaces, and *C* and *D* are the fitting parameters for the experimental data. The first parameter characterizes the strength of the force, while the second parameter characterizes its distance range. The second parameter is often referred to as decay length. In general, the stronger the hydrophobic force is, the more negative the value of *C* and the larger the value of *D* becomes.

The force data were also fitted by a double exponential force law in the following

form[20, 28, 29]:

$$F / R = C_1 \exp\left(-H / D_1\right) + C_2 \exp(-H / D_2) \qquad (1.6)$$

in which C_1 and C_2 represent the magnitudes of the short- and long-range hydrophobic forces, respectively, and D_1 and D_2 are the respective decay lengths.

Another way of representing the hydrophobic forces measured in experiment is to use a power law[20]:

$$F / R = -K_{131} / 6H^2 \qquad (1.7)$$

where K_{131} is the hydrophobic force constant between two solids **1** in water **3**. Equation (1.7) has only one fitting parameter as compared to two in Equation 1.5 and four in Equation 1.6. Equation 1.7 is of the same form as the van der Waals dispersion force; therefore, the value of K_{131} is directly comparable with the Hamaker constant (A_{131}).

1.2.2 Factors Affecting Hydrophobic Force

In 1982, Israelachivili and Pashley[6] published a seminal paper in Nature, which showed the presence of a third surface force. They measured an additional attractive force between two mica surfaces hydrophobized by cetyltrimethylammonium bromide (CTAB). Naturally, the non-DLVO attractive force was named hydrophobic force, which was not only stronger than the van der Waals force but was also longer-ranged, that is, the force was discernable at longer separation distances. The work of Israelachvili and Pashley created interests among many colloid chemists, with numerous follow-up measurements on different types of hydrophobic surfaces using a range of different methods of hydrophobization, as has been reviewed recently[7, 13, 30-33].

A wide range of factors affecting the hydrophobic force have been investigated, which are summarized as follows:

1. *Type of hydrophobic surface*. Christenson and Claesson[7] presented a state of the art review of the hydrophobic force from an experimental perspective. Recognizing the large variation of the measured interaction is dependent on the type of hydrophobic surface, they classified the non-DLVO attractive forces observed in water between hydrophobic surfaces into three different categories. (I) Stable hydrophobic surfaces, *e.g.*, polymerized Langmuir-Blodgett (LB) films deposited on mica[34, 35], bulk polymer surfaces[22], show a fairly short-range but strongly attractive force, much stronger than the van der Waals force. (II) Very hydrophobic surfaces, *e.g.*, silica or glass surfaces made hydrophobic by silylation[36-38], gold surfaces made hydrophobic by self-assembly of thiol[25, 39, 40], give an attraction of variable strength and range caused by the presence of small bubbles sporadically adhering to hydrophobic surfaces. (III) Results obtained with a variety of hydrophobic surfaces, *e.g.*, LB films of surfactants or lipids on mica or silica[28, 41-43], *in-situ* adsorbed surfactant on silica[38, 44-47], appear to give rise to a very-long range attractive force with exponential decay.
2. *Surface hydrophobicity*. Rabinovich and Yoon[20] measured the hydrophobic force between a silica bead and a silica plate surfaces, which were hydrophobized with varying amounts of octadecylchlorosilane (OTS) or trimethylchlorosilane (TMS) as a means of controlling contact angle. The range of the measured hydrophobic force depended on the contact angle, varying from approximately 30 nm for the surface contact angle θ_a = 88º to over 100 nm for θ_a = 115º. Yoon and Ravishankar[48] measured hydrophobic forces

between mica surfaces in dodecylammonium chloride (DAHCl) solutions in the presence of dodecanol or octanol. The results showed that when θ_a < 90º, only short range hydrophobic forces were measured with decay lengths of around 1.3 nm. Long-ranged hydrophobic forces, resulting from the formation of domains of close-packed hydrocarbon chains, were observed at $\theta_a \geq$ 90º. Ederth and Liedberg[49] investigated the influence of wetting properties on the long-range hydrophobic interaction between gold surfaces hydrophobized by self-assembly of methyl- and hydroxyl-functionalized alkanethiols. The results showed that whenever the advancing water contact angle on the hydrophobized gold surfaces exceeded 90º, long-range attraction appeared and the attractive force curves had steps or discontinuities. When the contact angle was lower than 90°, the interaction was a van der Waals force.

3. *Salt effect*. Claesson *et al*.[28] first investigated the electrolyte effect, and they found that the interaction between water-stable hydrophobic LB monolayers on mica was weakly dependent on KBr concentration up to a concentration of 0.01 M. Christenson *et al*.[50] studied the effect of divalent electrolyte (0.01 M magnesium sulfate sand 0.1 M magnesium sulfate solutions) on the hydrophobic attraction between two mica surfaces coated with LB film of dimethyldioctadecylammonium bromide (DDOABr). They found that the magnitude of the hydrophobic attraction was reduced with increasing electrolyte concentration but remained much larger than the van der Waals force. Parker *et al*.[36] conducted surface force measurements using chemically fluorinated glass surfaces in the presence of KBr and NaCl. They found that no reduction in force upon addition of electrolyte, except at very high salt concentrations (5 M NaCl) where the strength of the

attractive forces increased slightly. Meagher and Craig[22] measured the hydrophobic interaction between two polypropylene surfaces in NaCl solutions. The results showed that increasing NaCl concentration up to 1 M had little or no effect on the range of the interaction. Craig *et al*.[51] demonstrated that the hydrophobic attraction was undiminished between silica surfaces in soluble cetylpyridinium chloride in the presence of 0.1 M NaCl. Kekicheff and Spalla[17] measured surface force between electrically neutral glass surfaces in aqueous solution of cetyltrimethylammonium bromide (CTAB) at *p*H about 5.7. It was found that the long-range attractive force decayed with the addition of KBr (10^{-5}−10^{-2} M). Zhang *et al*.[46] conducted AFM force measurements between silica sphere and fused-silica plate in aqueous octadecyltrimethylammonium chloride (C_{18}TACl) solutions. The results showed the attractive force was screened by an added electrolyte (NaCl).

4. *Dissolved gas*. Meagher and Craig[22] used a modified AFM to measure the hydrophobic interaction between polypropylene surfaces in NaCl solutions. They showed that the measured attraction in dilute NaCl solutions was reduced upon removal of the gas. Rabinovich and Yoon[21] demonstrated that attractive interaction between OTS-coated silica surfaces in water became considerably stronger when the water was saturated with argon. Craig *et al*.[52] measured the hydrophobic forces between silica surfaces hydrophobized by adsorption of cetylpyridinium chloride (CPC). The effect of dissolved gas on the measured interaction was studied. It was shown that the removal of dissolved gas decreased the range and magnitude of the attraction at long range. Mahnke *et al*.[53] investigated the influence of dissolved gas on the interactions between silica surfaces

hydrophobized by either dehydroxylation or methylation. They found degassing caused a significant reduction in large jump distance (> 25 nm), but not in the smaller jump distance. For dehydroxylated silica surfaces interacting in CO_2 saturated solution, they found the jump distance were considerably larger than in the presence of air or argon. Considine *et al*.[54] measured the surface forces between two polystyrene latex spheres in aqueous solution containing different amount of gas. They found that the range of the attraction decreased significantly when the level of dissolved gas in the water was reduced. Sakamoto *et al*.[55] conducted force measurements between silica surfaces in aqueous C_{18}TACl solutions in the presence and absence of dissolved gas. They concluded that long-range attractive force was not observed in carefully degassed solutions. Zhang *et al*.[46] repeated the experiment of Sakamoto *et al*., however, they found instead that the long-range hydrophobic force still existed in degassed solution. Stevens *et al*.[56] studied the effects of degassing on the long-range attractive force between hydrophobic amorphous fluoropolymer surfaces. They found the range of the attraction was significantly decreased in degassed water, but the range and magnitude of the attraction remained greater than the van der Waals attraction. The effect of dissolved gas on the hydrophobic attraction between dimethyldioctadecylammonium bromide-(DODAB) coated mica was studied by Meyer *et al*.[57] using a surface forces apparatus (SFA). Removal of dissolved gas was seen to reduce the range of the attraction while the short-range attraction (< 25 nm) remained unchanged.

5. *Temperature effect*. Tsao *et al*.[29] measured the attractive forces between two hydrophobized mica surfaces immersed in water at three different temperatures in the

range 25−50ºC. The results showed that a very long range attractive force changed dramatically with temperature, the attraction decreasing with increasing temperature. They attributed the decrease in attractive force to the change of the state of the hydrocarbon chains on the surface when the temperature was increased. Parker *et al*.[36] investigated the effect of temperature using stable surfaces prepared by covalent modification of silica with fluorocarbon silane. It was shown that there was a significant increase in the strength of the interaction measured between silane-coated mica surfaces when the temperature was increased from room temperature to 41ºC.

6. *Ethanol effect*. Parker *et al*.[36] showed that the addition of ethanol reduced the strength of the long range forces between silane-coated silica surfaces. Kokkoli *et al*.[58] also showed that addition of ethanol to water resulted in a decrease in the strength of the hydrophobic attraction between self-assembled monolayers of hexadecanethiol on gold. As the ethanol concentration was increased further (75% mole fraction), the hydrophobic attraction became comparable to the van der Waals force. Ederth[40] showed that the attractive force measured between two hexadecanethiol-coated gold surfaces in water containing 12.5 % ethanol (by weight) was slightly shorter-ranged than that in pure water. As the ethanol concentration was increased to 20%, the attractive force measured was the van der Waals force. Nguyen *et al*.[37] measured attraction between silanated glass surfaces in water-ethanol mixtures. The results showed that the strong attractive force decreased with an increase in the ethanol content and disappeared in pure ethanol.

7. *Chain order*. Rabinovich *et al*.[59] investigated the dependence of hydrophobic force on the chain order for mica surfaces coated by double-chain surfactant

(dimethyldioctadecylammonium, DDOA) monolayers. It was found the hydrophobic force increased with the ordering the hydrocarbon chains. It was thus suggested that the hydrophobic force was related to the hydrocarbon chains ordering, which in turn may affect the structure of vicinal water.

1.3 Scientific Discussion

Many research groups around the world conducted surface force measurements with different types of hydrophobic surfaces, and showed the existence of long-range attractions. However, the results are far from being consistent. Therefore, many investigators cast doubts about the long-range force being the real hydrophobic force. Nevertheless, various theoretical models and ideas have been rendered to explain the experimental results. Eriksson *et al*.[60] carried out a theoretical analysis to suggest that the long range hydrophobic attraction is due to the enhanced hydrogen bonding of the water molecules in the vicinity of a hydrophobic solid. Some other investigators considered that they are due to surface-induced perturbation in the adjacent fluid[61], ion-ion correlations[62], mobile charged patches[15], correlated in plane dipoles[48, 63], lack of stability of hydrophobic surface groups[64], and rearrangement of the charged patchy bilayers[33]. However, these models cannot be reconciled with all of the experimental data, particularly with regards to salt effect. In particular, Miklavic *et al.*[15] predicted that the attraction due to charge correlation should decay exponentially with a decay length equal to one-half of the Debye length (κ^{-1}). Although there are some experiment results consistent with this theory[61, 62], more and more experimental data show that the force is independent of ionic strength[22, 36, 51].

More recently, many investigators showed evidence that the non-DLVO attractions observed during the force measurements are artifacts introduced during the measurement. Tyrrell and Attard[65, 66] and Ishida *et al.*[67] showed that the "so-called" hydrophobic force is caused by the small bubbles (nanobubbles) preexisting on hydrophobic surfaces. Christenson and Claesson[14] and Yaminsky and Ninham[68] suggested that the very long range forces measured are a consequence of cavitations between microscopic hydrophobic surfaces. The most frequently quoted evidences for the air-bubbles were the discontinuities (or steps) observed in force *versus* distance curves[36], each step representing coalescence of nanobubbles. When two bubbles coalesce, gas bridges (or cavities) are formed between two surfaces, which give rise to capillary forces. Tyrell and Attard [66] and Yang *et al.*[69] actually showed AFM images of the nanobubbles formed on hydrophobic surfaces. It is interesting that the nanobubbles were flat, which, according to the authors, was necessary to minimize the gas pressure inside the nanobubbles.

Seemingly definitive evidence for the microscopic bubbles theory was given by Sakamoto *et al.*[55], who conducted AFM force measurements between a glass sphere and silica plate immersed in octadecyltrimethylammonium chloride (C_{18}TACl) solutions. They found that the long-range attractions were observed only when the measurements were conducted in air-saturated solutions and not in carefully degassed solutions. This observation leads the authors to the conclusion that "long-range attraction never appears in completely air-free C_{18}TACl solutions".

This theory seems appealing, because the existence of the bubbles solves the range problem. The apparent ranges of the forces depend on the heights of bubbles with varying

dimensions. However, a primary setback for this theory is that very small air bubbles in the bulk water phase are short-lived[70]. Stevens *et al.*[56] showed the range and strength of the attraction between hydrophobic amorphous fluoropolymer surfaces in deaerated water remain significantly greater than the van der Waals force. Meyer *et al.*[57] conducted SFA force measurements between mica surfaces coated by a Langmuir-Blodgett (LB)-deposited hydrophobic monolayer of double-chain cationic surfactant (DODAB) both in the presence and absence of dissolved gases. In the presence of dissolved gases, they observed long-range attractive forces, while in degassed solutions only short-range attraction forces were observed. The authors concluded, therefore, that "true" hydrophobic force exists even in degassed solutions. They stated further that the longer range attractive force may be unrelated to hydrophobicity. On the other hand, Zhang *et al.*[46] observed long-range attractive forces with a decay length as large as 36 nm even after degassing a C_{18}TACl solution.

Thus, the questions concerning the existence of the hydrophobic force and its origins remain controversial. It has been shown that the classical DLVO theory cannot explain the coagulation of strongly hydrophobic particles and the coalescence of air bubbles at low surfactant concentrations[8, 9, 71, 72]. Both of these phenomena are important in flotation as they affect particle and bubble size distributions. Also, modeling bubble-particle interactions is not possible without recognizing the existence of hydrophobic force[10-12]. Furthermore, most of the surface force measurements conducted in the past was made between mica and silica surfaces using surfactants that are not commonly used for flotation.

1.4 Research Objectives

The main objective of these studies is to examine the existence of the long range hydrophobic forces between thiol- and xanthate-coated gold surfaces in air-equilibrated water. The factors that may affect the hydrophobic force will be investigated. The results will be used to study the nature of hydrophobicity and the origin of hydrophobic force.

The specific objectives for this research are:

1. Conduct AFM force measurements between two gold macroscopic surfaces in aqueous solution to determine the Hamaker constant of gold (Chapter 2).

2. Conduct force measurements with gold surfaces pretreated by *ex-situ* adsorption of alkanethiols as functions of surfactant concentration and immersion time (Chapter 2 and Chapter 3).

3. Conduct force measurements with gold surfaces pretreated by *ex-situ* adsorption of alkanethiols as function of chain length (Chapter 3).

4. Conduct force measurements with gold surfaces pretreated by *in-situ* adsorption of water-soluble xanthate surfactants as functions of surfactant concentration and immersion time (Chapter 4).

5. Conduct force measurements in the presence of various solutes such as inorganic electrolytes, surfactants and alcohols that can affect the properties (*e.g.*, structure) of the thin water films between two hydrophobic surfaces (Chapter 3, Chapter 4 and Chapter 5).

6. Measure the surface forces at different temperatures to determine the changes in film entropies ($\Delta S^{f,ex}$) and enthalpies ($\Delta H^{f,ex}$) across the film thickness (Chapter 6).

1.5 References

1. Derjaguin, B. V.; Laudau, L., *Acta Physicochim. U. R. S. S.* **1941,** 14, 622-633.

2. Verwey, E. J. W.; Overbeek, J. T. G., *Theory of the Stability of Lyophobic Colloids*. Elsevier: Amsterdam, 1948.

3. Derjaguin, B. V.; Churaev, N. V., *Colloids Surf.* **1989,** 41, 223-237.

4. Laskowski, J.; Kitchener, J. A., *J. Colloid Interface Sci.* **1969,** 29, 670-679.

5. Israelachvili, J. N., *Surf. Sci. Rep.* **1992,** 14, 109-159.

6. Israelachvili, J. N.; Pashley, R. M., *Nature* **1982,** 300, 341-342.

7. Christenson, H. K.; Claesson, P. M., *Adv. Colloid Interface Sci.* **2001,** 91, 391-436.

8. Xu, Z.; Yoon, R.-H., *J. Colloid Interface Sci.* **1989,** 132, (2), 532-541.

9. Xu, Z.; Yoon, R.-H., *J. Colloid Interface Sci.* **1990,** 134, (2), 427-434.

10. Yoon, R.-H.; Mao, L., *J. Colloid Interface Sci.* **1996,** 181, 613-626.

11. Yoon, R.-H. In *Hydrodynamic and Surface Forces in Bubble-Particle Interactions*, XVII International Mineral Processing Congress, Dresden, Germany, 1991; Aufbereitungs-Technik: Dresden, Germany, 1991; pp 474-485.

12. Mao, L.; Yoon, R.-H., *Int. J. Miner. Process* **1997,** 51, 171-181.

13. Attard, P., *Adv. Colloid Interface Sci.* **2003,** 104, 75-91.

14. Christenson, H. K.; Claesson, P. M., *Science* **1988,** 239, (4838), 390-392.

15. Miklavic, S. J.; Chan, D. Y. C.; White, L. R.; Healy, T. W., *J. Phys. Chem.* **1994,** 98, 9022-9032.

16. Podgornik, R., *J. Chem. Phys* **1989,** 91, (9), 5840-5849.

17. Kekicheff, P.; Spalla, O., *Phys. Rev. Lett.* **1995,** 75, (9), 1851-1855.

18. Meyer, E. E.; Lin, Q.; Hassenkam, T.; Oroudjev, E.; Israelachvili, J. N., *Proc. Nat. Acad. Sci. U.S.A* **2005,** 102, 6839-6842.

19. Derjaguin, B. V., *Kolloid Zeits* **1934,** 69, 115-164.

20. Rabinovich, Y. I.; Yoon, R.-H., *Langmuir* **1994,** 10, 1903-1909.

21. Rabinovich, Y. I.; Yoon, R.-H., *Colloids and Surfaces* **1994,** 93, 263-273.

22. Meagher, L.; Craig, V. S. J., *Langmuir* **1994,** 10, 2736-2742.

23. Vinogradova, O. I.; Yakubov, G. E., *J. Chem. Phys.* **2001,** 114, (18), 8124-8131.

24. Muster, T. H.; Toikka, G.; Hayes, R. A.; Prestidge, C. A.; Ralston, J., *Colloids and Surf., A* **1996,** 106, 203-211.

25. Wang, J.; Yoon, R.-H., *Langmuir* **2008,** 24, 7889-7896.

26. Israelachvili, J.; Pashley, R., *Nature* **1982,** 300, 341-342.

27. Christenson, H. K.; Claesson, P. M.; Berg, J.; Herder, P. C., *J. Phys. Chem.* **1989,** 93, 1472-1478.

28. Claesson, P. M.; Blom, C. E.; Herder, P. C.; Ninham, B. W., *J. Colloid Interface Sci.* **1986,** 114, (1), 234-242.

29. Tsao, Y.-H.; Yang, S. X.; Evans, D. F.; Wennerstrom, H., *Langmuir* **1991,** 7, 3154-3159.

30. Spalla, O., *Curr. Opin. Colloid Interface Sci.* **2000,** 5, 5-12.

31. Eriksson, J. C.; Yoon, R.-H., The Nature of Hydrophobic Attraction Forces. In *Froth Flotation A Century of Innovation*, Fuerstenau, M. C.; Jameson, G.; Yoon, R.-H., Eds. Society for Mining, Metallurgy, and Exploration, Inc.: 2006; pp 133-178.

32. Eriksson, J. C.; Yoon, R.-H., Hydrophobic Attraction in the Light of Thin-Film Thermodynamics. In *Colloid Stability: The Role of Surface Forces*, Tadros, T. F., Ed.

WILEY-VCH Verlag GmbH & Co. KGaA: Weinheim, Germany, 2007; Vol. 1, pp 99-132.

33. Meyer, E. E.; Rosenberg, K. J.; Israelachvili, J., *Proc. Nat. Acad. Sci. U.S.A* **2006,** 103, 15739-15746.

34. Wood, J.; Sharma, R., *Langmuir* **1994,** 10, 2307-2310.

35. Wood, J.; Sharma, R., *Langmuir* **1995,** 11, (12), 4797-4802.

36. Parker, J. L.; Claesson, P. M.; Attard, P., *J. Phys. Chem.* **1994,** 98, 8468-8480.

37. Nguyen, A. V.; Nalaskowski, J.; Miller, J. D.; Butt, H.-J., *Int. J. Miner. Process.* **2003,** 72, 215-225.

38. Ishida, N.; Kinoshita, N.; Miyahara, M.; Higashitani, K., *J. Colloid Interface Sci.* **1999,** 216, 387-393.

39. Ederth, T.; Claesson, P.; Liedberg, B., *Langmuir* **1998,** 14, 4782-4789.

40. Ederth, T., *J. Phys. Chem. B* **2000,** 104, 9704-9712.

41. Hato, M., *J. Phys. Chem.* **1996,** 100, 18530-18538.

42. Kurihara, K.; Kunitake, T., *J. Am. Chem. Soc.* **1992,** 114, 10927-10933.

43. Lin, Q.; Meyer, E. E.; Tadmor, M.; Israelachvili, J. N.; Kuhl, T. L., *Langmuir* **2005,** 21, 251-255.

44. Parker, J. L.; Yaminsky, V. V.; Claesson, P. M., *J. Phys. Chem.* **1993,** 97, 7706-7710.

45. Rutland, M. W.; Parker, J. L., *Langmuir* **1994,** 10, 1110-1121.

46. Zhang, J.; Yoon, R.-H.; Mao, M.; Ducker, W. A., *Langmuir* **2005,** 21, 5831-5841.

47. Zhang, J.; Yoon, R.-H.; Eriksson, J. C., *Colloids Surf., A* **2007,** 300, 335-345.

48. Yoon, R.-H.; Ravishankar, S. A. R., *J. Colloid Interface Sci.* **1996,** 179, 391-402.

49. Ederth, T.; Liedberg, B., *Langmuir* **2000,** 16, 2177-2184.

50. Christenson, H. K.; Fang, J.; Ninham, B. W.; Parker, J. L., *J. Phys. Chem.* **1990,** 94, 8004-8006.

51. Craig, V. S. J.; Ninham, B. W.; Pashley, R. M., *Langmuir* **1998,** 14, (12), 3326-3332.

52. Craig, V. S. J.; Ninham, B. W.; Pashley, R. M., *Langmuir* **1999,** 15, 1562-1569.

53. Mahnke, J.; Stearnes, J.; Hayes, R. A.; Fornasiero, D.; Ralston, J., *Phys. Chem. Chem. Phys.* **1999,** 1, 2793-2798.

54. Considine, R. F.; Hayes, R. A.; Horn, R. G., *Langmuir* **1999,** 15, 1657-1659.

55. Sakamoto, M.; Kanda, Y.; Miyahara, M.; Higashitani, K., *Langmuir* **2002,** 18, 5713-5719.

56. Stevens, H.; Considine, R. F.; Drummond, C. J.; Hayes, R. A.; Attard, P., *Langmuir* **2005,** 21, 6399-6405.

57. Meyer, E. E.; Lin, Q.; Israelachvili, J. N., *Langmuir* **2005,** 21, 256-259.

58. Kokkoli, E.; Zukoski, C. F., *J. Colloid Interface Sci.* **1999,** 209, 60-65.

59. Rabinovich, Y. I.; Guzonas, D. A.; Yoon, R.-H., *Langmuir* **1993,** 9, 1168-1170.

60. Eriksson, J. C.; Ljunggren, S.; Claesson, P. M., *J. Chem. Soc., Faraday Trans. 2* **1989,** 85, (3), 163-176.

61. Attard, P., *J. Phys. Chem* **1989,** 93, 6441-6444.

62. Spalla, O.; Belloni, L., *Phys. Rev. Lett.* **1995,** 74, (13), 2515-2518.

63. Tsao, Y.-H.; Evans, D. F.; Wennerstrom, H., *Science* **1993,** 262, (5133), 547-550.

64. Christenson, H. K.; Yaminsky, V. V., *Colloids Surf., A* **1997,** 129-130, 67-74.

65. Tyrrell, J. W. G.; Attard, P., *Phys. Rev. Lett.* **2001,** 87, (17), 176104-1.

66. Tyrrell, J. W. G.; Attard, P., *Langmuir* **2002,** 18, 160-167.

67. Ishida, N.; Sakamoto, M.; Miyahara, M.; Higashitani, K., *J. Colloid Interface Sci.* **2002,** 253, 112-116.

68. Yaminsky, V. V.; Ninham, B. W., *Langmuir* **1993,** 9, 3618-3624.

69. Yang, J.; Duan, J.; Fornasiero, D.; Ralston, J., *J. Phys. Chem. B* **2003,** 107, 6139-4147.

70. Ljunggren, S.; Eriksson, J. C., *Colloids and Surf., A* **1997,** 129-130, 151-155.

71. Wang, L.; Yoon, R.-H., *Langmuir* **2004,** 20, 11457-11464.

72. Yoon, R.-H.; Aksoy, B. S., *J. Colloid Interface Sci.* **1999,** 211, 1-10.

Chapter 2

AFM Forces Measured between Gold Surfaces Coated with Self-Assembled Monolayers of 1-Hexadecanethiol*

2.1 Abstract

An atomic force microscope (AFM) was used to measure the forces between gold surfaces with and without hydrophobizing them by the self-assembly of 1-hexadecanethiol. The forces measured between bare gold surfaces were fitted to the Derjaguin-Landau-Verwey-Overbeek (DLVO) theory with a Hamaker constant of 1.2×10^{-20} J, which was close to the value determined using the methylene iodide contact angle method but was lower than that calculated using the Lifshitz theory. When the surfaces were hydrophobized in a 1×10^{-2} mM thiol-in-ethanol solution for 10 minutes, the measured forces exhibited a long-range force with a decay length of 35 nm. Despite its high water contact angle (105º), the force curve was smooth and exhibited no steps. When the surfaces were hydrophobized in a 1 mM thiol solution for longer than 6 hours, however, the force curves exhibited steps, indicating that the long-range attractions were caused by bridging bubbles. When the measurements were conducted after washing the substrates with organic solvents, the steps disappeared and long-range attractive force appeared. In the presence of ethanol, the water contact angle decreased below 90º, the attraction became weaker, and the force curves became smooth. On the basis of the results obtained in the present work, possible mechanisms for the long-range attractions are discussed.

2.2 Introduction

In colloid chemistry, the Derjaguin-Landau-Verwey-Overbeek (DLVO) theory has been used extensively to predict the kinetics of coagulation. It was derived to predict the stability of lyophobic colloids, that is, particles with low or no affinity with the dispersion medium, on the basis of a balance between the van der Waals (attractive) force and the electrical double layer (repulsive) force. Thus, the theory should work well with hydrophobic colloids when the medium is water. However, many hydrophobic particles[1, 2] and surfaces[3-8] exhibit attractions that are much stronger than the van der Waals attractions. In this regard, Derjaguin and Churaev[9] suggested that the DLVO theory should be applicable for "particles or surfaces having some limited degree of hydrophilicity". They recognized that hydrophobic attractions are detected experimentally when advancing contact angles (θ_a) are greater than 64^o,[3] while hydrophilic repulsions are detectable at $\theta_a < 15^o$.[10] It appears, therefore, that the DLVO theory has a limited applicability for colloids with a relatively narrow range of contact angles.

The DLVO theory faces even more difficult challenges when one wishes to predict the stability of the wetting films formed on hydrophobic surfaces. Thermodynamically, wetting films are unstable at $\theta > 0^o$, and rupture instantaneously once the film thickness is reduced to a critical value (H_{cr}). Blake and Kitchener[11] measured the values of H_{cr} to be in the range of 6-220 nm, while, according to the DLVO theory, no rupture should occur as both the double-layer and van der Waals forces are repulsive in wetting films.[12] Thus, one way of explaining the rupture of wetting films would be to consider the possibility of a non-DLVO force destabilizing the wetting film. Laskowski and Kitchener[13] speculated the presence of a

long-range “hydrophobic influence” operating in the flotation of methylated silica, while Blake and Kitchener[11] suggested the presence of “hydrophobic force” in wetting films.

Israelachvili and Pashley[14] were the first to actually measure the hydrophobic forces in the thin water films between two mica surfaces coated with cetyltrimethylammonium bromide (CTAB) using the surface force apparatus (SFA). They not only were stronger than the van der Waals force but also were longer-ranged. The work of Israelachvili and Pashley created interests among many colloid chemists and physicists, with numerous follow-up publications.[8, 15-19] Recognition of the hydrophobic force also made it possible to model the coagulation of hydrophobic particles[1, 2] and the bubble-particle adhesion occurring during flotation.[20-22]

There has been a great deal of controversy, however, regarding the existence and the nature of the hydrophobic force. Some investigators consider that it is due to the changes in water structure in the vicinity of hydrophobic solids,[16, 23-25] while others believe that it is an electrical effect due to the correlation between charged patches[26, 27] or between large dipoles[28, 29] formed on solid surfaces,[27, 28] metastability of the water films between hydrophobic surfaces,[5, 30] and bridging of preexisting nanobubbles.[31-33] Recently, the nanobubble theory gained momentum as many investigators showed the discontinuities (or steps) in their force *versus* distance curves,[33, 34] Tyrell and Attard[31] and Yang *et al*.[35] actually showed the AFM images of the nanobubbles formed on hydrophobic surfaces. Interestingly, the nanobubbles were flat, which was necessary to minimize the gas pressure inside the bubbles.

Seemingly definitive evidence for the nanobubble theory was presented by Sakamoto *et al*.,[36] who conducted AFM force measurements between a glass sphere and a silica plate

immersed in octadecyltrimethylammonium chloride (C_{18}TACl) solutions. They observed long-range attractions when the measurements were conducted in air-saturated solutions but not in carefully degassed solutions. These observations led to a statement that "long-range attraction *never* appears in completely air-free C_{18}TACl solutions". However, the repeat experiments conducted by Zhang *et al.*[17] on the same system showed that long-range attractions with decay lengths of 36 nm were observed in degassed solutions. Meyers *et al*.[19, 37] also conducted force measurements between mica surfaces coated with a double-chain (C-18) cationic surfactant both in the presence and absence of dissolved gases. In the former, they observed a long-range attractive force, while in the latter only a short-range attraction was observed. It was concluded, therefore, that only the short-range force observed at separations below 10 nm was the "true" hydrophobic force, while the long-range force observed above 20 nm was unrelated to hydrophobicity. Meyers *et al*.[27] suggested that the long-range attraction was due to the electrostatic attraction between the positively charged patches of cationic surfactants and the negatively charged bare mica surface. This explanation was similar to the charged-patch model of Miklavic *et al.,*[26] according to which the patches must be mobile to account for the long-range attractions observed in surface force measurements.

In the present work, AFM force measurements were conducted between gold substrates hydrophobized by the self-assembly of 1-hexadecanethiol (C_{16}SH). It is well known that *n*-alkanethiols form stable monolayers with the terminal -CH_3 groups in contact with the aqueous phase, providing hydrophobic surfaces whose surface free energy (19 mJ/m^2) is lower than any hydrocarbon surfaces studied to date.[38] Further, the strong covalent

Au-S bonding provides robust and immobile hydrophobic monolayer, which will preclude the possibility of mobile hydrophobic groups[39, 40] or mobile charged patches[19, 26, 27] creating the long-range forces.

Ederth[40] and Ederth *et al.*,[41] used a bimorph surface force apparatus (MASIF) to measure the forces between $C_{16}SH$-coated gold surfaces in water. The force curves obtained by these investigators showed steps, which led to their conclusion that the "excess" force was due to bubble coalescence. They concluded that the excess force was observed only when advancing contact angle (θ_a) exceeded 90^o and that no attraction beyond the van der Waals attraction was observed when $\theta_a < 90^o$. It has been found in the present work that strong and long-range hydrophobic forces can still be observed without the steps when gold substrates are contacted with $C_{16}SH$-in-ethanol solutions of lower concentrations and for shorter contact times than employed by Ederth and his co-workers. Further, the steps disappear when gold substrates hydrophobized at higher concentrations for a long period of time are washed with appropriate solvents.

2.3 Materials and Methods

2.3.1 Materials

a) Regents

A Nanopure II (Barnstead IA) water purification system was used to obtain double-distilled and deionized water with a resistivity of 18.2 MΩ/cm. To remove particulates, a submicron Postfilter (0.2 μm pore size) from Fisher Scientific was used in conjunction with the Nanopure water system. 1-hexadecanethiol ($C_{16}SH$, 97%) from TCI dissolved in 200

proof ethanol (AAPER Alcohol) was used to hydrophobize the gold surfaces. Sulfuric acid (98%) from VMR International and hydrogen peroxide (H_2O_2, 29.0-32.0%) from Alfa Aesar were used to clean gold plates.

b) Gold Plates

Gold microspheres and gold-coated glass slides were used for AFM surface force measurements. The gold-coated glass slides were obtained by depositing pure gold on glass using a vacuum evaporator. A 50 Å chromium layer was deposited first on the glass prior to coating it with a thin-layer (500 Å) of gold. The chromium coating was necessary to achieve strong bonding between gold and substrate. The coatings produced without the chromium adhesive layer were easily removed in acid solutions.

c) Gold Spheres

Gold spheres were produced by melting a gold micro-powder (1.5-3.0 μm, >99.96%, Alfa Aesar) in a furnace. The powder was placed in an alumina crucible, and heated until the temperature was raised above its melting point (1,064.18^{o}C). It was kept at 1,100^{o} C for 15 minutes and then cooled down slowly. The furnace was flushed with nitrogen to provide an oxygen-free atmosphere. The gold spheres obtained in this manner had a wide range of sizes. Only those with diameters of 15-20 μm were selected for AFM force measurements.

2.3.2 Cleaning Gold Substrates

To obtain high-quality thiol monolayers on gold, a substrate must be cleaned thoroughly prior to immersing it in a thiol solution.[42, 43] There are several cleaning procedures reported in the literature, including the methods of using piranha solution,[38, 44, 45] chromic

acid,[46, 47] UV/ozone treatment,[43, 48] etc. In the present work, the gold plates were cleaned first by immersing them in a boiling piranha solution (1:2 H_2O_2/H_2SO_4) for 20 minutes, and then washing it with nanopure water for 1 minute, followed by ethanol wash for 2 minutes. After the cleaning, the gold plate was immediately contacted with a thiol solution for hydrophobization. The piranha solution reacts violently with organic matter, especially when it is hot, and is extremely corrosive. Therefore, it is known to oxidize gold surfaces.[42] In the present work, the gold surfaces cleaned in the manner described above exhibited zero water contact angles, possibly due to the formation of gold oxide (Au_2O_3). After rinsing it with ethanol for 2 minutes, the contact angle was increased to 65°. It has been reported that the gold oxide is unstable at ambient and can be readily reduced by ethanol.[42, 43]

For the case of gold spheres, cleaning was done after they had been glued onto cantilever springs. To prevent the glues from being destroyed by the piranha solution, each gold sphere was flushed with ethanol, irradiated by UV irradiation (λ = 254 nm) for 2 hours, and then rinsed with ethanol again.

2.3.3 Hydrophobizing Gold Substrates

The gold plates and spheres cleaned in the manner described above were hydrophobized by contacting them in C_{16}SH-in-ethanol solutions. The specific interaction between sulfur and gold allowed the surfactant molecules to form robust self-assembled monolayers.[38] The kinetics of adsorption varied with the surfactant concentration.[49] In the present work, the hydrophobization was carried out in 10^{-2} or 1 mM C_{16}SH-in-ethanol solutions at room temperature. It was shown that good monolayers can be formed at a

concentration as low as 10^{-2} mM, given a sufficient contact time.[38] After the hydrophobization, the gold substrates were washed with ethanol and then dried in a nitrogen gas stream. For a given force measurement, a set of gold plate and sphere was immersed in a thiol solution for a predetermined length of time, so that the hydrophobicity of the two macroscopic surfaces would be the same. A gold sphere was glued onto a cantilever spring before being immersed into a thiol solution. Reversing the order made it difficult to glue the sphere onto a spring.

2.3.4 Contact Angle Measurement

Ederth[40] showed that $C_{16}SH$-coated gold exhibited very small contact angle hysteresis ($\Delta\cos\theta = 0.10$). Therefore, equilibrium water contact angles were measured on the hydrophobized gold plates using a goniometer (Ramé-Hart, Inc) under ambient conditions. Droplets of water (or ethanol solutions) of 1-2 mm diameter were placed on a horizontally placed plate by means of a syringe. The angles were measured on each side of a droplet. The measurements were conducted on a total of five droplets placed on different locations of a gold plate, and the results were averaged. The sessile drop technique was also used to measure the contact angles of methylene iodide on gold. The result was used to calculate the Hamaker constant of gold in water.[18]

2.3.5 Surface Force Measurement and AFM Imaging

Surface force measurements were conducted using a Nanoscope III (Digital Instruments, Inc., Santa Barbara, CA) atomic force microscope (AFM) equipped with a

standard fluid cell and a scanner "E". All the AFM force measurements were carried out in a manner described by Zhang *et al*.[17] Rectangular non-contact silicon cantilevers (dlevers, Model: 1930-00, Veeco Probes) were used for the force measurements. Their spring constants (k) were determined using the Cleveland method.[50] In each experiment, a gold sphere was glued onto a cantilever with EPON 1004 resin (Shell Chemical Co) using a homemade 3D micromanipulator under an Olympus BH-2 light microscope. The force measurements were conducted immediately after the thiol monolayers were formed on gold substrates. AFM images of a clean bare gold plate were taken using triangular Si_3N_4 cantilevers with nominal $k = 0.12$ Nm^{-1}. The image was obtained in the height mode.

2.3.6 ζ-Potential Measurement

A Pen Kem Model 501 Lazer Zee meter was used to measure the electrophoretic mobilities of gold spheres (1.5-3.0 μm). Micro-spheres of gold were suspended in water or in NaCl solutions by means of an ultrasonic vibration. The mobilities were converted to ζ-potentials using the Smoluchowski equation. The ζ-potentials reported in this communication represent the averages of at least five measurements.

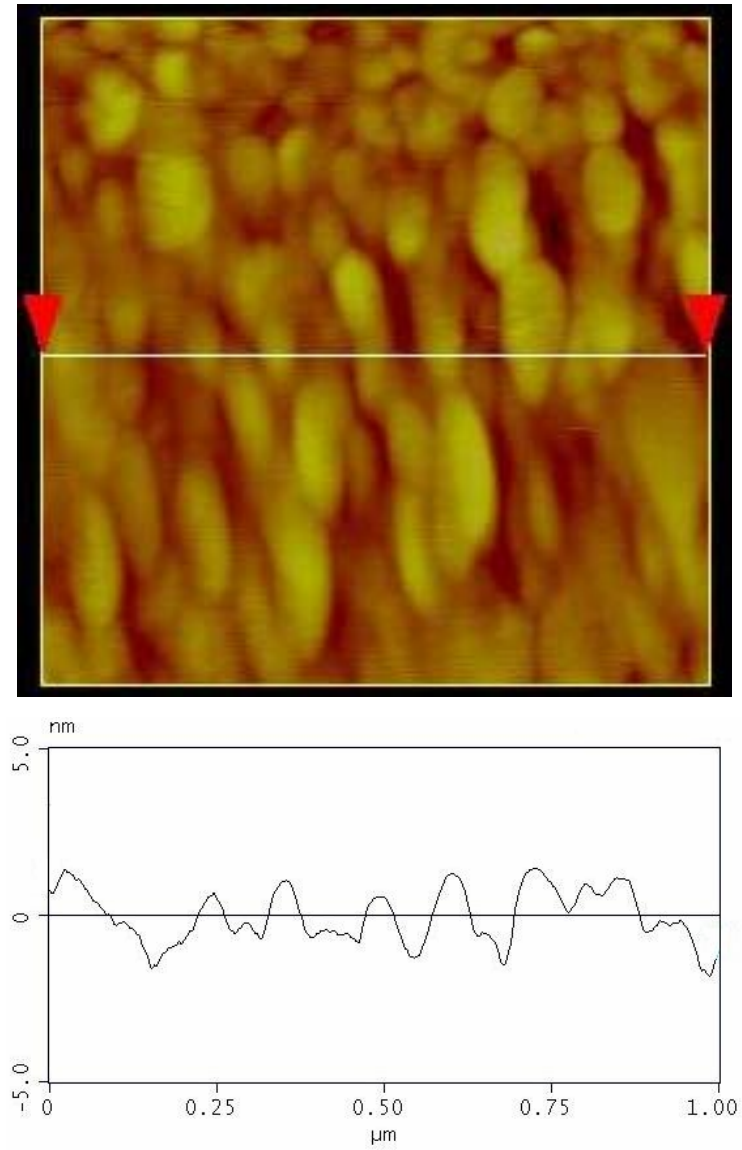

Figure 2.1. An AFM image (and its cross section) of the evaporated gold film on Cr-coated glass after treatment with piranha solution.

2.4 Results and Discussion

2.4.1 Surface Morphology

Figure 2.1 shows an AFM image of the surface of a clean gold plate as obtained using a regular silicon nitride tip. The surface consisted of different grains, with the maximum peak-to-valley distance of 3.3 nm and the root mean square (RMS) roughness of 0.8 nm over an area of 1 × 1 μm^2.

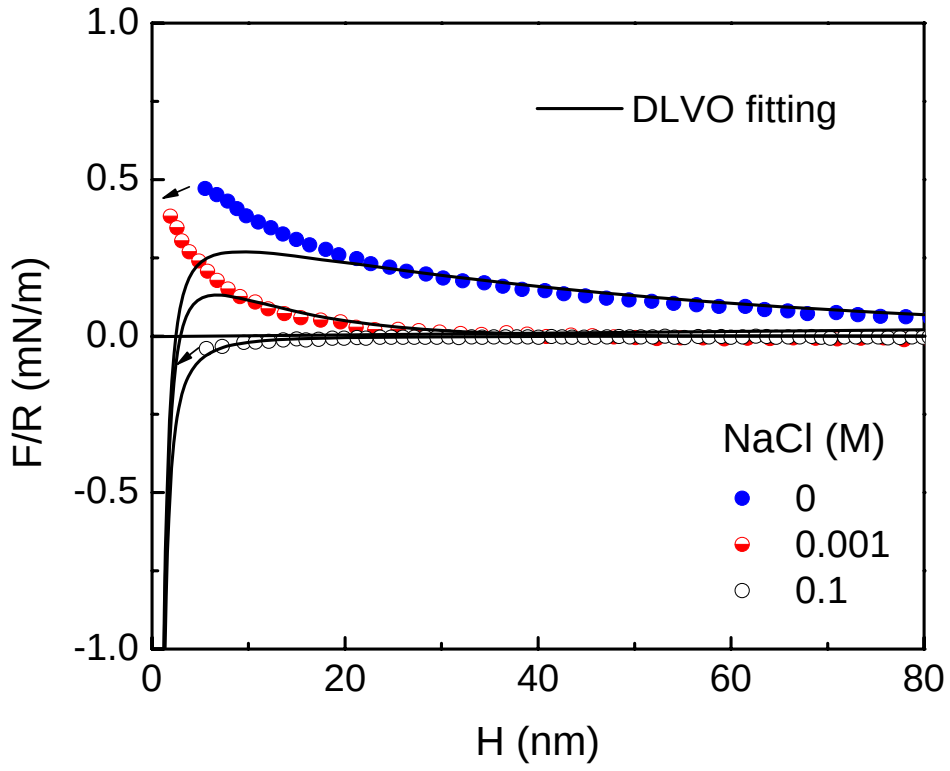

Figure 2.2. Surface forces measured between a microscopic gold sphere and a gold-coated glass plate in water, 1mM and 100 mM NaCl solutions. The data points have been fitted to the DLVO theory under conditions of constant potential using the following parameters: for water, ψ_0 = -55 mV, κ^{-1} = 424 Å; for 1mM NaCl, ψ_0 = -24 mV, κ^{-1} = 93 Å; for 100 mM NaCl, ψ_0 = -8 mV, κ^{-1} = 9 Å. A_{131} = 1.2 × 10^{-20} J.

2.4.2 van der Waals Attraction

Figure 2.2 shows the AFM force curves (*F/R versus H*) obtained between bare gold surfaces immersed in 0, 1, and 100 mM NaCl solutions. The force curves obtained in pure water and at 1 mM NaCl solution showed net repulsive forces over the entire separation distances investigated, while the results obtained at 100 mM showed no repulsive forces until the separation distance was reduced below approximately 20 nm. The solid lines represent the experimental data fitted to the DLVO theory. The fitting parameters were: A_{131} (Hamaker constant) = 1.2×10^{-20} J, ψ_0 (surface potential) = -55 mV, and κ^{-1} (Debye length) = 42.4 nm in pure water. At 1 mM NaCl, ψ_0 decreased to -24 mV and κ^{-1} to 9.3 nm due to double-layer compression. As the NaCl concentration was increased to 100 mM, ψ_0 decreased further to -8 mV and κ^{-1} to 0.9 nm. The double-layer potentials were calculated using the constant potential model of Oshima *et al*.[51] The values of ψ_0 obtained from the curve fitting exercise were close to the ζ-potentials measured in the present work as shown in Table 2.1.

Table 2.1. Comparison of the ζ-potentials of Gold Spheres and the DLVO and the DLVO Potentials in Water and NaCl solutions

Gold Substrate	NaCl Concentration (mM)	ζ-potential (mV)	DLVO Potential[1] (mV)
Uncoated	0	-56.9	-55
	1	-24.2	-24
	100	-8.0	-8
$C_{16}SH$ Coated	0	-57.2	-

[1]from AFM force curves in Figure 2.2

It may be of interest to compare the value of A_{131} determined from curve fitting in the manner described above with that determined using a different method. According to the combining rule,[52]

$$A_{131} = \left(\sqrt{A_{11}} - \sqrt{A_{33}}\right)^2 \qquad (2.1)$$

where A_{131} is the Hamaker constant of material **1** in medium **3** (water), A_{11} the same *in vacuo*, and A_{33} is the Hamaker constant of water *in vacuo*. It has been shown that A_{ii} can be determined for a variety of polar and apolar materials using the following relation:[53]

$$A_{ii} = 24\pi l_0^2 \gamma_i^{LW} \qquad (2.2)$$

in which $l_0 \approx 1.57$ Å. Substituting Equation 2.2 into Equation 2.1, one obtains that

$$A_{131} = 1.86 \times 10^{-21} (\sqrt{\gamma_1^{LW}} - \sqrt{\gamma_3^{LW}})^2 \qquad (2.3)$$

in which γ_1^{LW} is the dispersion component of the surface tension of gold and γ_3^{LW} is the same for water.

Table 2.2. Surface Tension and Methylene Iodide Contact Angle Data Used to Determine the Hamaker Constant for Gold in Water.

	γ (mN/m)	γ^{LW} (mN/m)	γ^{AB} (mN/m)	θ_m (degree)	A_{131} (J)
methylene iodide[1]	50.8	48.5	2.3	6	
Water[2]	72.8	21.8	51		
gold		52.9			
gold-water-gold					1.26×10^{-20}

[1]ref 18; [2]ref 53

In the present work, the value of γ_1^{LW} was determined using the following relation:[18]

$$\gamma_1^{LW} = [(1+\cos\theta_m)\gamma_m / 2\sqrt{\gamma_m^{LW}}]^2 \qquad (2.4)$$

in which θ_m is the contact angle of methylene iodide on gold, and γ_m and γ_m^{LW} are the surface tension of methylene iodide and its apolar component, respectively. The values of θ_m for the gold-coated glass surfaces used in the present work gave the value of 6° as shown in Table 2.2. By substituting this and the values of γ_m = 50.8 mN/m[18] and γ_m^{LW} = 48.5 mN/m[18] into Equation 2.4, one obtains γ_1^{LW} = 52.9 mN/m. This value is comparable to those reported by

Fowkes[54] (60-120 mN/m) and the value of 121.6 mN/m reported by Thelen.[55]

By substituting the value of γ_1^{LW} = 52.9 mN/m obtained in the present work and the value of γ_3^{LW} = 21.8 mN/m[53] into Equation 2.3, one obtains A_{131} = 1.26 × 10^{-20} J, which is close to that (A_{131} = 1.2 × 10^{-20} J) obtained from curve fitting. Both of these values are a little lower than that (4 × 10^{-20} J) obtained by Ederth[40] from AFM force measurement. On the other hand, Biggs and Mulvaney[47] conducted AFM force measurement between bare gold surfaces, that is, gold-coated silica sphere and gold plate, and obtained a value of A_{131} = 2.5 × 10^{-19} J, which was close to those (2.5~4 × 10^{-19} J) calculated using the Lifshitz theory. Biggs *et al.*[56] used these values to fit the AFM force curves obtained in different NaCl solutions. However, the fits were relatively poor at short separations. In later experiments, Kane and Mulvaney[44] used a considerably lower value of A_{131} (= 1 × 10^{-19} J) to fit their AFM force data. Further, Ducker and Senden[57] could not fit their AFM force curves obtained between gold-coated silica sphere and gold-coated mica surface to the DLVO theory using the value of A_{131} = 3.5 × 10^{-19} J from the Lifshitz theory. Giesbers *et al.*[45] also showed that the force curves obtained for the gold-gold interactions in water exhibited very weak van der Waals interactions.

That different researchers reported different Hamaker constants for gold-gold interactions may be attributed to the differences in coating thickness, contamination level, and surface roughness. Owing to the large Hamaker constants, as calculated from the Lifshitz theory, gold surfaces can be readily contaminated. Ducker and Senden[57] attributed the failure to fit their data with A_{131} = 3.5 × 10^{-19} J to the possible adsorption of organic materials on gold. It has actually been shown that the adsorption of citrate mediates the van der Waals interaction between gold surfaces.[58, 59] The same explanation could be extended to

silver-silver interactions. The AFM force measurements conducted between silver-coated glass plate and silica sphere gave a Hamaker constant of 2×10^{-20} J, which was much smaller than the value of 3×10^{-19} J calculated from the Lifshitz theory.[60]

According to Considine and Drummond,[61] surface roughness attenuates short-range forces such as van der Waals, steric, and hydration forces. Bhattacharjee *et al*.[62] showed also that random distribution of asperities can also reduce the interaction energies substantially.

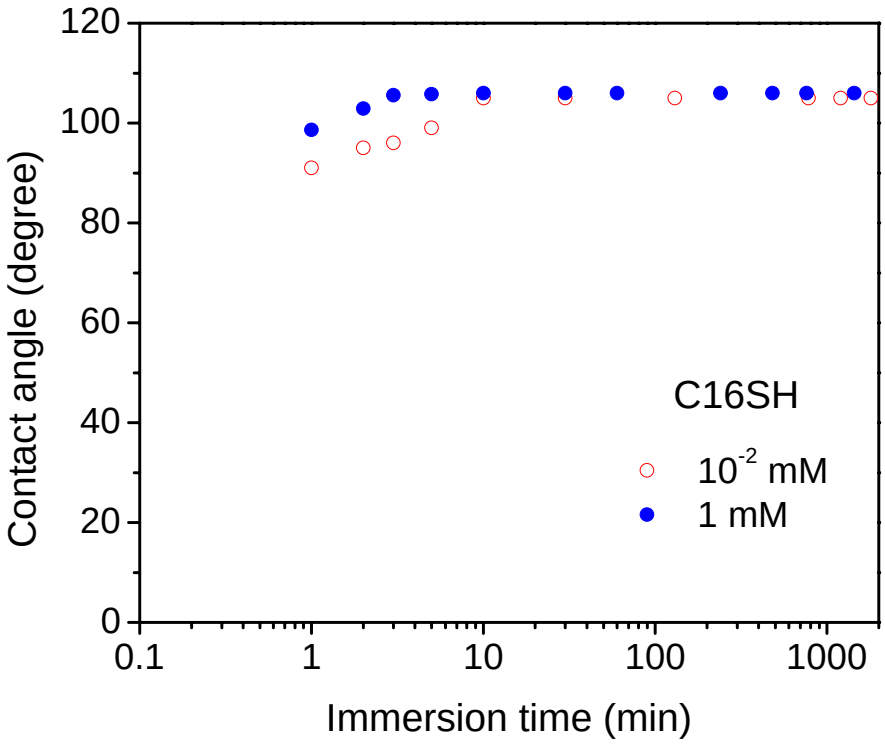

Figure 2.3. Changes in equilibrium water contact angle (θ) on gold plate as a function of immersion time in 0.01 and 1 mM 1-hexadecanethiol-in-ethanol solutions.

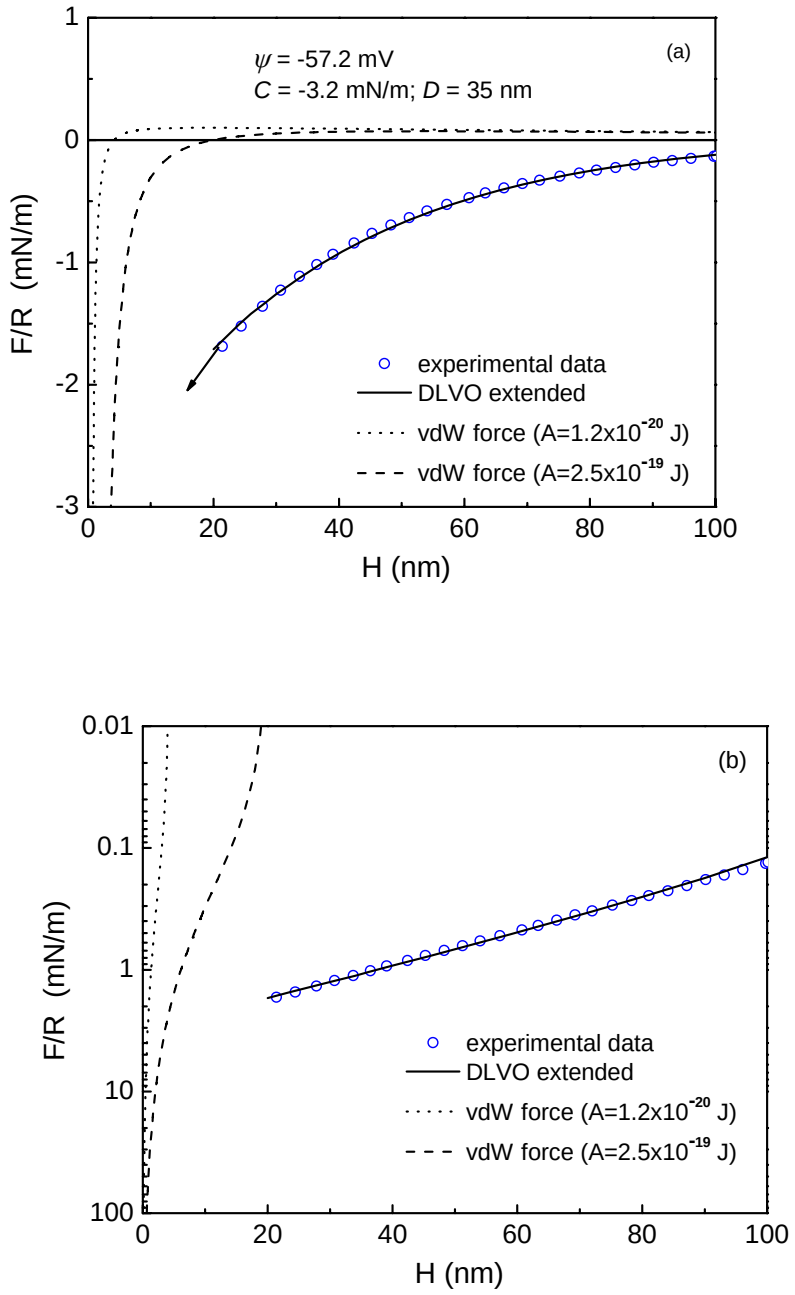

Figure 2.4. (a) A normalized AFM force curve obtained in water between gold surfaces hydrophobized in a 1×10^{-2} mM $C_{16}SH$-in-ethanol solution for 10 minutes. The dashed and dotted lines represent the force curves fitted to the DLVO theory with $A_{131} = 1.2 \times 10^{-20}$ J and $A_{131} = 2.5 \times 10^{-19}$ J, respectively, for the gold-water-gold system. The solid line represents the experimental data fitted to the DLVO theory extended to include the contributions from the hydrophobic force. The hydrophobic force is represented by the single-exponential force law ($F/R=C\exp(-H/D)$) with C = -3.2 mN/m and D = 35 nm as fitting parameters. (b) The same data plotted on a log-log scale to show the goodness of the fit.

2.4.3 Hydrophobic Force

Samples of gold spheres and plates were hydrophobized by immersing them in a 1×10^{-5} M $C_{16}SH$-in-ethanol solution for 10 minutes. Figure 2.3 shows the equilibrium water contact angles measured on these samples at different immersion times. As shown, the contact angle reached a maximum of 105° after 10 minutes of immersion time. Thus, the 10-minute immersion time should be sufficient to complete the formation of a monolayer.

Figure 2.4 shows a force *versus* distance curve obtained with a gold sphere and a gold plate hydrophobized in the matter described above. The measured forces were net attractive and long-ranged (0~80 nm), with the two surfaces jumping into contact at $H \approx 22$ nm where the force gradient exceeded the spring constant. The dashed and dotted lines represent the van der Waals force curves with $A_{131} = 1.2 \times 10^{-20}$ and $A_{131} = 2.5 \times 10^{-19}$ J, respectively, while the solid line represents the DLVO theory extended to include the contribution from the hydrophobic force. The force curve was smooth indicating that the long-range attraction was not caused by nanobubbles. Figure 2.4b shows the same experimental results plotted in a semi-log plot to show that the long-range attraction can be fitted to a single-exponential force law with a decay length of 35 nm. Thus, the long-range attractive force decays exponentially, and is much stronger and longer-ranged than the van der Waals forces considered in the present work.

It is well known that the forces measured between hydrophobic surfaces vary a great deal depending on the measuring apparatus used and the methods of hydrophobization employed. The measured forces reported in the literature have been classified into three groups,[8, 19] which include i) the short range, but strongly attractive, forces that are typically

observed between robust hydrophobic surfaces formed by the adsorption of chemisorbing surfactants,[63, 64] ii) the long-range, exponentially decaying forces observed between surfaces coated with physisorbed surfactants,[65-68] and iii) the attractive forces of random strengths and ranges, the force curves showing steps due to bubble coalescence. The third group of forces is observed typically with hydrophobic surfaces with very high contact angles.[31-33, 69]

It would be difficult to classify the results obtained in the present work to any one of the three groups. Since $C_{16}SH$ chemisorbs on gold and forms robust hydrophobic surfaces, they should belong to the first group. However, the forces measured in the present work are of very long-range and decay exponentially without steps.

2.4.4 Bubble Coalescence

Ederth[40] and Ederth *et al.*[41] used a bimorph surface force apparatus (MASIF) to measure the forces between $C_{16}SH$-coated gold surfaces in water and ethanol/water mixtures. They observed "excess" (long-range) attractions at $\theta > 90^{o}$, but the force curves showed steps at separations in the range of 20-50 nm. They concluded, therefore, that the excess attractions were caused by the coalescence of bubbles on the surface. It should be pointed out, however, that Ederth *et al.*[41] conducted the force measurements after immersing the substrates in 1 mM $C_{16}SH$-in-ethanol solutions for more than 15 hours. These conditions represented 2 orders of magnitude higher thiol concentration and longer contact time than employed in the present work to obtain the results shown in Figure 2.4.

Figure 2.5a shows the AFM force measurements conducted in the present work after hydrophobizing the gold substrates under the same conditions as employed by Ederth *et al.*[41]

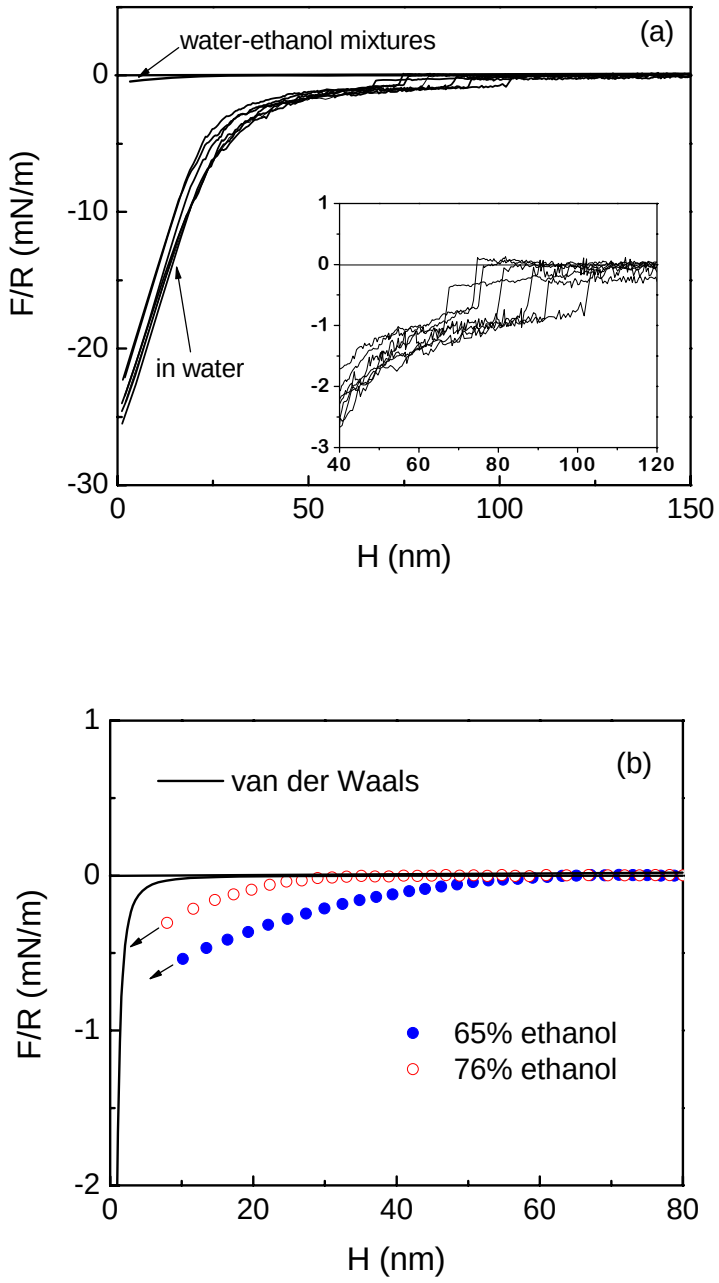

Figure 2.5. (a) Normalized forces measured in pure water and ethanol/water mixtures between gold surfaces contacted with a 1 mM $C_{16}SH$-in-ethanol solution for at least 15 hours; (b) The contact angles of gold in the ethanol-water mixtures were 44 and 39° in 65 and 76% ethanol, respectively.

The equilibrium water contact angle was 106°. The force curves obtained in water show steps, as reported by these investigators, but not in ethanol/water mixtures. In aqueous solutions containing 65 and 76% ethanol by volume, the steps disappeared completely as shown in

Figure 2.5b. This was not surprising because the contact angles were less than 90^{o}, that is, 44 and 39^{o} in 65 and 76% ethanol-in-water solutions, respectively. Under these conditions, bubble nucleation is thermodynamically not possible. Therefore, the net-attractive forces observed in the ethanol/water mixtures should be considered real hydrophobic forces. Note here that the magnitudes of the attractive forces measured in the ethanol/water mixtures were substantially less than in pure water, which may be attributed to the likelihood that the network of hydrogen bonds in solution became weaker in the presence of ethanol. Effects of ethanol on the AFM force measurements will be discussed further in detail in another communication.

The results presented in Figure 2.5a show that nanobubbles can indeed be formed when gold substrates are hydrophobized at a high thiol concentration for a long period of time. It is possible that the thiol monolayer can have defects (or pits) in which air bubbles can nucleate. It is possible that at lower concentrations (*e.g.*, 1×10^{-2} mM $C_{16}SH$) and shorter contact times smoother coatings are formed, which are less likely to trap nanobubbles and hence give rise to force curves with no steps, as shown in Figure 2.4. Sakamoto *et al.*[36] also showed steps in their AFM force curves obtained with silica surfaces coated with $C_{18}TACl$ solutions, and concluded that the long-range attractions were due to bridging bubbles. In support of this claim, they showed that the long-range attractions disappeared when the solution was degassed. On the other hand, Zhang *et al.*[17] showed that long-range attractions were still observed in degassed solutions. However, the long-range attractions observed in degassed solutions were an order of magnitude weaker than those measured by Sakamoto *et al.*[36] Thus, the long-range attractions observed by Zhang *et al.*[17] were considered true

hydrophobic forces while those measured by Sakamoto *et al.*[36] were actually capillary forces. Likewise, the long-range attraction observed in the present work between gold surfaces hydrophobized at 1×10^{-2} mM $C_{16}SH$ for 10 minutes may also be considered a true hydrophobic force.

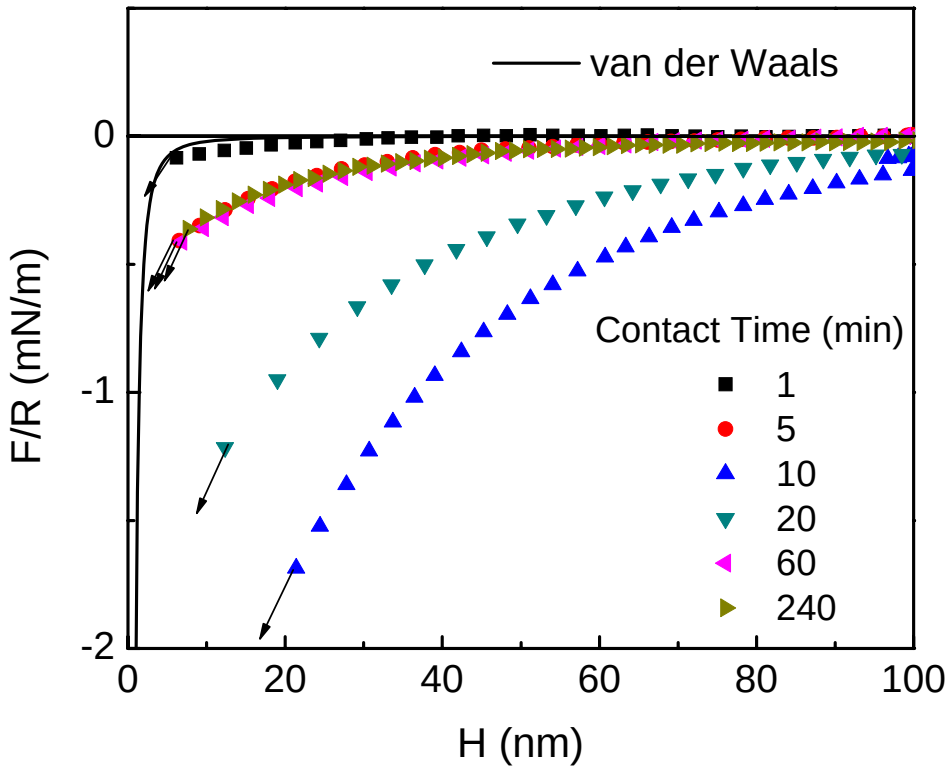

Figure 2.6. Effects of the contact time between gold substrates and a 0.01 mM $C_{16}SH$-in-ethanol solution on the AFM forces measured in pure water.

Figure 2.6 shows a set of AFM force curves obtained with the gold surfaces immersed in a 1×10^{-2} mM $C_{16}SH$-in-ethanol solution for different periods of time. As the contact time was increased from 1 to 10 minutes, the measured forces became stronger, reached a maximum, and then decreased as the contact time was further increased. Also, none of the force curves shows steps, indicating that the attractive forces were not created by bubble

coalescence. Thus, all of the force curves shown in Figure 2.6 may be considered to represent true hydrophobic attractions.

The forces measured after 240 minutes of contact time were substantially lower than the maximum observed after only 10 minutes of contact time, as shown in Figure 2.6. It was found, however, that the maximum force was fully restored after washing the substrates with appropriate organic solvents. The washing procedure involved flushing the AFM cell, mounted with both the plate and sphere, first with ethyl ether and then with ethanol for a few seconds each, followed by flushing with a sufficient amount of nanopure water. It is likely that after a long contact time, the $C_{16}SH$ adsorption resulted in a multi-layer coating, and that solvent washing removed only the species adsorbing on top of the first monolayer. The solvents would not remove the monolayer of the chemisorbed thiol. Thus, the solvent washing would expose the $-CH_3$ groups, which should increase the hydrophobicity and, hence, the long-range attraction (or hydrophobic force).

It is well known that alkyl xanthates and thionocarbamates form multi-layers on sulfide minerals (*e.g.*, Cu_2S, and copper-activated ZnS) and precious metals (*e.g.*, Au, Ag, and Au-Ag alloys), and that the species adsorbing in the multi-layers are metal xanthates.[70-73] It is known also that the head groups of various metal xanthates have varying degrees of hydrophobic character, depending on the difference in electronegativities of the sulfur and metal ions.[74] Xanthates are commonly used as hydrophobizing reagents (collectors) in the base metals flotation industry, and they behave similarly as *n*-alkanethiols. Thus, gold surfaces coated with multi-layers of C_{16}-thiol should still be hydrophobic. In fact, the water contact angles does not change with increasing contact time in 1×10^{-2} mM $C_{16}SH$-in-ethanol

solutions, as shown in Figure 2.3, which makes it difficult to explain the restoration of the full hydrophobic force by the solvent washing. One possible explanation would be that thiol-coated gold surfaces become smoother after the solvent washing. It has been shown that smoother surfaces gives stronger attractive forces.[75]

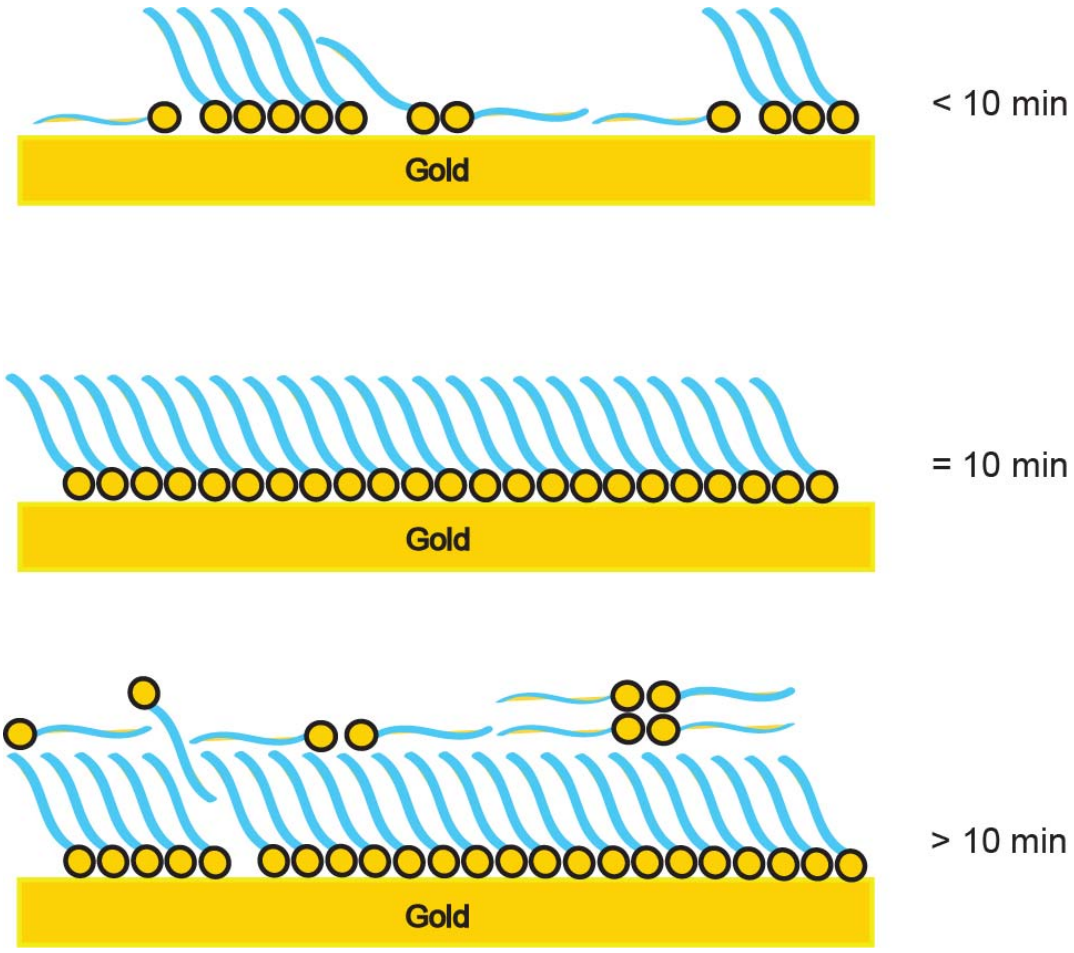

Figure 2.7. A model for the adsorption of $C_{16}SH$ on gold. The surface coverage and orientation are shown to change with the contact time in a 10^{-2} mM thiol-in-ethanol solution.

Figure 2.7 may depict a mechanism for the adsorption of $C_{16}SH$ on gold at a relatively low concentration (*e.g.*, 1×10^{-2} mM). At a short contact time, the surface coverage will be low, which may be responsible for a weak hydrophobic force. After an optimum contact time of 10 minutes, a close-packed monolayer is formed, which gives rise to a maximum

hydrophobic force as shown in Figure 2.6. At a longer contact time, the hydrophobic force diminishes possibly due to the exposure of the -SH or -SAu groups toward the aqueous phase, or the surface roughness created by multi-layer coatings. When a gold substrate is hydrophobized at a very high concentration (*e.g.*, 1 mM), for a very long time (*e.g.*, overnight), the surface roughness may be greatly increased. The force curves obtained under such conditions (see Figure 2.5a and Ederth *et al.*[41]) show steps, indicating that nanobubbles are trapped in between the aspirates and the valleys of rough surfaces. Solvent washing would remove the species adsorbed on top of monolayers, provide a smooth hydrophobic surface, and hence create a strong long-range attraction. In order to explore this possibility, a set of gold sphere and plate were hydrophobized in a 1 mM C_{16}SH-in-ethanol solution overnight (12 hours) in the same manner as Ederth *et al.*,[41] and then washed with ethanol and subsequently with pentane. The residual solvents were evaporated off the surface in a nitrogen gas stream. The force measurements were then conducted a Nanoscope IVa, which was equipped with a standard fluid cell and a scanner "J". Just before the measurement, the gold substrates were washed again by flushing the liquid cell with pure ethanol for a few seconds and subsequently with a plenty of nanopure water. As shown in Figure 2.8, the measured force was net negative and the force curve was smooth with no steps. It appears, therefore, that the solvent washing replaced the capillary force with a true hydrophobic force.

It has been shown in the present work that the long-range attractions observed in the present work between thiol-coated gold surfaces are much larger than the van der Waals force, and that they are not caused by the preexisting bubbles on the surface. If the long range attraction with a decay length of 35 nm cannot be attributed to a hydrophobic attraction, one

might consider the possibility that it originates from an electrostatic attraction between charged patches.[26] For this theory to work, however, it is necessary that the patch sizes be large (larger than the size of hemimicelles) and mobile.[76] The latter is unlikely in view of the fact that thiols chemisorb on gold.[77] Further, the thiolated gold has almost the same ζ-potential as bare gold as shown in Table 2.1. What is left then would be the possibility that the long-range attraction is related to the changes in water structure around hydrophobic surfaces. A problem with this approach is that the computer simulations show that the surface-induced water structure can be extended up to several layers of water molecules only.[78-80] As suggested by Ninham,[81] the hydrophobic force may be related to the gas molecules (oxygen and nitrogen) dissolved in water. At 1 atm, the concentration of the dissolved gas molecules is 5×10^{-2} M, above which the DLVO theory breaks down and the Hofmeister effects begin to show up. It is possible that the dissolved gas molecules, which are hydrophobic and are likely to concentrate near hydrophobic surfaces, may promote the structuring of water at larger distances away from hydrophobic surfaces. In degassed solutions, the surface-induced structuring may not be extended too far into the solution, thereby making the hydrophobic force disappear,[82] or only the short-range hydrophobic force remain.[37]

Although the force measurements conducted by Zhang *et al.*[17] in degassed solutions showed long-range forces, it would be difficult to claim that the AFM cell was completely sealed off from the ambient during the measurement. Thus, the long-range force observed by Zhang *et al*. could have been affected by a small amount of dissolved gases still present in the system. Pashley *et al*.[82-85] showed recently that hydrocarbon oils can be readily emulsified in

water without a surfactant when the mixture was thoroughly (> 97%) degassed. These investigators suggested that degassing eliminated the hydrophobic force, making the emulsions to be stabilized by the double-layer force as predicted by the DLVO theory.

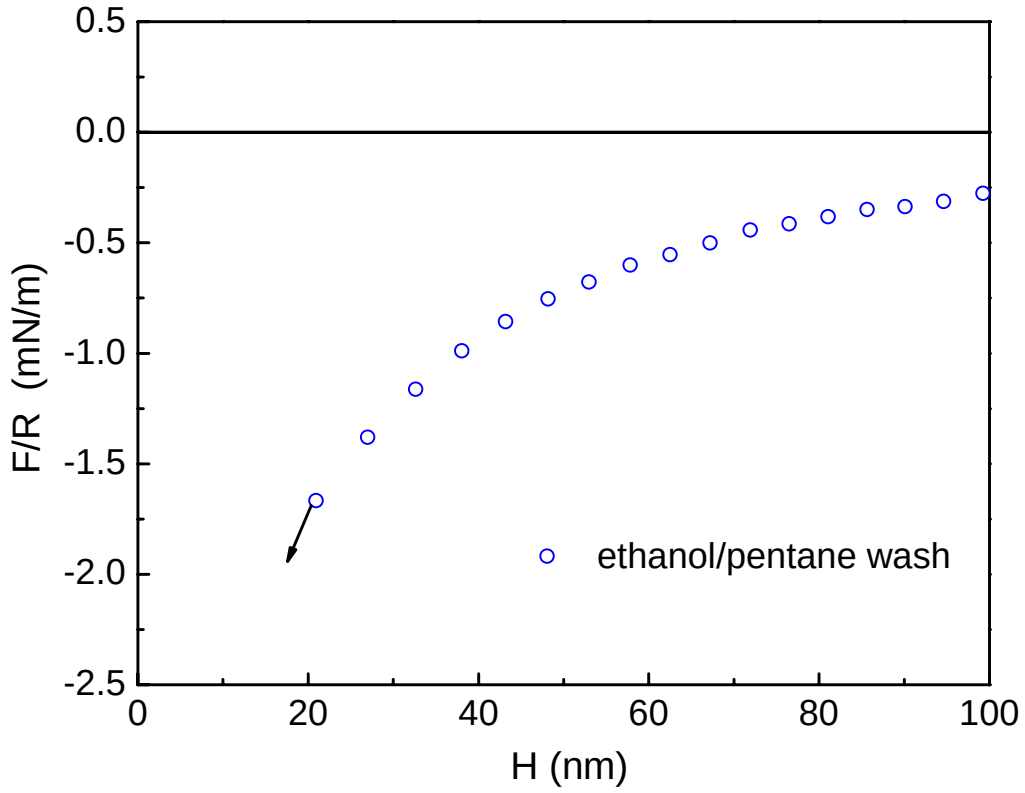

Figure 2.8. An AFM force curve obtained between gold surfaces immersed in a 1 mM $C_{16}SH$-in-ethanol solution for 12 hours and then washed with organic solvents before the measurements. The solvent washing eliminated the steps shown in Figure 2.5a and gave rise to a smooth attractive force curve.

The charged-patch model[26, 27] may be useful for explaining the long-range forces observed between mica or silica surfaces coated with physisorbing cationic surfactants.[27, 86, 87] It is difficult, however, to relate the mechanism to the gases dissolved in solution, while the long-range force observed (at H > 20 nm) in air-saturated solutions disappears upon degassing.[37]

2.5 Conclusions

The Hamaker constant for the gold-gold interactions in water was determined to be 1.2×10^{-20} J by fitting the AFM force curves obtained between bare gold surfaces to the DLVO theory. This value is close to that (1.26×10^{-20} J) determined using the methylene iodide contact angle method. However, these values are substantially lower than those ($2.5\sim4 \times 10^{-19}$ J) obtained from the Lifshitz theory. The lower Hamaker constants measured in the present work may be due to possible contamination of the gold surface, which may be difficult to avoid in view of the large Hamaker constant of the heavy metal.

AFM force measurements were also conducted using gold surfaces hydrophobized by the self-assembly of 1-hexadecanethiol. When the surfaces were hydrophobized in a 1 mM thiol-in- ethanol solution longer than 6 hours, the measured forces were net-attractive and long-ranged. However, the force curves exhibited steps, indicating that the measured forces were due to bridging bubbles. Bubble nucleation was warranted as the water contact angles of the thiolated gold surfaces were over 90^{o}. These results were in agreement with those of Ederth *et al.*[40] When the AFM force measurements were conducted in ethanol/water mixtures, the contact angles became less than 90^{o}, and hence prevented bubble nucleation and gave rise to smooth force curves without steps. The measured forces were weaker than in pure water, but were still net attractive, long-ranged, and stronger than the van der Waals force.

When the gold substrates were hydrophobized in a dilute (1×10^{-2} mM) thiol solution at a relatively short contact time (10 minutes), a long-range attractive force which decayed exponentially with a decay length of 35 nm was obtained. The force curve exhibited no steps indicating that the long-range attraction was not due to bridging bubbles. Steps appeared

when the gold substrates were hydrophobized in a strong (1 mM) thiol solution at a long contact time (overnight). When the force measurements were conducted after washing the substrates with appropriate solvents, the steps in force curves disappeared and long-range hydrophobic forces appeared.

The results obtained in the present work show that the long-range attraction observed between thiolated gold surfaces in water and ethanol solutions are not due to bridging nanobubbles or electrostatic attraction between charged patches. This leaves the possibility that the long-range attraction is caused by the changes in water structure near hydrophobic surfaces. Further work is needed to obtain stronger evidence that the long-range hydrophobic forces are indeed of structural origin.

2.6 Acknowledgement

The authors would like to express their sincere appreciation to Professor Jan Christer Eriksson for his encouragement and helpful discussions. They would also like to acknowledge the financial support from the National Energy Technology Laboratory, U.S. Department of Energy (DE-FC26-02NT41607).

2.7 References

1. Xu, Z.; Yoon, R.-H., *J. Colloid Interface Sci.* **1989,** 132, (2), 532-541.
2. Xu, Z.; Yoon, R.-H., *J. Colloid Interface Sci.* **1990,** 134, (2), 427-434.
3. Israelachvili, J. N.; Pashley, R. M., *J. Colloid Interface Sci.* **1984,** 98, (2), 500-514.
4. Pashley, R. M.; Mcguiggan, P. M.; Ninham, B. W., *Science* **1985,** 229, 1088-1089.

5. Claesson, P. M.; Christenson, H. K., *J. Phys. Chem* **1988,** 92, 1650-1655.

6. Rabinovich, Y. I.; Derjaguin, B. V., *Colloids Surf.* **1988,** 30, 243-251.

7. Parker, J. L.; Cho, D. L.; Claesson, P. M., *J. Phys. Chem.* **1989,** 93, 6121-6125.

8. Christenson, H. K.; Claesson, P. M., *Adv. Colloid Interface Sci.* **2001,** 91, 391-436.

9. Derjaguin, B. V.; Churaev, N. V., *Colloids Surf.* **1989,** 41, 223-237.

10. Churaev, N. V., *Usp. Kolloidn, Khim., FAN, Tashkent* **1987**, 70-78.

11. Blake, T. D.; Kitchener, J. A., *J. Chem. Soc., Faraday Trans. 1* **1972,** 68, 1435-1442.

12. Hough, D. B.; White, L. R., *Adv. Colloid Interface Sci.* **1980,** 14, 3-41.

13. Laskowski, J.; Kitchener, J. A., *J. Colloid Interface Sci.* **1969,** 29, 670-679.

14. Israelachvili, J. N.; Pashley, R. M., *Nature* **1982,** 300, 341-342.

15. Rabinovich, Y. I.; Yoon, R.-H., *Langmuir* **1994,** 10, 1903-1909.

16. Eriksson, J. C.; Ljunggren, S.; Claesson, P. M., *J. Chem. Soc., Faraday Trans. 2* **1989,** 85, (3), 163-176.

17. Zhang, J.; Yoon, R.-H.; Mao, M.; Ducker, W. A., *Langmuir* **2005,** 21, 5831-5841.

18. Yoon, R.-H.; Pazhianur, R., *Colloids and Surf., A* **1998,** 144, 59-69.

19. Meyer, E. E.; Rosenberg, K. J.; Israelachvili, J., *Proc. Nat. Acad. Sci. U.S.A* **2006,** 103, 15739-15746.

20. Yoon, R.-H., *Aufbereit. Tech* **1991,** 32, 474-485.

21. Yoon, R.-H.; Mao, L., *J. Colloid Interface Sci.* **1996,** 181, 613-626.

22. Mao, L.; Yoon, R.-H., *Int. J. Miner. Process* **1997,** 51, 171-181.

23. Eriksson, J. C.; Yoon, R.-H., Hydrophobic Attraction in the Light of Thin-Film Thermodynamics. In *Colloid Stability: The Role of Surface Forces*, Tadros, T. F., Ed.

WILEY-VCH Verlag GmbH & Co. KGaA: Weinheim, Germany, 2007; Vol. 1, pp 99-132.

24. Yoon, R.-H.; Wang, L., Hydrophobic Forces in Foam Films. In *Colloid Stability. The Role of Surface Forces-Part I*, Tadros, T. F., Ed. Wiley-VCH: 2007; Vol. 1, pp 161-186.

25. Eriksson, J. C.; Henriksson, U., *Langmuir* **2007,** 23, 10026-10033.

26. Miklavic, S. J.; Chan, D. Y. C.; White, L. R.; Healy, T. W., *J. Phys. Chem.* **1994,** 98, 9022-9032.

27. Meyer, E. E.; Lin, Q.; Hassenkam, T.; Oroudjev, E.; Israelachvili, J. N., *Proc. Nat. Acad. Sci. U.S.A* **2005,** 102, 6839-6842.

28. Tsao, Y.-H.; Evans, D. F.; Wennerstrom, H., *Science* **1993,** 262, (5133), 547-550.

29. Yoon, R.-H.; Ravishankar, S. A. R., *J. Colloid Interface Sci.* **1996,** 179, 391-402.

30. Christenson, H. K.; Claesson, P. M., *Science* **1988,** 239, 390-392.

31. Tyrrell, J. W. G.; Attard, P., *Langmuir* **2002,** 18, 160-167.

32. Attard, P.; Moody, M. P.; Tyrrell, J. W. G., *Physica A* **2002,** 314, 696-705.

33. Parker, J. L.; Claesson, P. M.; Attard, P., *J. Phys. Chem.* **1994,** 98, 8468-8480.

34. Nguyen, A. V.; Nalaskowski, J.; Miller, J. D.; Butt, H.-J., *Int. J. Miner. Process.* **2003,** 72, 215-225.

35. Yang, J.; Duan, J.; Fornasiero, D.; Ralston, J., *J. Phys. Chem. B* **2003,** 107, 6139-6147.

36. Sakamoto, M.; Kanda, Y.; Miyahara, M.; Higashitani, K., *Langmuir* **2002,** 18, 5713-5719.

37. Meyer, E. E.; Lin, Q.; Israelachvili, J. N., *Langmuir* **2005,** 21, 256-259.

38. Bain, C. D.; Troughton, E. B.; Tao, Y.-T.; Evall, J.; Whitesides, G. M.; Nuzzo, R. G., *J. Am. Chem. Soc.* **1989,** 111, 321-335.

39. Christenson, H. K.; Yaminsky, V. V., *Colloids Surf., A* **1997,** 129-130, 67-74.

40. Ederth, T., *J. Phys. Chem. B* **2000,** 104, 9704-9712.

41. Ederth, T.; Claesson, P.; Liedberg, B., *Langmuir* **1998,** 14, 4782-4789.

42. Ron, H.; Rubinstein, I., *Langmuir* **1994,** 10, 4566-4573.

43. Ron, H.; Rubinstein, I., *J. Am. Chem. Soc.* **1998,** 120, 13444-13452.

44. Kane, V.; Mulvaney, P., *Langmuir* **1998,** 14, 3303-3311.

45. Giesbers, M.; Kleijin, J. M.; Stuart, M. A. C., *J. Colloid Interface Sci.* **2002,** 252, 138-148.

46. Hillier, A. C.; Kim, S.; Bard, A. J., *J. Phys. Chem.* **1996,** 100, 18808-18817.

47. Biggs, S.; Mulvaney, P., *J. Chem. Phys.* **1994,** 100, (11), 8501-8505.

48. Sondag-Huethorst, J. A. M.; Fokkink, L. G. J., *Langmuir* **1992,** 8, 2560-2566.

49. Karpovich, D. S.; Blanchard, G. J., *Langmuir* **1994,** 10, 3315-3322.

50. Cleveland, J. P.; Manne, S.; Bocek, D.; Hansma, P. K., *Rev. Sci. Instrum.* **1993,** 64, (2), 403-405.

51. Ohshima, H.; Healy, T. W.; White, L. R., *J. Colloid Interface Sci.* **1982,** 89, 484-493.

52. Israelachvili, J. N., *Proc. R. Soc. London, Ser. A* **1972,** 331, 39-55.

53. Oss, C. J. v., *Interfacial Forces in Aqueous Media*. 2 ed.; CRC Press: 2006.

54. Fowkes, F. M., *Ind. Eng. Chem.* **1964,** 56, (12), 40-52.

55. Thelen, E., *J. Phys. Chem.* **1967,** 71, (6), 1946-1948.

56. Biggs, S.; Mulvaney, P.; Zukoski, C. F.; Grieser, F., *J. Am. Chem. Soc.* **1994,** 116, (20), 9150-9157.

57. Ducker, W. A.; Senden, T. J., *Langmuir* **1992,** 8, 1831-1836.

58. Larson, I.; Chan, D. Y. C.; Drummond, C. J.; Grieser, F., *Langmuir* **1997,** 13, 2429-2431.

59. Wall, J. F.; Grieser, F.; Zukoski, C. F., *J. Chem. Soc., Faraday Trans.* **1997,** 93, (22), 4017-4020.

60. Dagastine, R. R.; Grieser, F., *Langmuir* **2004,** 20, 6742-6747.

61. Considine, R. F.; Drummond, C. J., *langmuir* **2001,** 17, 7777-7783.

62. Bhattacharjee, S.; Ko, C.-H.; Elimelech, M., *Langmuir* **1998,** 14, 3365-3375.

63. Parker, J. L.; Claesson, P. M., *Langmuir* **1994,** 10, 635-639.

64. Parker, J. L.; Claesson, P. M.; Wang, J.-H.; Yasuda, H. K., *Langmuir* **1994,** 10, 2766-2773.

65. Claesson, P. M.; Blom, C. E.; Herder, P. C.; Ninham, B. W., *J. Colloid Interface Sci.* **1986,** 114, (1), 234-242.

66. Lin, Q.; Meyer, E. E.; Tadmor, M.; Israelachvili, J. N.; Kuhl, T. L., *Langmuir* **2005,** 21, 251-255.

67. Christenson, H. K.; Fang, J.; Ninham, B. W.; Parker, J. L., *J. Phys. Chem.* **1990,** 94, 8004-8006.

68. Hato, M., *J. Phys. Chem.* **1996,** 100, 18530-18538.

69. Ishida, N.; Sakamoto, M.; Miyahara, M.; Higashitani, K., *Langmuir* **2000,** 16, (13), 5681-5687.

70. Mielczarski, J. A.; Yoon, R.-H., *J. Phys. Chem.* **1989,** 93, 2034-2038.

71. Mielczarski, J. A.; Yoon, R.-H. In Proceedings of the Engineering Foundation Conference, Palm Coast, Florida, January 10-15, 1989; Moudgil, B. M.; Scheiner, B. J., Eds. United Engineering Trustees, Inc., New York: Palm Coast, Florida, 1989; pp 619-630.

72. Mielczarski, J. A.; Yoon, R.-H., *J. Colloid Interface Sci.* **1989,** 131, (2), 423-432.

73. Mielczarski, J. A.; Yoon, R.-H., *Langmuir* **1991,** 7, 101-106.

74. Leja, J., Surface Chemistry of Froth Flotation. In Plenum Press: Vancouver, 1982; p 510.

75. Walz, J. Y.; Suresh, L.; Piech, M., *J. Nanopart. Res.* **1999,** 1, 99-113.

76. Zhang, J.; Yoon, R.-H.; Eriksson, J. C., *Colloids Surf., A* **2007,** 300, 335-345.

77. Ulman, A., *Chem. Rev.* **1996,** 96, (4), 1533-1554.

78. Fa, K.; Nguyen, A. V.; Miller, J. D., *J. Phys. Chem.* **2005,** 109, (27), 13112-13118.

79. Forsman, J.; Jonsson, B.; Woodward, C. E., *J. Phys. Chem.* **1996,** 100, (36), 15005-15010.

80. Sakurai, M.; Tamagawa, H.; Ariga, K.; Kunitake, T.; Inoue, Y., *Chem. Phys. Lett.* **1998,** 289, 567-571.

81. Ninham, B. W., *Prog. Colloid Polym. Sci.* **2006,** 133, 65-73.

82. Maeda, N.; Rosenberg, K. J.; Israelachvili, J. N.; Pashley, R. M., *Langmuir* **2004,** 20, 3129-3137.

83. Pashley, R. M., *J. Phys. Chem. B* **2003,** 107, 1714-1720.

84. Francis, M. J.; Gulati, N.; Pashley, R. M., *J. Colloid Interface Sci.* **2006,** 299, 673-677.

85. Francis, M. J.; Pashley, R. M., *Colloids Surf., A* **2006,** 287, 36-43.

86. Tsao, Y.-H.; Evans, D. F.; Wennerstrom, H., *Langmuir* **1993,** 9, 779-785.

87. Claesson, P. M.; Herder, P. C.; Blom, C. E.; Ninham, B. W., *J. Colloid Interface Sci.* **1987,** 118, 68-79.

Chapter 3

Surface Force Measurements between Gold Surfaces Hydrophobized with Alkanethiols of Different Chain Lengths

3.1 Abstract

An atomic force microscope (AFM) was used to measure the surface forces between two macroscopic gold surfaces. A microsphere of gold and a gold-coated glass plate were immersed in thiol-in-ethanol (1×10^{-2} mM or 1 mM) solutions to hydrophobize the surfaces. The degree of hydrophobization was controlled by varying immersion time and using thiols of different chain lengths. In the present work, alkanethiols, such as ethanethiol (C_2SH), 1-butanethiol (C_4SH), 1-dodecanethiol ($C_{12}SH$) and 1-hexadecanethiol ($C_{16}SH$) were used. The equilibrium water contact angle obtained with C_2SH was 67º. The contact angles were greater than 90º on gold surfaces coated with the other thiols of longer chain lengths. Regardless of whether the contact angle was larger than 90º or not, the force curves obtained were smooth and showed no steps, and the measured forces were substantially larger and longer-ranged than the van der Waals force. When the thiol-coated surfaces were exposed for prolonged periods of times in the atmospheric air or contaminated, discontinuities or steps on the force curves were observed. The maximum equilibrium water contact angles obtained with C_4SH, $C_{12}SH$ and $C_{16}SH$ were 94º, 105º and 105º, respectively, and the strongest hydrophobic attractions were measured on surfaces exhibiting maximum contact angles. The strongest hydrophobic force measured on C_4SH-coated gold was weaker than those measured on $C_{12}SH$- and $C_{16}SH$-coated gold surfaces. The latter two surfaces were indistinguishable

with respect to the measured strongest hydrophobic forces.

It was found that the strengths and ranges of the hydrophobic attractive forces decreased in the presence of NaCl electrolyte and a cationic surfactant C_{12}TACl. The decay lengths of the hydrophobic forces were not equal to one half of the Debye lengths, contrary to the predictions from the electrostatic models. The results obtained in the present work suggest that the long-range attractions measured may represent true hydrophobic forces originating from the structural change of water in the vicinity of hydrophobic surfaces. Solvable foreign species added to the system, *e.g.*, cationic surfactant C_{12}TACl and NaCl, break the hydrogen bond network, and reduce the hydrophobic forces.

3.2 Introduction

The classic Derjaguin-Landau-Verwey-Overbeek (DLVO) theory, which combines the effects of the van der Waals attraction and electrostatic double layer repulsion, has been successfully applied to many colloidal systems. However, some colloidal systems comprising hydrophobic particles[1, 2] or oil droplets[3] exhibit additional attraction which is much stronger than the van der Waals force considered in DLVO theory. Early experiments carried out in 1972 by Blake and Kitchener[4] on the stability of wetting films sandwiched between an air bubble and hydrophobic silica indicated the existence of a long-range hydrophobic attraction force. In 1982, the hydrophobic force was first measured directly by Israelachvili and Pashley[5] on two mica surfaces hydrophobized by the *in-situ* adsorption of hexadecyltrimethylammonium bromide (CTAB) in aqueous solutions using a surface force apparatus (SFA). The pioneering works of Blake and Kitchener, and Israelachvili and Pashley

had established that in addition to the traditional DLVO forces, a long-range attractive force called “hydrophobic force” operates between hydrophobic surfaces in aqueous media. The hydrophobic force plays an important role in many scientific and technological fields, such as surface and colloid science, biology, and minerals processing. In the field of minerals processing, recognition of the long-range hydrophobic attraction force is important in the modeling the coagulation of hydrophobic particles[1, 2] and the process of bubble-particle attachment in flotation.[6-8]

The significant role of the hydrophobic force in many scientific and technological fields has led to a great deal of study. During the past two decades or more, several instruments, *e.g.*, surface force apparatus (SFA), measurement and analysis of surface interaction force (MASIF), and atomic force microscope (AFM), have been used for the direct measurement of the hydrophobic force. Numerous reports published document the existence of this long-range attractive force. Different research groups used different types of hydrophobic surfaces and a range of hydrophobization methods. However, the results were far from being consistent. The magnitudes and ranges of the forces varied from one experiment to another. Also the origin of the long-range attractive forces has been debated without consensus. Various theoretical models have been brought forward to explain the experimental results. Eriksson *et al*.[9] attributed the long-range attractive force to the enhanced hydrogen bonding of the water molecules confined between two hydrophobic surfaces. However, computer simulations[10-13] showed that the change in the structure of the water near the hydrophobic surface only extend the distance of several molecular diameters, while many experimentalist reported that the force can be measured at the separation distances of up to 80

nm. Other investigators suggested that the long-range hydrophobic attraction is due to the correlations between the charged patches[14, 15] formed as a result of surfactant adsorption, between mobile surface groups[16] when the two surfaces approach to each other, or between large dipoles associated with the patches of adsorbed surfactants.[17, 18] However, some of these models can not be reconciled with all the experimental data. In particular, Miklavic *et al*.[14] predicted that the attraction due to correlation should be exponentially decaying with decay lengths equal to one half the Debye lengths upon increasing the electrolyte concentration. Although there were some experimental results supporting this theory, more recent experimental data show that the force is independent of ionic strength.

More recently, many investigators proposed that the non-DLVO attractive forces observed from the force measurements are caused by bridging submicroscopic bubbles preexisting on the hydrophobic surfaces[19-23] or cavities.[24-29] The most frequently quoted evidence for this was the discontinuities (or steps) observed in force *versus* distance curves, each step representing the coalescence of nanobubbles.[19] When two bubbles coalesce, gas bridges (or cavities) are formed between two surfaces, which give rise to capillary forces. This theory seems appealing, because the existence of the bubbles solves the range problem, and the range of the forces depends on the size of the bubbles involved. A primary setback for this theory is that very small air bubbles in bulk water are short-lived.[30] In addition, experiments showed that long-range hydrophobic attractions were observed for hydrophobic surfaces on which there were no signs of bubbles.[31, 32] Stevens *et al*.[33] found that the range and strength of the attraction between two hydrophobic amorphous fluoropolymer surfaces in deaerated water was significantly greater than that of the van der Waals attraction. Meyers *et*

al.[34] conducted SFA force measurements between mica surfaces coated by a Langmuir-Blodgett (LB)-deposited hydrophobic monolayer of DODAB both in the presence and absence of dissolved gases. In the presence of dissolved gases, they observed long-range attractive forces, while in degassed solutions only short-range attraction forces (under ~ 250 Å) were observed. They concluded, therefore, that 'true' hydrophobic force exists even in degassed solutions.

Ederth and Liedberg[35] and Ederth[23] have conducted direct force measurement between thiolated-gold surfaces in water, water/ethanol mixtures by MASIF. The wettability of the surfaces was controlled by changing the mole ratios of 1-hexadecanethiol ($C_{16}SH$) and 16-hydroxyhexanedecanethiol ($HOC_{16}SH$), and by changing the mixing ratios between water and ethanol. They showed that when the contact angle of the thiolated-gold surface was larger than 90º, long-range attractions with step-like profiles which were observed due to the coalescences of microscopic air bubbles on the surfaces. When the contact angle was less than 90º, the attraction was actually the same as the van der Waals attraction. In the present work, an AFM force microscope was used to measure the surface forces between two macroscopic gold surfaces in water, aqueous NaCl electrolytes and cationic surfactant dodecyltrimethylammonium chloride ($C_{12}TACl$) solutions. We also chose the self-assembled monolayers of thiols on gold as interacting surfaces, because they are robust, well characterized and easy to prepare. Spheres of gold and gold-coated glass plates were immersed in quiescent thiol-in-ethanol solutions to hydrophobize the gold surfaces. The degree of hydrophobization was controlled by varying immersion times or using thiols of different chain lengths. The results are used to test existing theoretical models and discuss the

possible origins of the long-range hydrophobic force.

3.3 Materials and Methods

3.3.1 Materials

A Millipore direct-Q 3 ultrapure (Millipore, MA) water system was purchased and used to obtain deionized water with a resistivity of 18.2 MΩ/cm at 25ºC. Alkanethiol such as ethanethiol (C_2SH, 98%, TCI America), 1-butanethiol (C_4SH, 99%, Aldrich), 1-dodecanethiol ($C_{12}SH$, 98%, Aldrich) and 1-hexadecanethiol ($C_{16}SH$, 97%, TCI America) dissolved in 200 proof ethanol (AAPER alcohol) were used to hydrophobize the gold surfaces. They were used without further purification. Sulfuric acid (98%) from Fisher Scientific and hydrogen peroxide (H_2O_2, 29−32% w/w) from Alfa Aesar were used as received to clean gold plates. Sodium Chloride (99.999%, Sigma-Aldrich) was roasted in air at 560ºC to decompose organic impurities and dissolved in pure water. Dodecyltrimethylammonium chloride ($C_{12}TACl$, 99%) was purchased from Acros Organics Co. Gold wire (0.0127 mm dia, 99.9%, Alfa Aesar) was used to make gold microspheres.

Gold microspheres and gold-coated glass plate were used for AFM force measurements. The gold-coated glass plates were produced by depositing pure gold on a clean glass slide using a vacuum evaporator. A 50 Å chromium layer was deposited first on the glass prior to coating it with a thin-layer (500 Å) of pure gold. The chromium coating was necessary to achieve strong bonding between gold and substrate. The AFM image showed that the flat gold surfaces were smooth, with maximum peak-to-valley distance of 3.3 nm. Gold spheres with appropriate diameters were produced according to the procedure

developed by Raiteri *et al.*[36] The two ends of a thin gold wire were connected to a power supply (120 V, AC) and briefly short circuited in a glass tray as shown in Figure 3.1. A small cloud of gold particles were produced in the spark. In this manner, gold spheres with a wide size range were produced. The spheres with radius of 4.5~10 μm were chosen for the present experiments.

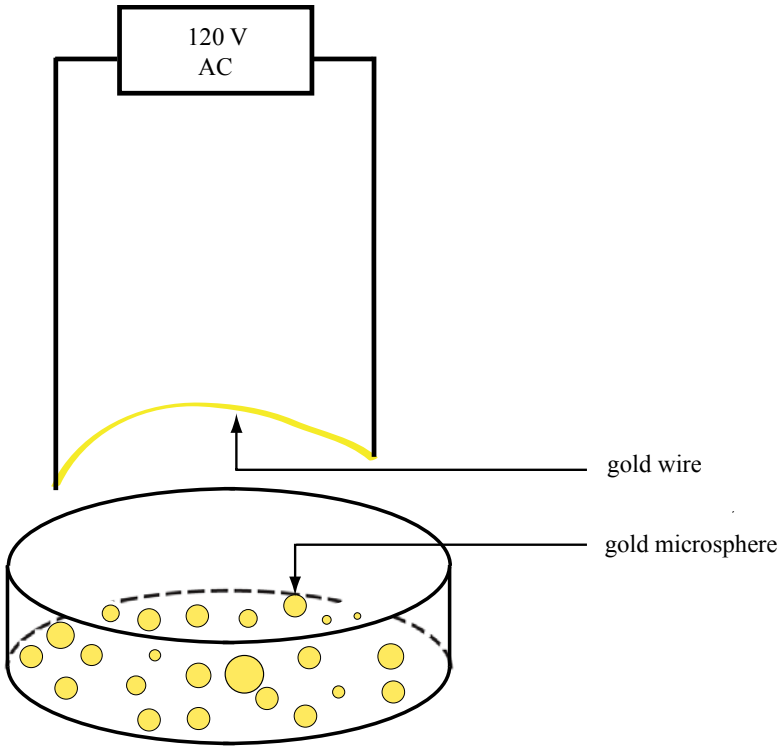

Figure 3.1. Schematic illustration of the method for making gold microspheres.

3.3.2 Hydrophobizing Gold Surfaces

The cleanliness of the gold surface is critically important in the process of self-assembly of thiol on gold.[32, 37-40] To ensure the high-quality thiol monolayers on gold, gold surfaces must be cleaned thoroughly prior to soaking them in thiol-in-ethanol solutions. In the present work, the gold plate surfaces were cleaned first by immersing them in a boiling H_2SO_4/H_2O_2 (2:1 by volume) at 120ºC for 20 minutes, and then rinsed in ultra pure water for

1 minute, followed by ethanol wash for 2 minutes to remove the oxides produced in the piranha solution. After cleaning, the gold plates were immediately exposed to quiescent thiol solutions for hydrophobization in a fume hood. For the case of gold spheres, cleaning procedure was performed after they had been glued onto the tips of AFM cantilever springs. To prevent gold spheres from being washed away by strong acid solution, before hydrophobization, each gold sphere was flushed with ethanol, irradiated by a UV lamp (λ = 254 nm) for 2 hours to remove possible organic contaminants, and then rinsed with ethanol again.

The cleaned gold plates and spheres were hydrophobized by soaking them in thiol-in-ethanol solutions at room temperature *via* chemical reaction. To ensure the accuracy of the force measurement, for every set of experiment, only the fresh thiol surfactants were used to prepare thiol-in-ethanol solutions, because the thiol surfactant in ethanol will degrade with time. After hydrophobization, the gold substrates were washed with ethanol and then dried in a nitrogen gas stream. For a given force measurement, a set of gold plate and sphere on cantilever was immersed in a thiol solution for a desired period of time, so that the hydorphobicity of the two microscopic surfaces would be the same.

3.3.3 Contact Angle Measurement

Equilibrium water contact angles on the hydrophobized gold plates were measured with the sessile drop method using a goniometer (Ramé-Hart, Inc) under ambient conditions. Droplets of pure water of 1−2 mm diameter were placed on the surface of a horizontally placed thiolated-gold plate using a Norm-Ject syringe. The angles were measured on each

side of a water droplet. The measurements were conducted using a total of five droplets placed on different locations of a gold surface, and the results were averaged. For the contact angles of thiol-coated gold in NaCl solutions, aqueous NaCl solution with different concentrations drops were employed instead of pure water as the contacting liquid.

3.3.4 AFM Surface Force Measurement

A Nanoscope Ⅲ (Digital Instruments, CA) multi-mode atomic force microscope (AFM) equipped with a standard fluid liquid cell and a piezoelectric scanner "E" was used for the force measurements. The surface interactions between a gold-coated glass and a gold microsphere in water medium were measured at room temperature (~ 22ºC) using the colloidal probe technique.[41] The separation distance (H) between the spherical probe (gold sphere) and the flat substrate (gold-coated glass) was determined by monitoring the deflection of the cantilever on which the sphere was attached. Triangular silicon nitride (NP-20, Veeco probes) cantilevers with a nominal spring constant (k) of 0.58 N/m were used in this study, and their spring constants were determined using the Cleveland method.[42] For each experiment, a gold sphere was glued onto the end of a cantilever with EPON-1004 resin (Shell Chemical Co.) using a homemade three-dimensional micromanipulator under an optical microscope (Olympus BH-2). The fluid cell made of glass was cleaned in pure water in an ultrasonic cleaner and blow-dried with nitrogen gas before each experiment. The force measurements were conducted immediately after the thiol monolayers were formed on gold substrates.

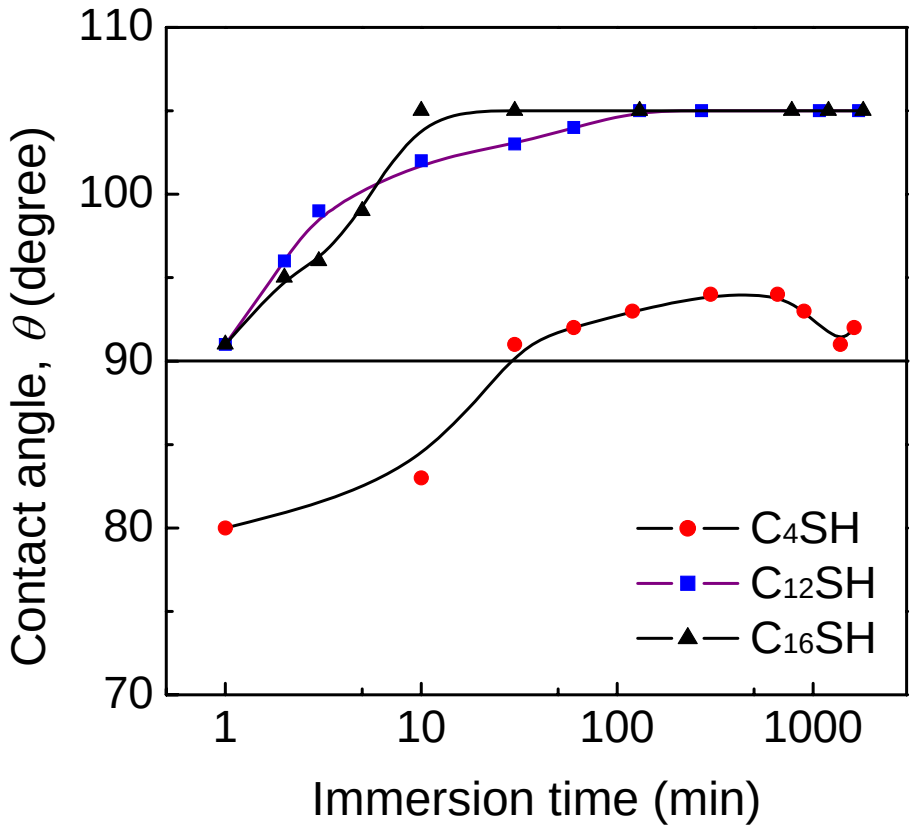

Figure 3.2. Changes in the equilibrium water contact angles (θ) on gold plates as functions of immersion time in 1×10^{-2} mM C_4SH-, $C_{12}SH$-, and $C_{16}SH$-in-ethanol solutions.

3.4 Results

3.4.1 Contact Angle Measurement

Samples of gold spheres and plates were hydrophobized by immersing them in 1×10^{-2} mM $C_{16}SH$-in-ethanol, $C_{12}SH$-in-ethanol or C_4SH-in-ethanol solutions for different periods of times. Figure 3.2 shows the water contact angles measured on these samples as functions of immersion time. As shown, the contact angles reached a maximum values of $\theta =$ 105º with both $C_{16}SH$- and $C_{12}SH$-coated gold surfaces. The immersion time of 10 minutes

and 2 hours were employed for $C_{16}SH$ and $C_{12}SH$, respectively. With the C_4SH-coated gold surfaces, the maximum contact angle was θ = 94º. The contact time employed in this case was 5 hours. It appears that the contact angles reached a maximum more quickly as the hydrocarbon chain length was increased, which is in line with the studies by Bain *et al.*[43]. These investigators found that the kinetics of adsorption is faster for longer chain thiols. This finding was attributed to the fact that van der Waals interaction between the hydrocarbon chains of alkanethiol increased with chain length.[44] With the C-12 and C-16 thiols only 1 minute dipping time was sufficient to obtain contact angles above 90º.

3.4.2 Force Measurements in Water

Figure 3.3 shows the surface forces (F/R) measured between $C_{12}SH$-coated gold microspheres (with radius R) and gold-coated glass plates in water as functions of the closest distance (H) separating the two macroscopic surfaces. The gold substrates were immersed in 1×10^{-2} mM $C_{12}SH$-in-ethanol solutions for different period of time. The trend is the same as observed on $C_{16}SH$,[32] that is, the attractive force increases with immersion time, and then decreases. All the forces measured were stronger and longer-ranged than the van der Waals force. The van der Waals force curve shown in Figure 3.3 was plotted based on the Hamaker constant ($A_{131} = 1.2 \times 10^{-20}$ J) determined experimentally.[32] At the immersion time of 1 minute, the force was only slightly stronger than the van der Waals force. However, the attractive force was detected at a separation distance $H \approx 30$ nm. At the immersion time of 30 minutes, the strength and range of the attraction increased with the attractive forces being detected at $H > 100$ nm. At the immersion time of 60 minutes, the strength of the force

further increased. The strongest attraction was obtained at the 120 minutes immersion time. As the immersion time was further increased to 360 minutes, both the strength and the range of the attraction were reduced.

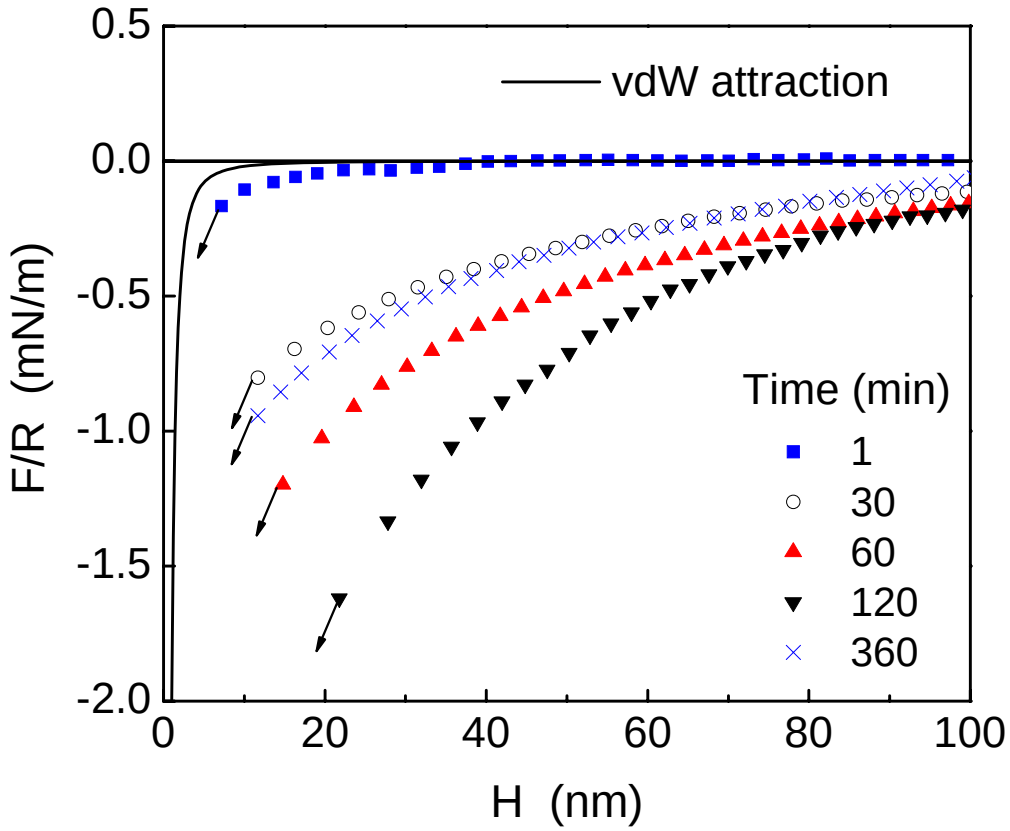

Figure 3.3. Effects of the immersion times of gold substrates in a 1×10^{-2} mM $C_{12}SH$-in-ethanol solution on the AFM forces measured in pure water. The solid line represents the non-retarded van der Waals force acting between two gold surfaces in water.

As shown in Figure 3.2, the equilibrium water contact angles (θ) on $C_{16}SH$-coated gold were 91º, 99º, 105º, 105º, 105º and 105º as the immersion times were 1, 5, 10, 20, 60 and 240 minutes. On $C_{12}SH$-coated gold, they were 91º, 103º, 104º, 105º and 105º at the immersion times of 1, 30, 60, 120 and 360 minutes, respectively. In view of the force

measurements conducted with $C_{12}SH$-coated surfaces, from immersion time t = 1 to 120 minutes, the attraction became gradually stronger with contact angle; beyond t = 120 minutes, the attraction became weaker, while the contact angle was constant. The vanished attractive forces on $C_{16}SH$- and $C_{12}SH$-coated gold prepared with longer immersion time were restored to the original full strengths after rinsing the hydrophobic thiol-coated surfaces in the liquid cell with ether. Based on this observation, it is supposed that the hydrophobic force response is reduced due to trapping of extra thiol molecules with the –SH groups turned outward to water, thus forming a kind of adlayer. This physisorbed thiol layer could be removed by means of rinsing with ether.

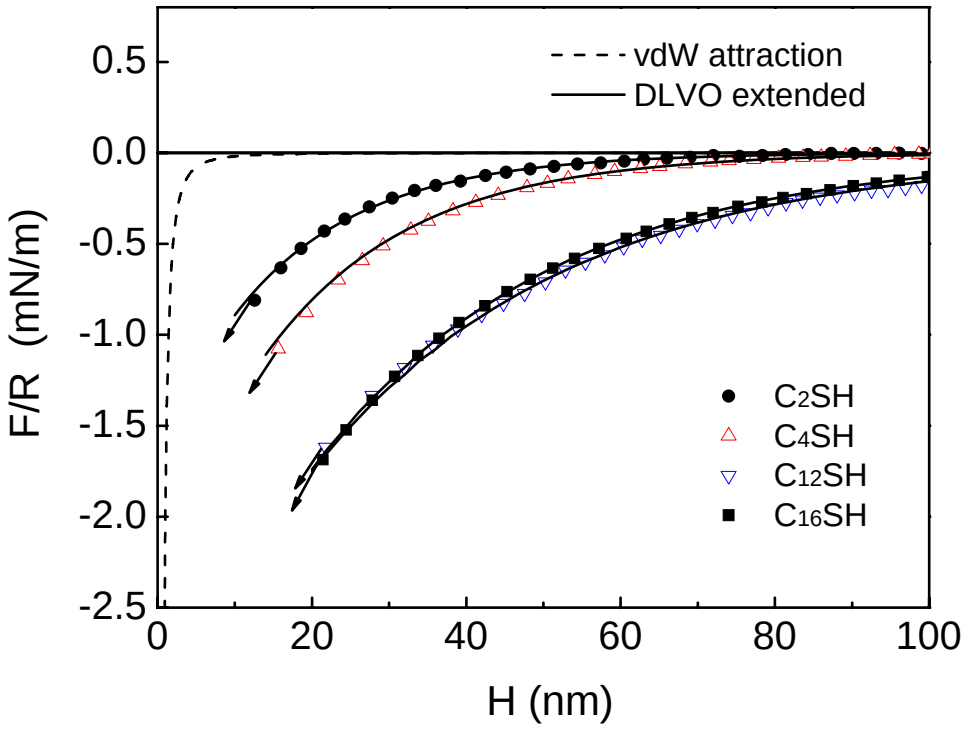

Figure 3.4. Surface forces (*F/R*) *versus* separation distances (*H*) between hydrophobized gold surfaces prepared using alkanethiols with different chain lengths. The solid lines represent the fittings of surface force data points using single-exponential laws (Equations 3.1). The dashed line represents the van der Waals force.

Figure 3.4 shows the surface force measurements performed in water on gold surfaces hydrophobized by self-assembly of alkanethiols with different chain lengths. The strongest attractive force curves measured which were shown in Figure 3.3 on $C_{12}SH$-coated gold surfaces and on $C_{16}SH$-coated gold[32] are re-drawn in Figure 3.4. Also included in Figure 3.4 are surface forces data in water on C_4SH- and C_2SH-coated gold surfaces. According to the contact angle measurements on C_4SH-coated gold (Figure 3.2), the contact angle approaches the maximum value ($\theta = 94^o$) after 5 hours of immersion time. In Figure 3.4, the surface force between C_4SH-coated gold surfaces in water was shown when the C_4SH coatings were prepared with an immersion time of 5 hours. The attractive force measured on surfaces prepared under this condition should be the strongest according to the relation between contact angle and hydrophobic force (Figure 3.3). The strongest hydrophobic force on C_4SH-coated gold is measurable at the separation distance $H \approx 70$ nm. The surface force between C_2SH-coated gold surfaces in water was measured when the C_2SH coatings were prepared by immersing a gold microsphere and a gold coated-glass plate in 1 mM solution for an immersion time of 6 hours. The water contact angle measured on C_2SH-coated gold surface prepared under this condition was $\theta = 67^o$, and the measured force between these surfaces was purely attractive within a separation distance $H \approx 60$ nm. All the force curves shown in Figure 3.3 and 3.4 are smooth, without showing steps or discontinuities, indicating that the hydrophobic surfaces were relatively free of contaminations or air bubbles. All the attractions are much stronger and longer-ranged than the non-retarded van der Waals force.

All of the surface force curves in Figure 3.4 were fitted to a single-exponential force law, that is:

$$\frac{F}{R} = C\exp\left(-\frac{H}{D}\right) \qquad (3.1)$$

where *F/R* denotes the normalized surface force, *R* is the radius of the gold sphere, *C* is a constant and *D* is the decay length. *H* is the closest separation distance between two approaching surfaces. Since the hydrophobic force is overwhelmingly larger compared to the double layer repulsive force on thiol-coated gold,[32] we assume the surfaces of the hydrophobized gold are neutral, thus only the hydrophobic and van der Waals forces are considered in the fittings. The Hamaker constant of $A_{131} = 1.2 \times 10^{-20}$ J[32] as determined by measuring the interaction between two bare gold surface in water and salt solutions was used in this study. The fitting was carried out after subtracting the forces due to van der Waals interaction from the measured forces, and the values for *C* and *D* were derived and are shown in Table 3.1. As shown, the decay length *D* and *C* values of the attractive force depend on both the chain length and the water contact angle. The decay length (*D* = 16.5 to 33 nm) and *C* value (from 1.6 to 3.2 mN/m) increase with chain length (from *n* = 2 to 12) and contact angle (from θ = 67º to 105º). For the thiols with chain length of 12 and 16, the contact angles (θ = 105º) are the same, the attractive forces appear to coincident with each other, and the decay lengths (*D* = 31 *versus* 33 nm) and *C* values (3.3 *versus* 3.2 mN/m) are similar.

Table 3.1. The Parameters Obtained by Fitting the Surface Data between Gold Surfaces Coated by Alkanethiols with Different Chain Lengths in Pure Water with Extended DLVO Theory

	θ (degree)	*C* (mN/m)	*D* (nm)
C_2SH	67	-1.6	16.5
C_4SH	94	-2.3	19
$C_{12}SH$	105	-3.2	33
$C_{16}SH$	105	-3.3	31

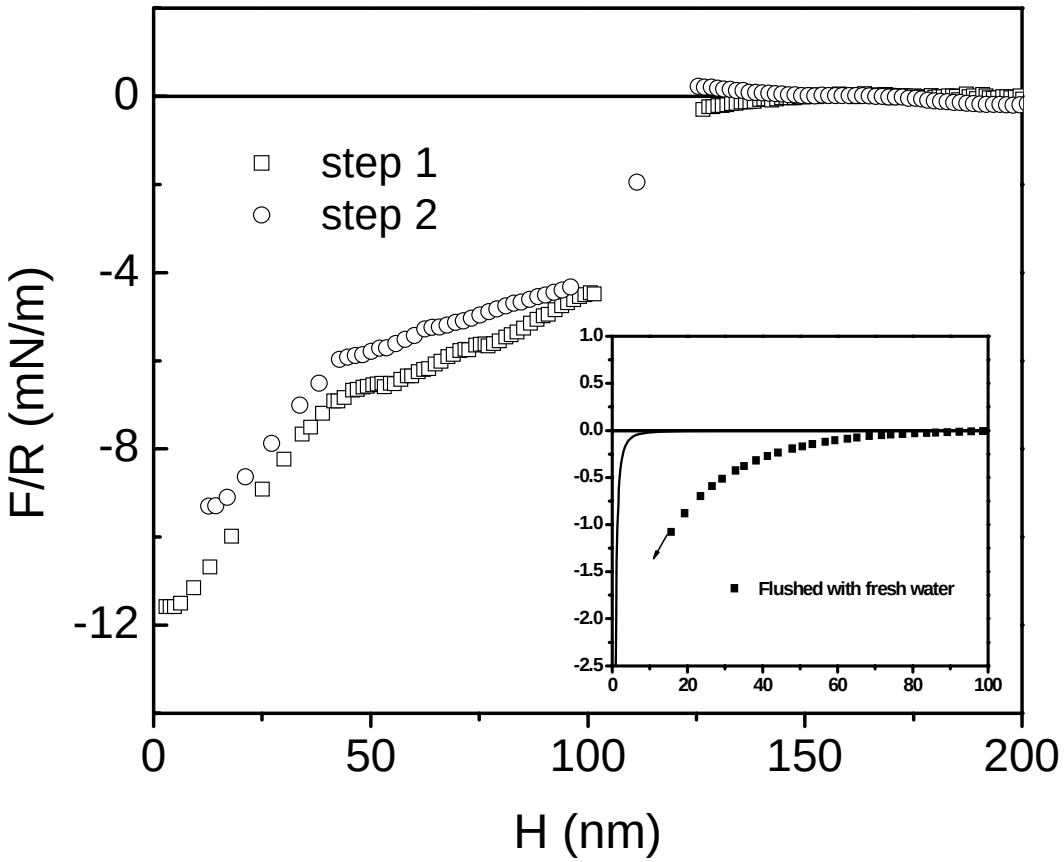

Figure 3.5. Normalized forces (*F/R*) between gold surfaces which were hydrophobized in a 1×10^{-2} mM C_4SH-in-ethanol solution for 6 hours. The step-like force curves were obtained under the condition that C_4SH-coated gold plate was exposed in air for elongated time prior to the commencement of force measurement. The inset represents the force obtained on the same surfaces flushed with fresh water. The contamination of hydrophobized surfaces or the air bubbles could give rise to the steps or discontinuities shown on the force curves.

Figure 3.5 shows the results of the AFM force measurements conducted between two C_4SH-coated gold surfaces in water. The C_4SH coatings on gold were prepared in a 1×10^{-2} mM C_4SH-in-ethanol solution for 5 hours. The step-like force curves were obtained under the condition that C_4SH-hydrophobized gold surfaces were exposed in air for a prolonged period of time prior to the commencement of the force measurement. After the AFM liquid cell and the gold surfaces were flushed with fresh water, the extremely large attractions with steps disappeared, and a much smaller, smooth force curve was obtained. The steps were attributed

to the bridging of contaminating air bubble from the air which can easily form on the C_4SH-coated hydrophobic surfaces during the "drying" coating preparation process.

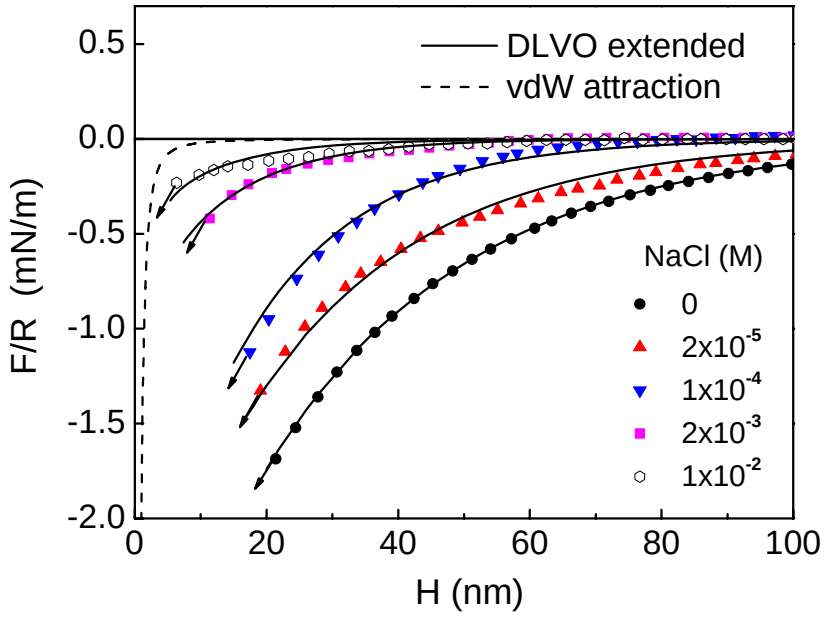

Figure 3.6. Effect of NaCl on the forces measured between gold surfaces hydrophobized in a 1×10^{-2} mM $C_{16}SH$-in-ethanol solution for 10 minutes. The solid lines represent the fittings of surface force data points using single-exponential laws (Equations 3.1). The dashed line represents the van der Waals force.

3.4.3 Force Measurements in NaCl Aqueous Solutions

Figure 3.6 and 3.7 show the effect of NaCl concentration on the hydrophobic forces measured on $C_{16}SH$- and $C_{12}SH$-coated gold surfaces, respectively. The $C_{16}SH$-coated surfaces were prepared in a 1×10^{-2} mM $C_{16}SH$-in-ethanol solution for 10 minutes, and the $C_{12}SH$-coated surfaces were prepared in a 1×10^{-2} mM $C_{12}SH$-in-ethanol solution for 2 hours. The forces measured on $C_{16}SH$- and $C_{12}SH$-coated gold in pure water were the strongest attractions and of the same magnitude and range. On both the $C_{16}SH$- and $C_{12}SH$-coated gold surfaces, the attractive forces decreased in range and magnitude as the NaCl concentration

was increased from 0 to 1 × 10^{-2} M. As shown in Figure 3.6 and 3.7, the attractive forces measured in the most concentrated NaCl solution (1 × 10^{-2} M) were still stronger and longer-ranged than the van der Waals force. After finishing the experiments with NaCl, the AFM liquid cell was flushed with fresh water in order to remove the NaCl electrolyte, and the strong attractive forces in water reappeared. It is demonstrated that the $C_{16}SH$ and $C_{12}SH$ monolayer coatings on gold were very stable, and the surface properties of these chemisorbed surfactant layers were not changed upon increasing concentration of NaCl. Sessile drop contact angle measurement using NaCl aqueous drops indicates that the contact angle on the thiol surfaces did not change with the changed concentration of NaCl. It is suggested that the surfaces did not become less hydrophobic in NaCl solutions.

In all cases, the attractive forces decreased exponentially as two surfaces approached

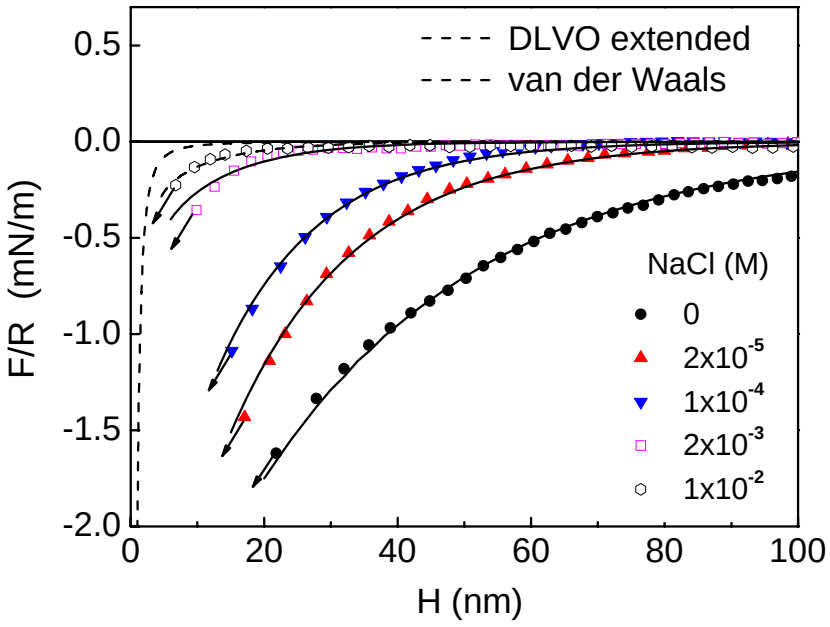

Figure 3.7. Effect of NaCl on the forces measured between gold surfaces hydrophobized in a 1 × 10^{-2} mM $C_{12}SH$-in-ethanol solution for 2 hours. The solid lines represent the fittings of surface force data points using single-exponential laws (Equations 3.1). The dashed line represents the van der Waals force.

each other. The measured force curves were fitted to the exponential function (Equation 3.1). The decay length D and constant C were derived and are shown in Table 3.2. Also shown in the table are the Debye lengths (κ^{-1}) calculated according to the NaCl concentration used. The values of C and D obtained from the force curves measured on $C_{16}SH$- and $C_{12}SH$-coated gold surfaces show the same trend upon adding the NaCl although the values are not exactly the same. With the concentration of NaCl increasing from 0 to 10 mM, the Debye length decreased from 134.2 to 3 nm. At the same time, both C values (from 3.3 to 0.4 nm) and D values (from 31 to 12 nm) obtained on $C_{16}SH$-coated gold decrease with the increasing concentration of NaCl. On $C_{12}SH$-coated gold, the C values decrease from 3.2 to 0.3 nm, the D values decrease from 33 to 10 nm.

Table 3.2. Effects of NaCl on Debye Lengths (κ^{-1}) and Decay Lengths (D) between $C_{12}SH$-coated Gold Surfaces and $C_{16}SH$-coated Gold Surfaces

		$C_{12}SH$		$C_{16}SH$	
NaCl (mM)	κ^{-1} (nm)	C (mN/m)	D (nm)	C (mN/m)	D (nm)
0	134.2	-3.2	33	-3.3	31
0.02	67.1	-3.3	19	-2.8	26
0.1	30	-2.8	15	-2.7	18
2	6.7	-0.6	11	-0.9	13
10	3	-0.3	10	-0.4	12

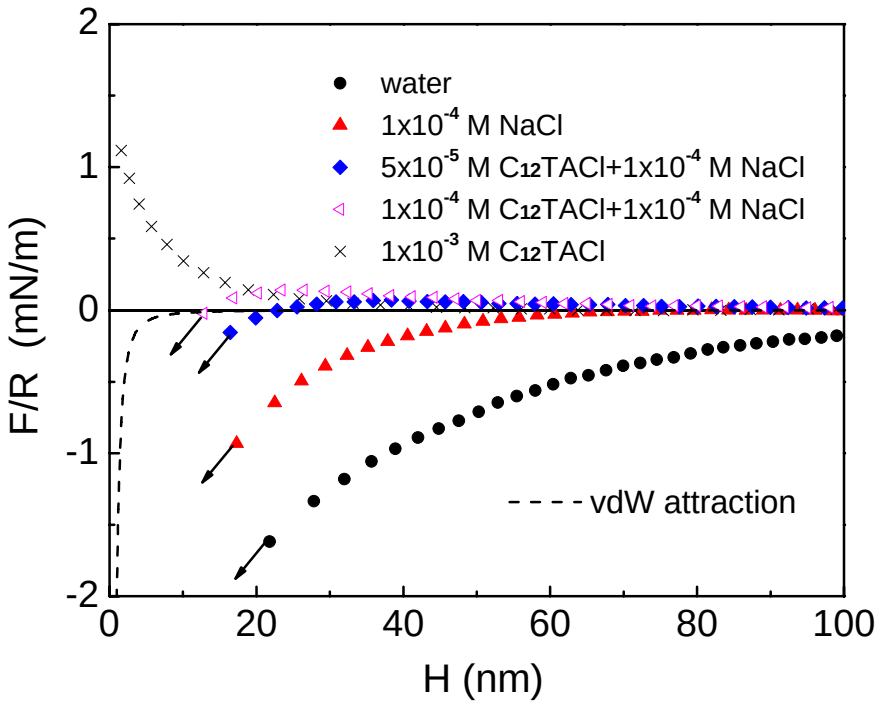

Figure 3.8. The AFM force curves obtained on $C_{12}SH$-coated gold surfaces immersed in NaCl, $C_{12}TACl$ solution, and in NaCl/$C_{12}TACl$ mixtures. The dashed line represents the van der Waals force.

3.4.4 Force Measurements in the Presence of $C_{12}TACl$ Surfactant

Figure 3.8 shows the surface forces measured between hydrophobic $C_{12}SH$-coated gold surfaces in NaCl, $C_{12}TACl$, and $C_{12}TACl$/NaCl aqueous solutions as functions of separation distance. The arrows indicate the jump distances. A gold microsphere and a gold-coated glass slide were hydrophobized in a 1×10^{-2} mM $C_{12}SH$-in-ethanol solution for 2 hours. Using this preparing procedure, the attractive force was the strongest in pure water as indicated in Figure 3.3. In the presence of 5×10^{-5} M $C_{12}TACl$ and 1×10^{-4} M NaCl, the force became repulsive at long range and became attractive at short range. The attractive force was

dramatically reduced to a much shorter-ranged attraction with a jump distance $H \approx 18$ nm, and a long-ranged double layer repulsive force operating at separation distance $H > 40$ nm appeared, most probably due to the inverse orientation of the $C_{12}TA^+$ ions.[45] At 1×10^{-4} M $C_{12}TACl$ and 1×10^{-4} M NaCl, the attractive force became progressively weaker and the surfaces jumped into contact from a distance $H \approx 16$ nm; and the double layer repulsive force became even stronger. The attractive force disappeared and the electrostatic repulsion dominated at all separation distances as the concentration of $C_{12}TACl$ increased to 1×10^{-3} M.

3.5 Discussion

3.5.1 The Existence of the Long-Range Hydrophobic Force

Although the long-range hydrophobic force has been observed experimentally on different types of hydrophobic surfaces using different surface force measurement techniques, the existence of this strong attractive force is still questioned by many people. In an attempt to explain the long-range attractions of variable strengths and ranges reported so far with a single theory, Hato *et al*.[46] and Meyer *et al*.[34] suggested that the various long-range attractive forces measured consist of two components; one is the real hydrophobic force, of rather short range (< 20 nm), and the other is the long-range attraction (> 20 nm) which is rather dependent on surface preparation method than the hydrophobicity of the surfaces. Surface force measurements[19, 20, 23, 35, 47-50] and the surface images[21, 22, 51] showed that the long-range attractive force is caused by the bridging of nano or submicro air bubbles preexisting on the two hydrophobic surfaces. Air bubbles adsorb and nucleate at the defective sites on the

hydrophobic surface, and steps on the force curve signify the coalescence of two air bubbles. The range of the measured attractive force is determined by the size of the bubble.

Ederth *et al*.[23, 35] had conducted surface force measurements on thiol-coated gold surface with a MASIF instrument. The microscopic gold surfaces were hydrophobized in a 1 mM $C_{16}SH$-in-ethanol solution overnight, and the contact angles measured on them were all above 90º. They attributed the steps or discontinuities on the obtained force-separation curves to the bridging of the two air bubbles preexisting on the hydrophobic thiol-coated gold surfaces. When the contact angles on thiol-coated gold were below 90º, which were obtained by using ethanol/water mixtures as solvents or by employing bi-functional thiol with –OH group on the other end as the co-surfactant, they obtained only the van der Waals force. It was suggested, therefore, that when the surface contact angle was above 90º, there was a long-range attractive force not considered in classic DLVO theory acting between two hydrophobic surfaces, which in turn was caused by the bridging of two air bubbles. At $\theta < 90º$, only the van der Waals force was measured.

In the present study, the gold substrates were hydrophobized in dilute solutions (1×10^{-2} mM for C_4SH, $C_{12}SH$ and $C_{16}SH$) of thiol-in-ethanol for significantly shorter period of time (1 minute to several hours). Figure 3.3 and 3.4 shows that all the force curves obtained were smooth and the long-range surface forces measured were net attractive and stronger than van der Waals, regardless of weather the contact angles were above 90º or not. Figure 3.5 shows the results of the force measurements in the presence and absence of air bubbles. When the C_4SH hydrophobized gold surfaces were exposed in atmospheric air for a longer period time before the force measurement, preexisting bubbles were present on the surface,

which gave rise to capillary forces. The hydrophobic surfaces were dried completely when exposed in air for a long period of time. As the surfaces were immersed in water, the surfaces did not get wet completely, leaving air bubbles on the surfaces. In the absent of air bubbles, or when the air bubbles were flushed away by fresh water, a smooth curve was obtained instead of discontinued one, and the measured force was still much stronger than the van der Waals force.

The contact angles on the C_4SH-, $C_{12}SH$- and $C_{16}SH$-coated gold surfaces prepared in this study were all above 90º, meaning that large-scale cavities may be formed due to the metastability of the intervening fluid between the hydrophobic surfaces.[24-29] The cavitation can occur when the surface tension (γ_{12}) of thiol-coated surface is less than the solid-liquid interfacial tension (γ_{13}).

$$\Delta G_c = \gamma_{12} - \gamma_{13} = \gamma_{23}\cos\theta \qquad (3.2)$$

Here, ΔG_c is the free energy of cavitation. The subscript 1 refers to solid, 2 refers to air, and 3 refers to liquid. The cavitations are expected to occur as the cavity state is the thermodynamically favored state under situations where the receding contact angle θ > 90º.[52]

Figure 3.4 shows surface force measured on C_2SH-coated gold in water. The water equilibrium contact angle on this surface was 67º, which was the mean value for the advancing and receding contacts. According to Equation 3.2, the cavitation is not possible in this case. However, the force measured on C_2SH-coated gold was still much stronger than the van der Waals force. Thus, it is concluded that long-range hydrophobic forces measured on thiol-coated gold are not of bridging air bubbles or cavitations origin.

Comparing the contact angle measurements (Figure 3.2) with the surface force measurements (Figure 3.3 and 3.4) on the same surfaces, it is found that the hydrophobic force is dependent on the contact angle, which denotes the degree of surface hydrophobicity. For C_{12}SH- and C_{16}SH-coated gold surfaces, the hydrophobic force increased with contact angle, which was varied by changing the immersion time. When the contact angle was controlled by using alkanethiols with different chain lengths, the measured forces showed the same relation with water contact angle. The hydrophobic forces measured on C_{12}SH- and C_{16}SH-coated gold surfaces are the same when they have the same contact angles. Indeed, the hydrophobic force more or less depends on the surface preparation methods.[53] With the immersion time longer than 10 minutes for C_{16}SH coating and 2 hours longer than C_{12}SH coating preparations, the contact angles were constant, but the hydrophobic forces diminished with time. As indicated previously, the reduction of the hydrophobic force is due to the physical adsorption of the multilayer of thiols, which can be removed by washing with non-polar solvent ether. The relationship between the contact angle and chain length of alkanethiol is in good agreement with the relation between the chain length and the structure of the SAM monolayer of alkanethiol. The IR spectroscopic and ellipsometric data indicated that self-assembled monolayers of short chain alkanethiols ($n < 9$) are disordered and liquid-like, while the long-chain thiols form a densely packed, crystalline-like monolayers which are free of pin holes.[54] With increasing chain length, the structure becomes increasingly ordered with higher packing density and coverage, which gives rise to the stronger long-range hydrophobic attractive force.[55, 56] Figure 3.9 shows the fitted decay lengths *D* and values *C* for the measured hydrophobic forces plotted against the water contact

angles (θ) of the thiol-coated gold surfaces with which the force measurements have been conducted. The values C and decay lengths D changed little until θ reached 94º, and then increased sharply above this value. The sharp increase in decay length at $\theta \geq 94$º may be due to the changes in the packing density of the hydrocarbon chains and, hence, the degree of ordering.[18]

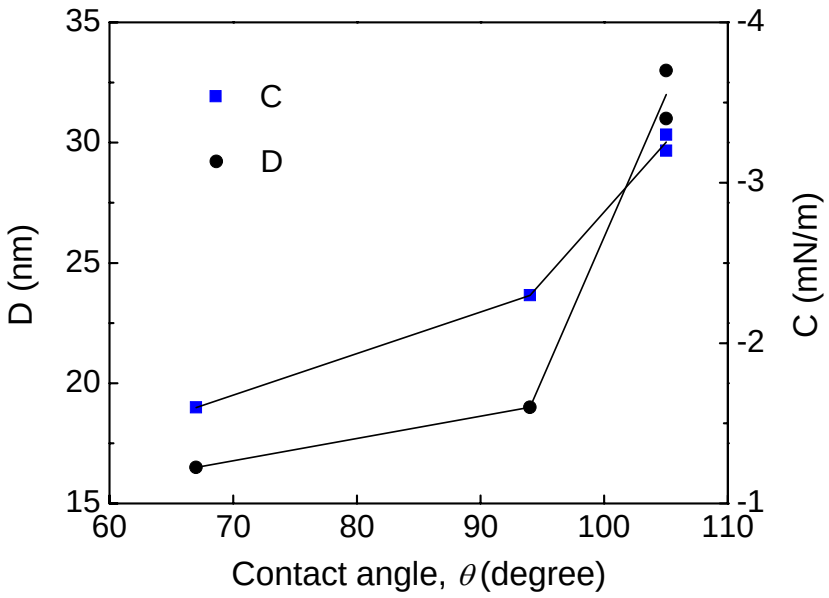

Figure 3.9. Decay length (D) and value C *versus* contact angle plots for the data obtained on C_2SH-, C_4SH-, C_{12}SH- and C_{16}SH-coated gold.

3.5.2 Effect of Surface Adsorption on the Hydrophobic Force

Figure 3.8 shows the surface forces measured in the presence of a cationic surfactant, C_{12}TACl, which ionizes in water to form charged $C_{12}TA^+$ species. Addition of a very small amount (5×10^{-5} M) of C_{12}TACl in water dramatically reduced the hydrophobic force between the C_{12}SH-coated gold surfaces. In the presence of 1×10^{-4} M NaCl and the cationic surfactant, repulsive forces were observed. The amphiphilic surfactant C_{12}TACl can adsorb

on the hydrophobic surfaces by hydrocarbon association. Earlier studies[45] on the surface forces between the mica surfaces hydrophobized with $C_{12}TACl$ in the presence of $C_{12}TACl$

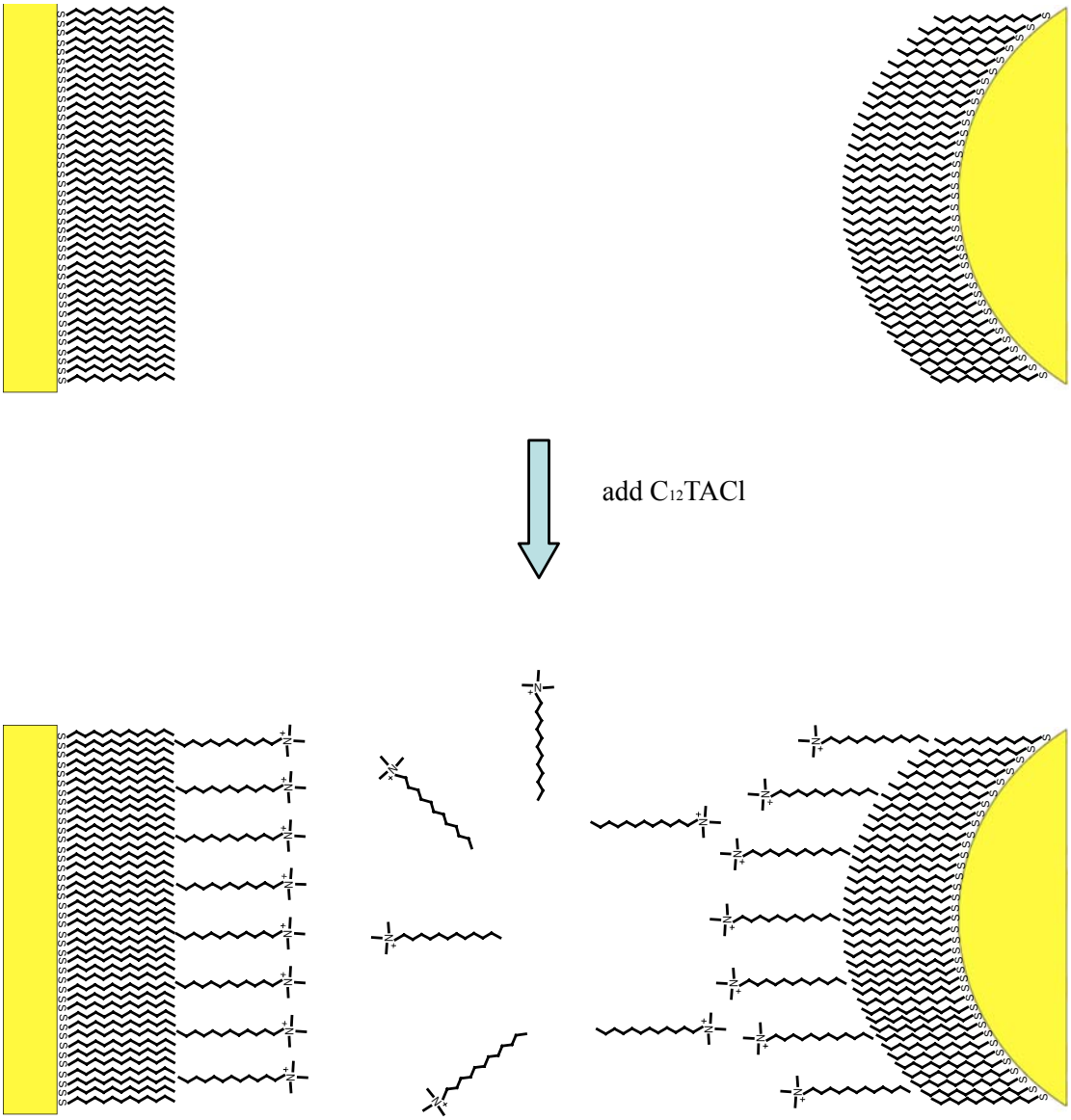

Figure 3.10. Schematic illustration for the effect of adding $C_{12}TACl$ in bulk solution.

showed that $C_{12}TA^+$ ions adsorb on hydrophobic surfaces with inverse (or flip-flop) orientation, as depicted in Figure 3.10. The inverse orientation exposes the charged head groups ($-N(CH_3)_3^+$) toward the aqueous phase, changes the interfacial water structure, and causes the surface to be less hydrophobic. In addition, the charged head groups on both

surfaces can generate the electrostatic repulsion. On the $C_{12}SH$-coated gold surfaces, the attractive hydrophobic force decreased and the electrostatic repulsive force increased in the presence of $C_{12}TACl$. At 1×10^{-3} M, the attractive force was completely suppressed, and only the repulsive force was operating at the short separation distance. In the concentration range of $5 \times 10^{-5} \sim 1 \times 10^{-3}$ M, the physically adsorbed $C_{12}TACl$ molecules may not be saturated on the hydrophobic surfaces, meaning some molecules were "lying down" while some were "standing up". As the concentration increased, more and more molecules were "standing up" and the surface became much less hydrophobic, causing a decrease in the attractive force. At the same time, the surface charge and hence the potential increased due to the adsorption of the $C_{12}TA^+$ species, which gave rise to a stronger electrostatic repulsion.

Also shown in Figure 3.8 are the effects of NaCl. In the presence of 1×10^{-4} M NaCl, the hydrophobic force was greatly reduced. This can be attributed to the possibility that the hydrogen bond network diminished in the presence of NaCl. In the presence of NaCl, the adsorption of the $C_{12}TA^+$ species may increase due to charge neutralization which in turn increases surface activity of a charged surfactant. The residual $C_{12}TA^+$ species left in solution may also contribute to diminishing the H-bonded water structure and decrease the hydrophobic force, as suggested by Zhang *et al*.[45]

Figure 3.2 shows the kinetics of adsorption of alkanethiols (C_4SH, $C_{12}SH$ and $C_{16}SH$) of different chain lengths on gold as monitored by the changes in contact angle with time. The data indicates that, the water contact angles of the thiol-coated gold surfaces reached the maximum after an exposure time of 5 hours, 2 hours and 10 minutes with C_4SH, $C_{12}SH$ and $C_{16}SH$, respectively. Thus, it takes less time for an alkanethiol with a longer chain to

completely cover the gold surface and form a self-assembled monolayer. There is a large body of information reported in the literature on the kinetics of alkanethiol adsorption on gold. However, the experimental results obtained with various analytical methods regarding the time required for the ordered monolayer formation are conflicting. Bain *et al*.,[43] measured the kinetics of formation of the self-assembled monolayer (SAM) of 1-octadecanethiol ($C_{18}SH$) on gold by measuring water contact angles. At thiol concentration below 1 mM, it took from hours to days to form a perfectly-ordered monolayer. Pan *et al*.[39] reported a contact time of 800 minutes for the monolayer formation in a 5 mM $C_{12}SH$ ethanol solution on gold as monitored by a quartz crystal microbalance (QCM) *in situ*. On the other hand, the X-ray photoelectron spectroscopy (XPS) analysis and scanning tunneling microscopy (STM) imaging by Kawasaki *et al*.[58] showed that almost complete monolayer coverage of octanethiol (C_8SH) SAM was obtained well within a few minutes, *e.g*., in a 1×10^{-2} mM alcoholic solution at room temperature. Campbell and Mutharasan[59] observed a $C_{16}SH$ SAM monolayer formation within 1 hour at various concentrations (1 nM to 10 mM) using a piezo-excited millimeter-sized gold-coated cantilever sensor. The infrared spectroscopy studies by Truong and Rowntree[60] indicated a shorter time scale of 1-10 minutes for the ordered C_4SH SAM formation from a 5 mM solution. Pan *et al*[39]. attributed the discrepancies among these reports to the contaminants on the gold surfaces. The pre-adsorbed contaminants can retard the adsorption process, because it is necessary to displace the adsorbed contaminants before thiol adsorption.

The surface force data obtained with $C_{12}SH$ (Figure 3.3) and $C_{16}SH$-coated gold[32] show that the hydrophobic forces were the strongest when the water contact angles

approached the maximum values after immersion time longer than 1 minute. As the immersion time was extended, the contact angles remained the same. On the other hand, the long-range attractions significantly decreased after longer immersion time. When the thiol-coated surfaces were flushed with non-polar solvent such as ether and then the fresh water was re-introduced in liquid cell, the strongest attractive forces were detected on C_{12}SH- and C_{16}SH-coated gold substrates. It is suggested that the decrease of hydrophobic force was caused by the physical adsorption of the bilayers of thiol.[32] Apparently, the "ethanol wash" step after hydrophobization step can not ensure that the physisorbed multilayer is completely removed. The adsorption of a thiol on a gold surface may be represented as follows:

$$Au \rightarrow \underline{Au}^{+} + e \qquad (3.3)$$

$$\underline{Au}^{+} + RSH \rightarrow \underline{Au} - SR + H^{+} \qquad (3.4)$$

where the underscore refers to the gold species remaining on the surface. Thus, the chemisorption yields the Au^{+} species on the surface, which uptakes the thiol in solution. After a long immersion time, however, some gold species may enter the bulk ethanol solution and form gold-thiol complex, which subsequently adsorb on the top of the chemisorbed thiol monolayer. Although the bi-layer formation does not cause a decrease in water contact angle, the presence of the gold-thiol complex in the adsorption layer can render the surface less ordered, which may cause a decrease in hydrophobic force. When such species are removed by appropriate solvent wash, a more ordered hydrophobic surface is exposed on the surface, which may give rise to a strong hydrophobic force.

3.5.3 Electrostatic Origin?

Based on the early studies[31, 61-65] showing that the hydrophobic forces decrease in range and magnitude in the presence of electrolytes, it was suggested that the hydrophobic force may be a electrostatic force in origin due to surface-induced perturbation in the fluid,[66] ion-ion correlations,[67, 68] mobile charged patches,[14] correlated in plane dipoles,[17, 18] instability of hydrophobic surface groups,[16] and rearrangement of the charged patchy bilayers.[15] The appealing point of this theory is that the classical electrostatic interaction is able to give rise to long-range force of exponential function measured for the hydrophobic attraction.

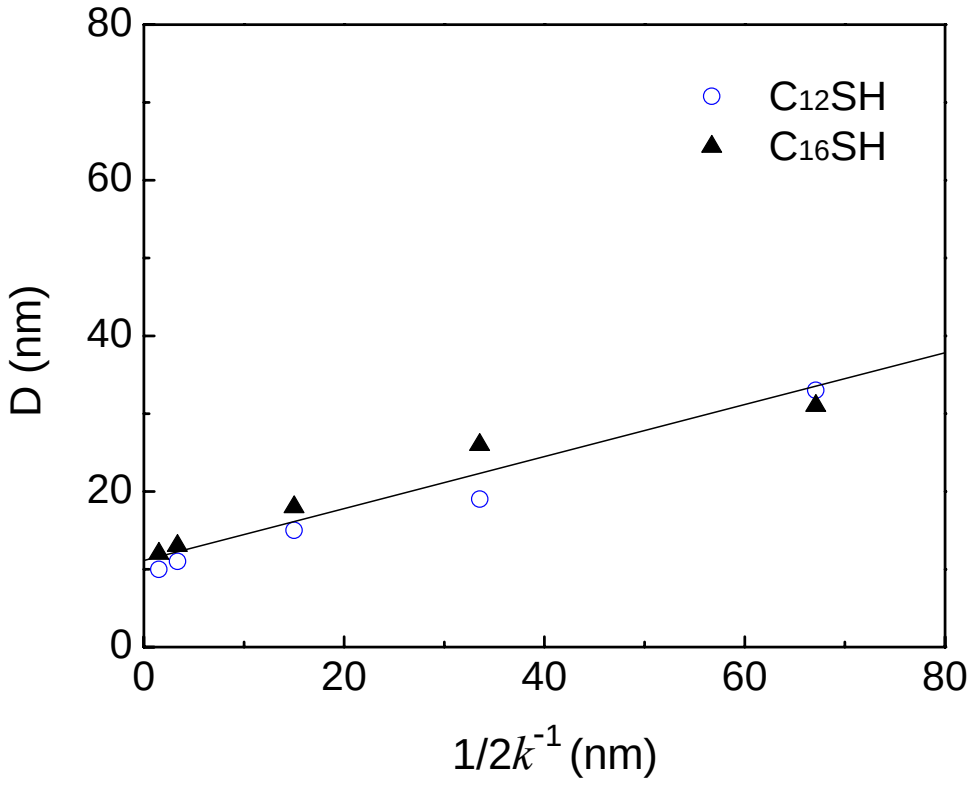

Figure 3.11. Decay length (D) *versus* the Debye length (κ^{-1}) plots for the data obtained on $C_{12}SH$- and $C_{16}SH$-coated gold in NaCl aqueous solutions with different concentrations.

Recently, more and more surface force measurements were performed using different

types of hydrophobic surfaces to determine the dependence of the range and strength of the hydrophobic force on the concentrations of the electrolytes. However, detailed experiments have shown that increased NaCl concentration up to 1 M has little or no effect on the range of the interaction,[69] the hydrophobic attraction is undiminished in the presence of concentrated electrolyte (0.1 M NaCl),[70] and electrolyte has negligible effect on the range and strength of the measured force, the strength of the attractive forces increases slightly even at very high salt concentrations.[19] These results can not be reconciled with the above models that attribute an electrostatic attraction to the hydrophobic force.

Figure 3.6 and 3.7 show the electrolyte (NaCl) effect on the hydrophobic forces measured on C_{12}SH- and C_{16}SH-coated gold surfaces. As shown in Table 3.2, analysis by fitting the force data points with extended DLVO theory which includes the contribution from the hydrophobic force confirms that the value *C* and decay length *D* decrease as the concentration of NaCl increases. The stability of C_{12}SH- and C_{16}SH-coated gold surfaces in NaCl aqueous solutions was evaluated by surface force and contact angle measurements. The experimental results show the decreased surface forces measured in NaCl solutions were restored when the NaCl solutions were replaced by fresh water, and the hydrophobicity did not change in the presence of NaCl electrolyte. According to the electrostatic models developed by Attard,[66] Miklavic *et al.*,[14] Podgornik,[67] and Spalla and Belloni,[68] the attraction decreases exponentially with a decay length *D* equal to the one half of the Debye length (κ^{-1}). In Figure 3.11, the values *D* obtained at different NaCl concentrations are plotted *versus* $1/2\kappa^{-1}$. However, it is shown that the *D* values are not equal to $1/2\kappa^{-1}$, except the *D* values obtained in 0.1 mM NaCl solution, the *D* (15 nm for C_{12}SH and 18 nm for C_{16}SH surfaces)

values are approximately $1/2\kappa^{-1}$ (30 nm). At the concentration of NaCl less than 0.1 mM, the obtained *D* values are smaller than the values of $1/2\kappa^{-1}$, while at NaCl concentration above 0.1 mM, the *D* values are much larger than $1/2\kappa^{-1}$. In addition, the thiol molecules formed immobile and robust monolayers on gold *via* chemical reaction, which can not meet the requirement of the theoretical models that assume that the surfaces are covered by movable charges,[14] mobile hydrophobic surface groups,[16] or "rolling" bilayer.[15] This conclusively rules out any electrostatic mechanism on stable thiol-coated gold surfaces.

The very long-range hydrophobic forces observed on thiol-coated surfaces may be explained by the changes in water structure across the thin film between the hydrophobic surfaces. A problem with this approach is that the computer simulations show the surface-induced structure can be extended up to only several layers of water molecules. It was argued by Eriksson *et al.*[71] that the classical simulations of Lee *et al.*[10] based on a simplistic water potential was not appropriate because it only explored density changes in thin water film. In fact, structural rearrangement of water can occur without volume changes.[71] Based on the water structure theory, the effects of organic surfactant and inorganic electrolyte ions across water thin film between thiol-coated hydrophobic surfaces on the hydrophobic force can be explained. It is suggested that the cationic surfactant C_{12}TACl and NaCl broke the hydrogen bond network[45] or the hydrations of Na^+ and Cl^- altered the water structure[57, 72] present in thin films between hydrophobic surface, and thus reducing the hydrophobic force. Ninham[73] suggested that the hydrophobic force may also be related to the gas molecules dissolved in water, because degassing can stabilized the surfactant-free emulsions[74] and can reduce the range and magnitude of the hydrophobic attractive force.[34] It

was shown that the solubility of oxygen in water decreases with increasing NaCl concentration, so the bubble coalescence is inhibited by the presence of NaCl.

3.6 Conclusions

AFM force measurements were conducted using gold surfaces hydrophobized by the self-assembly of alkanethiols with $n = 2-16$. We have observed net-attractive and long-range (~100 nm) forces between thiol-coated surfaces regardless of whether the water contact angle is greater than 90º or not, and the strengths and ranges of the attractions depends on the surface hydrophobicity. The force curves do not show discontinuities or steps at all separation distances except when the prepared thiol-coated hydrophobic surfaces were exposed in air for a prolonged period of time before being immersed in water for force measurement. We have tentatively exposed C_4SH-coated gold surfaces in atmospheric air for prolonged time after they were prepared *ex-situ* in thiol-in-ethanol solution. The force curves exhibited steps, indicating that the measured forces were due to bridging bubbles, which were trapped on the hydrophobic surfaces when C_4SH-coated surfaces were brought into water. When the air bubbles were washed away using water, the steps in force curves disappeared and long-range hydrophobic forces appeared. When gold surfaces were hydrophobized with C_2SH, the contact angle was less than 90°. In this case, no cavitation is possible. Yet, the AFM force measurement gave a long-range attraction, although it was weaker than those measured with gold surfaces coated with longer chain thiols. That long-range attractions are still observed under conditions cavitation is not thermodynamically possible suggest that hydrophobic force is not due to bubbles formed on hydrophobic surfaces.

The attractive forces measured on $C_{12}SH$- and $C_{16}SH$-coated gold surfaces were effectively reduced by electrolyte (NaCl), indicating that they may be of electrostatic origin. For this mechanism to work, it is necessary to assume that the charged patches must be mobile when two surfaces approach each other to maximize the correlation and give rise to a long-range attraction. However, the strong covalent Au-S bonding provides robust and immobile hydrophobic monolayers, which precludes the possibility of charged patches being mobile. Further, there is no reason that thiol adsorption produces charged patches as the thiol chemisorbs on gold.

Our work leaves the possibility that the long-range attraction is caused by the changes in water structure near hydrophobic surfaces. It is possible that the electrolyte NaCl and surfactant $C_{12}TACl$ in solution break the H-bonded water structure confined between two hydrophobic surfaces, and thus, reduce the hydrophobic force.

3.7 Acknowledgement

The authors would like to express their sincere appreciation to Professor Jan Christer Eriksson for his encouragement and helpful discussions. They would also like to acknowledge the financial support from the National Energy Technology Laboratory, U.S. Department of Energy (DE-FC26-02NT41607).

3.8 References

1. Xu, Z.; Yoon, R.-H., *J. Colloid Interface Sci.* **1989,** 132, (2), 532-541.

2. Xu, Z.; Yoon, R.-H., *J. Colloid Interface Sci.* **1990,** 134, (2), 427-434.

3. Demetriades, K.; Coupland, J. N.; McClements, D. J., *J. Food Sci.* **1997,** 62, (3), 462-467.

4. Blake, T. D.; Kitchener, J. A., *J. Chem. Soc., Faraday Trans. 1* **1972,** 68, 1435-1442.

5. Israelachvili, J.; Pashley, R., *Nature* **1982,** 300, 341-342.

6. Yoon, R.-H. In *Hydrodynamic and Surface Forces in Bubble-Particle Interactions*, XVII International Mineral Processing Congress, Dresden, Germany, 1991; Dresden, Germany, 1991; pp 17-31.

7. Yoon, R.-H.; Mao, L., *J. Colloid Interface Sci.* **1996,** 181, 613-626.

8. Mao, L.; Yoon, R.-H., *Int. J. Miner. Process* **1997,** 51, 171-181.

9. Eriksson, J. C.; Ljunggren, S.; Claesson, P. M., *J. Chem. Soc., Faraday Trans. 2* **1989,** 85, (3), 163-176.

10. Lee, C. Y.; McCammon, J. A.; Rossky, P. J., *J. Chem. Phys.* **1984,** 80, (9), 4448-4455.

11. Forsman, J.; Jonsson, B.; Woodward, C. E., *J. Phys. Chem.* **1996,** 100, (36), 15005-15010.

12. Sakurai, M.; Tamagawa, H.; Ariga, K.; Kunitake, T.; Inoue, Y., *Chem. Phys. Lett.* **1998,** 289, 567-571.

13. Fa, K.; Nguyen, A. V.; Miller, J. D., *J. Phys. Chem.* **2005,** 109, (27), 13112-13118.

14. Miklavic, S. J.; Chan, D. Y. C.; White, L. R.; Healy, T. W., *J. Phys. Chem.* **1994,** 98, 9022-9032.

15. Meyer, E. E.; Lin, Q.; Hassenkam, T.; Oroudjev, E.; Israelachvili, J. N., *Proc. Nat. Acad. Sci. U.S.A* **2005,** 102, 6839-6842.

16. Christenson, H. K.; Yaminsky, V. V., *Colloids Surf., A* **1997,** 129-130, 67-74.

17. Tsao, Y.-H.; Evans, D. F.; Wennerstrom, H., *Science* **1993,** 262, (5133), 547-550.

18. Yoon, R.-H.; Ravishankar, S. A. R., *J. Colloid Interface Sci.* **1996,** 179, 391-402.

19. Parker, J. L.; Claesson, P. M.; Attard, P., *J. Phys. Chem.* **1994,** 98, 8468-8480.

20. Nguyen, A. V.; Nalaskowski, J.; Miller, J. D.; Butt, H.-J., *Int. J. Miner. Process.* **2003,** 72, 215-225.

21. Ishida, N.; Sakamoto, M.; Miyahara, M.; Higashitani, K., *J. Colloid Interface Sci.* **2002,** 253, 112-116.

22. Tyrrell, J. W. G.; Attard, P., *Phys. Rev. Lett.* **2001,** 87, (17), 176104-1.

23. Ederth, T., *J. Phys. Chem. B* **2000,** 104, 9704-9712.

24. Yushchenko, V. S.; Yaminsky, V. V.; Shchukin, E. D., *J. Colloid Interface Sci.* **1983,** 96, (2), 307-314.

25. Yaminsky, V. V.; Ninham, B. W., *Langmuir* **1993,** 9, 3618-3624.

26. Yaminsky, V. V., *Colloids and Surf., A* **1999,** 159, 181-195.

27. Craig, V. S. J.; Ninham, B. W.; Pashley, R. M., *Langmuir* **1999,** 15, 1562-1569.

28. Christenson, H. K.; Claesson, P. M., *Science* **1988,** 239, 390-392.

29. Wood, J.; Sharma, R., *Langmuir* **1995,** 11, (12), 4797-4802.

30. Ljunggren, S.; Eriksson, J. C., *Colloids and Surf., A* **1997,** 129-130, 151-155.

31. Zhang, J.; Yoon, R.-H.; Mao, M.; Ducker, W. A., *Langmuir* **2005,** 21, 5831-5841.

32. Wang, J.; Yoon, R.-H., *Langmuir* **2008,** 24, 7889-7896.

33. Stevens, H.; Considine, R. F.; Drummond, C. J.; Hayes, R. A.; Attard, P., *Langmuir* **2005,** 21, 6399-6405.

34. Meyer, E. E.; Lin, Q.; Israelachvili, J. N., *Langmuir* **2005,** 21, 256-259.

35. Ederth, T.; Liedberg, B., *Langmuir* **2000,** 16, 2177-2184.

36. Raiteri, R.; Preuss, M.; Grattarola, M.; Butt, H.-J., *Colloids Surf., A* **1998,** 136, 191-197.

37. Ron, H.; Rubinstein, I., *Langmuir* **1994,** 10, (12), 4566-4573.

38. Ron, H.; Rubinstein, I., *J. Am. Chem. Soc* **1998,** 120, (51), 13444-13452.

39. Pan, W.; Durning, C. J.; Turro, N. J., *Langmuir* **1996,** 12, (18), 4469-4473.

40. Xu, S.; Cruchon-Dupeyrat, S. J. N.; Garno, J. C.; Liu, G.-Y.; Jennings, G. K.; Yong, T.-H.; Laibinis, P. E., *J. Chem. Phys.* **1998,** 108, (12), 5002-5012.

41. Ducker, W. A.; Senden, T. J., *Langmuir* **1992,** 8, (7), 1831-1836.

42. Cleveland, J. P.; Manne, S.; Bocek, D.; Hansma, P. K., *Rev. Sci. Instrum.* **1993,** 64, (2), 403-405.

43. Bain, C. D.; Troughton, E. B.; Tao, Y.-T.; Evall, J.; Whitesides, G. M.; Nuzzo, R. G., *J. Am. Chem. Soc.* **1989,** 111, 321-335.

44. Ulman, A., *An Introduction to Ultrathin Organic Films From langmuir-Blodgett to Self-Assembly*. Academic Press: Rochester, New York, 1991.

45. Zhang, J.; Yoon, R.-H.; Eriksson, J. C., *Colloids Surf., A* **2007,** 300, 335-345.

46. Hato, M., *J. Phys. Chem.* **1996,** 100, 18530-18538.

47. Attard, P., *Adv. Colloid Interface Sci.* **2003,** 104, 75-91.

48. Carambassis, A.; Jonker, L. C.; Attard, P.; Rutland, M. W., *Phys. Rev. Lett.* **1998,** 80, (24), 5357-5360.

49. Ishida, N.; Sakamoto, M.; Miyahara, M.; Higashitani, K., *Langmuir* **2000,** 16, (13), 5681-5687.

50. Sakamoto, M.; Kanda, Y.; Miyahara, M.; Higashitani, K., *Langmuir* **2002,** 18,

5713-5719.

51. Yang, J.; Duan, J.; Fornasiero, D.; Ralston, J., *J. Phys. Chem. B* **2003,** 107, 6139-6147.

52. Meyer, E. E.; Rosenberg, K. J.; Israelachvili, J., *Proc. Nat. Acad. Sci. U.S.A* **2006,** 103, 15739-15746.

53. Christenson, H. K.; Claesson, P. M., *Adv. Colloid Interface Sci.* **2001,** 91, 391-436.

54. Porter, M. D.; Bright, T. B.; Allara, D. L.; Chidsey, C. E. D., *J. Am. Chem. Soc.* **1987,** 109, (12), 3559-3568.

55. Tsao, Y.-H.; Yang, S. X.; Evans, D. F.; Wennerstrom, H., *Langmuir* **1991,** 7, 3154-3159.

56. Rabinovich, Y. I.; Guzonas, D. A.; Yoon, R.-H., *Langmuir* **1993,** 9, 1168-1170.

57. Weissenborn, P. K.; Pugh, R. J., *J. Colloid Interface Sci.* **1996,** 184, 550-563.

58. Kawasaki, M.; Sato, T.; Tanaka, T.; Takao, K., *Langmuir* **2000,** 16, (4), 1719-1728.

59. Campbell, G. A.; Mutharasan, R., *Langmuir* **2005,** 21, (25), 11568-11573.

60. Truong, K. D.; Rowntree, P. A., *Prog. Surf. Sci.* **1995,** 50, (1-4), 207-216.

61. Rabinovich, Y. I.; Derjaguin, B. V., *Colloids Surf.* **1988,** 30, 243-251.

62. Claesson, P. M.; Blom, C. E.; Herder, P. C.; Ninham, B. W., *J. Colloid Interface Sci.* **1986,** 114, (1), 234-242.

63. Tsao, Y.-H.; Evans, D. F.; Wennerstrom, H., *Langmuir* **1993,** 9, 779-785.

64. Kekicheff, P.; Spalla, O., *Phys. Rev. Lett.* **1995,** 75, (9), 1851-1855.

65. Christenson, H. K.; Claesson, P. M.; Berg, J.; Herder, P. C., *J. Phys. Chem.* **1989,** 93, 1472-1478.

66. Attard, P., *J. Phys. Chem.* **1989,** 93, (17), 6441-6444.

67. Podgornik, R., *J. Chem. Phys* **1989,** 91, (9), 5840-5849.

68. Spalla, O.; Belloni, L., *Phys. Rev. Lett.* **1995,** 74, (13), 2515-2518.

69. Meagher, L.; Craig, V. S. J., *Langmuir* **1994,** 10, 2736-2742.

70. Craig, V. S. J.; Ninham, B. W.; Pashley, R. M., *Langmuir* **1998,** 14, (12), 3326-3332.

71. Eriksson, J. C.; Yoon, R.-H., Hydrophobic Attraction in the Light of Thin-Film Thermodynamics. In *Colloid Stability: The Role of Surface Forces*, Tadros, T. F., Ed. WILEY-VCH Verlag GmbH & Co. KGaA: Weinheim, Germany, 2007; Vol. 1, pp 99-132.

72. Craig, V. S. J.; Ninham, B. W.; Pashley, R. M., *Nature* **1993,** 364, 317-319.

73. Ninham, B. W., *Prog. Colloid Polym. Sci.* **2006,** 133, 65-73.

74. Pashley, R. M., *J. Phys. Chem. B* **2003,** 107, 1714-1720.

Chapter 4

Surface Force between Gold Surfaces in Xanthate Solutions and Its Implication in Flotation

4.1 Abstract

Understanding the wetting behavior of sulfide and precious minerals in xanthate solutions and the surface forces in flotation is essential for improving the process of flotation. Contact angle and surface force measurements were conducted on the potassium amyl xanthate (PAX)-gold system. Monolayer structures of PAX were formed by spontaneous adsorption at different concentrations and contact (or adsorption) times. Captive bubble contact angle measurements showed that chemisorption of PAX on gold was concentration dependent. A monolayer was formed more readily on gold in a 1×10^{-5} M than in a 5×10^{-6} M PAX solution. The contact angle measurements conducted in 1×10^{-5} M and 5×10^{-6} M PAX solutions showed a rapid increase in contact angle to a peak value of 94º, followed by a slower period of decreasing contact angle.

Surface forces were measured using an atomic force microscope (AFM) with gold substrates hydrophobized by PAX coatings. The results showed the existence of long-range hydrophobic forces, which were closely related to the surface hydrophobicity. The strongest hydrophobic force with a decay length of 23 nm was measured when the water contact angle was the largest. The hydrophobic force decreased when the contact angle was decreased due to the physisorption of additional xanthate ions on the underlying monolayer possibly with reverse orientation. It was found that the residual xanthate species left in solution caused a

decrease in hydrophobic force, possibly because their presence in solution is detrimental to maximizing the cohesive energy of water.

4.2 Introduction

Froth flotation is the most important solid-solid separation process in the mining industry. Owing to its simplicity, the process is widely used for extracting many minerals from their ores, cleaning coals, and recycling plastics, *etc*, by exploiting the differences in hydrophobicity. In froth flotation, a stream of small air bubbles is introduced to the bottom of a flotation cell, in which a mixture of finely grounded ore particles is suspended in water. The air bubbles rise to the top of the tank under a buoyancy force. During the process, only the hydrophobic particles adhere to the surface of air bubbles and are carried to the upper surface of the pulp. Rendering a desired mineral particle more hydrophobic than the others determines the selectivity, and is the key to the success of a flotation process. For this reason, during the early stages of flotation research, most of the efforts were focused on hydrophobizing minerals with surfactants (collectors) and monitoring the changes in surface hydrophobicity by measuring contact angles. However, surface chemistry parameters such as contact angle, are thermodynamic properties and do not provide kinetic information. On the other hand, flotation is a kinetic process and the industry strives to improve flotation kinetics and, thus, increase recovery and throughput.

Froth flotation can be described as a first order process with a rate constant proportional to the probability of particle collection (P).[1] The probability of particle collection (P) is represented by:

$$P = P_c P_a (1 - P_d) \qquad (4.1)$$

where P_c is the probability of air bubble and mineral particle collision, P_a is the probability of bubble particle adhesion, and P_d is the probability of detachment. In mineral flotation, it is believed that both the adhesion and detachment processes are determined by the surface force between the air bubble and mineral particle. Derjaguin and Dukhin[2, 3] were the first to describe the bubble particle interaction in flotation by considering surface forces. However, the authors only considered the traditional DLVO force, *i.e.*, van der Waals and electrostatic forces, which can not explain the strong attraction between air bubbles and hydrophobic mineral particles in flotation. Laskowski and Kitchener[4] were the first to recognize the existence of the hydrophobic force by studying the interaction across a thin water film between an air bubble and a silicate plate hydrophobized by trimethylchlorosilane (TMCS). The air bubble readily adheres on the hydrophobic silica surface, even though both the van der Waals and electrostatic force in the wetting film are repulsive. Therefore, they speculated the existence of a third force, which is responsible for the bubble particle adhesion. Furthermore, they said the long range hydrophobic influence may be responsible for the flotation. In 1972, Blake and Kitchener[5] were the first to use the term hydrophobic force in wetting films. Recent studies of hydrophobic forces are focused on thin aqueous films between solid hydrophobic surfaces. Most of the force measurements have been based on employing the surface force apparatus (SFA) and atomic force microscope (AFM). In 1982, an attractive force much larger than the van der Waals force between two curved mica surfaces immersed in hexadecyltrimethylammonium bromide (CTAB) solution was first measured by Israelachvili and Pashley[6] using a SFA. They referred to the additional attractive

force as a hydrophobic force. More recently, Yoon and Aksoy[7] and Wang and Yoon[8] suggested that the hydrophobic forces are also present in soap films.

Xanthates (dithiocarbonates) are used as collectors for sulfide mineral flotation, and are known to chemisorb on them. Xanthates also adsorb to noble metals such as silver, copper and gold, in a manner similar to thiols.[9] Most of the hydrophobic force measurements conducted in the past was made with mica and silica surfaces using surfactants that are not commonly used for flotation. Therefore, in the present study, it is proposed to conduct AFM force measurements with gold substrates by xanthate adsorption. The results of the present work may be useful for better understanding the mechanisms on the origin of hydrophobic force, and help improve flotation technology.

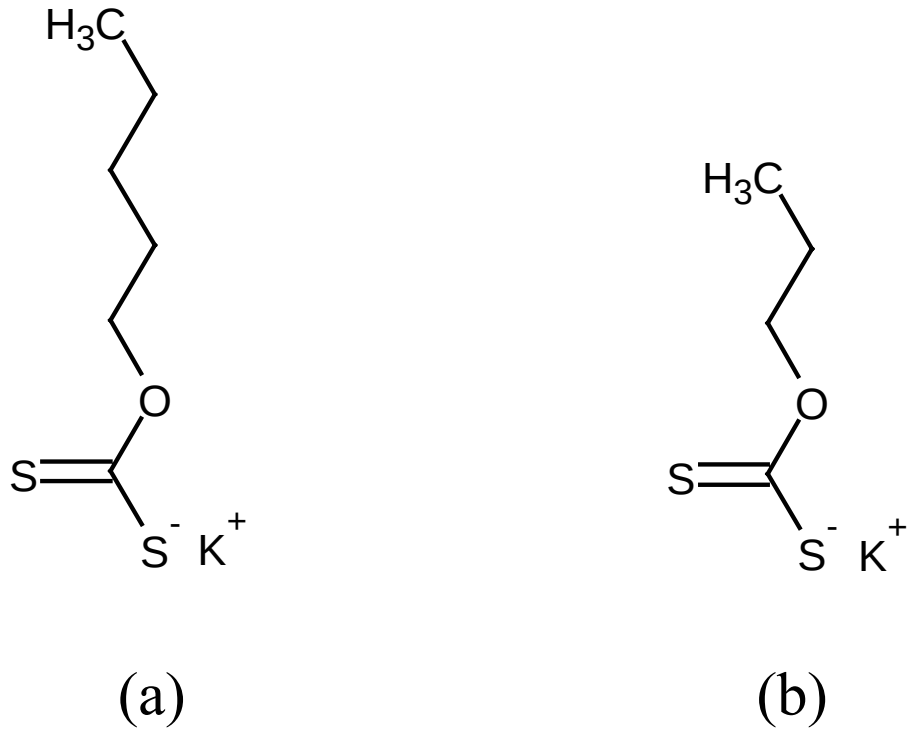

Figure 4.1. Molecular structure of (a) potassium amyl xantahte (PAX) (b) and potassium ethyl xanthate (KEX).

4.3 Materials and Methods

4.3.1 Materials

Potassium amyl xanthate (PAX, $C_6H_{11}KOS_2$, > 90.0%) and potassium ethyl xanthate (KEX, $C_3H_5KOS_2$, > 90.0%) were obtained from TCI America. The molecular structures of potassium amyl xanthate and potassium ethyl xanthate are shown in Figure 4.1. The xanthates were purified by dissolution in acetone (HPLC grade, Fisher Scientific, Inc.), filtration and recrystallization with diethyl ether (≥ 99.9%, Sigma-Aldrich, Inc.), as described in the literature.[10] Alkyl xanthate is unstable in water and decomposes to form CS_2. The xanthates were recrystallized at least twice prior to use. Sodium perchlorate monohydrate ($NaClO_4 \cdot H_2O$, 97%), potassium ferrocyanide trihydrate ($K_4Fe(CN)_6 \cdot 3H_2O$, 100%) and potassium ferricyanide ($K_3Fe(CN)_6$, 90%) were obtained from Fisher Scientific, and used for electrochemical study. High purity sodium chloride (NaCl, 99.999%) from Sigma-Aldrich was used as electrolyte. A Nanopure water treatment unit was used to obtain deionized water with a resistivity of 18.2 MΩ cm^{-1} at 22ºC. The feed to the water treatment system was double-distilled water. All of the aqueous solutions used in the present study were prepared using nanopure water.

Gold microspheres and gold-coated glass slides were used for AFM surface force measurements. The gold-coated glass slides were obtained by depositing pure gold on glass using a vacuum evaporator. A 50 Å chromium layer was deposited first on the glass prior to coating it with a thin layer (500 Å) of gold. The chromium coating was necessary to achieve strong bonding between the gold and glass substrate. The gold coatings produced without the

chromium adhesive layer were easily removed in acid solutions.

Gold spheres were produced by melting a gold micropowder (1.5–3.0 μm, > 99.6%, Alfa Aesar) in a high temperature furnace. The powder was placed in an alumina crucible and heated until the temperature was raised above its melting point (1064.18ºC). It was kept at 1100ºC for 15 minutes and then cooled down slowly. The furnace was flushed with nitrogen gas to provide an oxygen-free atmosphere. The gold spheres obtained in this manner had a wide range of sizes. Only those with radius of 3.5–7.5 μm were selected for AFM force measurements.

The gold plates were cleaned first by immersing them in a boiling piranha solution (30:70 H_2O_2/H_2SO_4) for 20 minutes and then washing them with nanopure water for 1 minute, followed by an ethanol wash for 2 minutes. The gold spheres were cleaned after they had been glued onto AFM cantilever springs. Because piranha solution would have destroyed the glue attaching the gold spheres to the AFM cantilever springs, each gold sphere was instead flushed with ethanol, exposed in UV light (λ = 254 nm) for two hours, and then rinsed with ethanol again.

4.3.2 Electrochemical Measurement

Cyclic voltammetry (CV) experiments were conducted in a standard three-electrode electrochemical cell under ambient conditions. The cell was equipped with a saturated calomel electrode (SCE, 0.242 V *versus* NHE) as reference electrode and a platinum mesh electrode as counter electrode. A gold-coated glass slide (1" × 1.5") was used as the working electrode, and 1×10^{-1} M $NaClO_4$ as the supporting electrolyte. The potential on the gold

electrode was controlled by a potentiostat (model 273A, EG&G Princeton Applied Research). The cyclic voltammetry experiments were carried out in 1×10^{-1} M $NaClO_4$ solutions containing 1×10^{-4} M PAX at a scan rate of 250 mV/s to study the adsorption mechanism. When testing the blocking capability of the xanthate layer on gold, an electrolyte solution containing 1×10^{-1} M $NaClO_4$, 1×10^{-5} M PAX, and 1×10^{-2} M $K_3Fe(CN)_6/K_4Fe(CN)_6$ at a scan rate of 200 mV/s was used. The potentials are reported against the standard hydrogen electrode (SHE), *i.e.*, assuming that the potential is 242 mV more negative than the saturated calomel electrode.

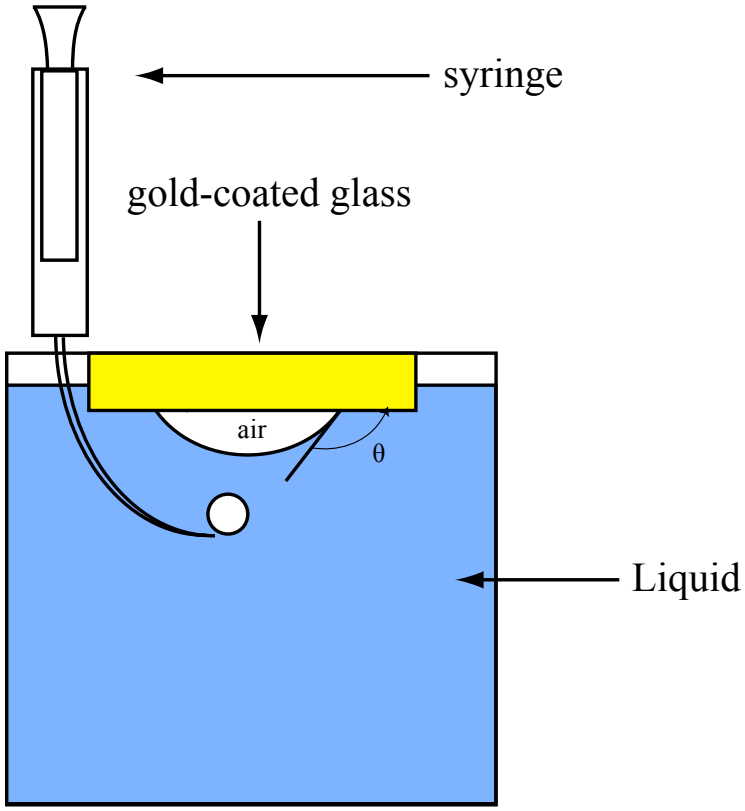

Figure 4.2. A schematic picture of the liquid cell for captive air bubble contact angle measurement.

4.3.3 Contact Angle Measurement

Contact angles of gold were measured using the captive air bubble technique in a

home-made plastic sample holder, which is shown in Figure 4.2. After the gold-coated glass slides were kept in xanthate solutions for a desired period of time, air bubbles were brought to contact using a syringe. Contact angles were measured by means of a contact angle goniometer (model 100-00 115, Ramé-Hart, Inc., Mountain Lakes, NJ). An average of at least five different individual measurements was used at a given experimental condition.

4.3.4 Surface Force Measurement

Surface force measurements were conducted using a nanoscope III (Digital Instruments, Inc., Santa Barbara, CA) atomic force microscope (AFM) equipped with a standard fluid cell and a piezoelectric scanner "E". All the AFM force measurements were carried out using the colloidal probe technique[11, 12] at room temperature (22±1ºC). Triangular silicon nitride cantilevers (NP-20, Veeco Probes, Inc.) were used for the force measurements. The spring constant (k) was determined using the resonant frequency technique.[13] In each experiment, a gold sphere was glued onto a cantilever spring with EPON 1004 resin (Shell Chemical Co.) using a homemade 3-D micromanipulator with a hot plate. The diameter of the gold sphere was measured using an Olympus BH-2 light microscope. The liquid cell, used to hold the sphere probe, was cleaned in an ultrasonic water bath. All of the measurements were conducted in air-equilibrated solution. The separation distance (H) between the gold sphere and the flat-gold coated glass plate was measured by monitoring the deflection of the cantilever on which the gold sphere was attached. Measured forces (F) were normalized with respect to the radii (R) of the gold spheres.

4.4 Results and Discussion

4.4.1 Electrochemical Characterization

The key chemical step in a flotation process is the interaction of the organic collectors with a selected mineral; thereby the mineral surface is rendered hydrophobic so that gas bubbles can adhere to them. Electrochemical techniques such as cyclic voltammetry have been used to study the mechanism of interaction between gold and xanthate.[14-17] In the present study, cyclic voltammetry was used to investigate the interaction and adsorption process between PAX and gold surfaces.

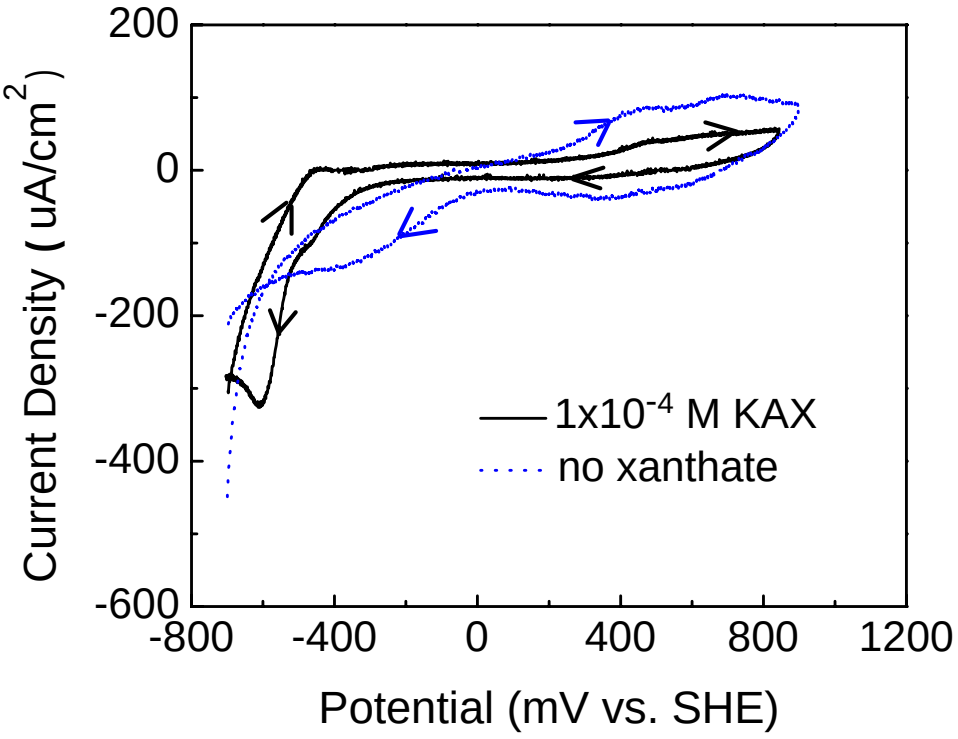

Figure 4.3. Cyclic voltammograms of gold recorded in 1×10^{-1} M $NaClO_4$ aqueous solutions with and without 1×10^{-4} M potassium amyl xanthate (PAX) using a scan rate of 250 mV/s.

Cyclic voltammograms of the gold working electrode obtained in 1×10^{-1} M $NaClO_4$ solution and 1×10^{-1} M $NaClO_4$ + 1×10^{-4} M PAX mixture solution are shown in Fig. 4.1. Potential scans were performed between -700 and 900 mV at a sweep rate of 250 mV/s. The dotted curve represents the relationship between current density and applied potential for a bare gold electrode in the absence of 1×10^{-4} M PAX, while the cyclic voltammogram for gold in the presence of 1×10^{-4} M PAX is represented by the solid line. As shown in Figure 4.3, the shape of the voltammogram changed dramatically when the xanthate was added. During the anodic scan, in the absence of xanthate, the small anodic current peak at potential around 400 mV is caused by the adsorption of perchloride ions on gold. The anodic peak observed at potential of about 650 mV is due to the oxidation of gold, which is consistent with previous work.[18] As the potential was swept in the reverse direction (cathodic scan), the reduction of gold began at a potential about 400 mV. In the presence of 1×10^{-4} M PAX, anodic at 450 mV and a cathodic current at -450 mV were observed. Previous CV studies on the adsorption of potassium ethyl xanthate (KEX) on gold suggest that in the presence of KEX, the chemisorption of xanthate ions (EX^-) begins at -470 mV[15] or -400 mV[16] and the oxidation of ethyl xanthate to ethyl dixanthogen occurs at +200 mV[15, 16] during the anodic scan. As the potential was swept in the cathodic direction, the reduction of dixanthogen began at a potential of about -400 mV[15] or -250 mV[16]. Thus, we cannot exclude the possibility that the same types of chemical reaction occurs for potassium amyl xanthate. In the presence of PAX, the anodic current peak at -450 mV is attributed to the adsorption of amyl xanthate ions on gold, and the peak at 450 mV is due to the oxidation of amyl xanthate ion (X^-) to amyl dixanthogen (X_2), which is bound to the underlying chemisorbed xanthate.[19] The cathodic

current peak around -450 mV is due to the reduction of amyl dixanthogen (X_2) to amyl xanthate ion (X^-). The cyclic voltammetry experiment shows that the amyl xanthate ions from aqueous solutions spontaneously chemisorb on gold and form a xanthate monolayer.

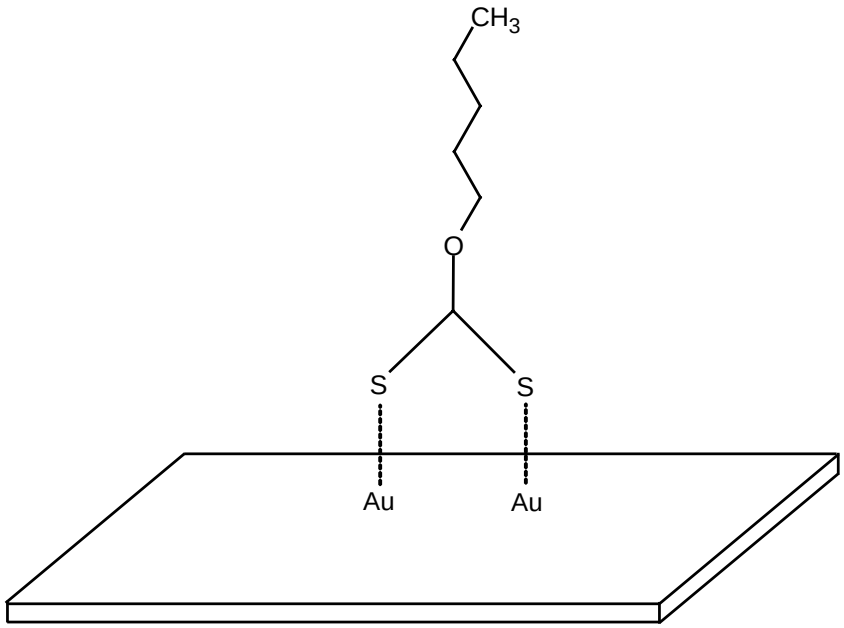

Figure 4.4. Schematic illustration for the arrangement and coordination of amyl xanthate ion on gold.

The chemical interaction of xanthates such as potassium *p*-methyl benzyl xanthate, potassium *p*-trifluoromethyl benzyl xanthate, ethyl and octyl xanthate ions with gold was also studied with infrared reflection absorption spectroscopy (IRAS) and x-ray photoelectron spectroscopy (XPS).[20, 21] The xanthate monolayers were prepared by immersing gold substrates in 1 to 10 μM aqueous solutions of the xanthates for different adsorption times. The experimental reflection-absorption (R-A) spectra of xanthate ions adsorbed on gold were compared with the calculated R-A spectrum of gold xanthate salts. According to the experimentally obtained peak positions, which were consistent with the calculated values, the chemical structure of the xanthate species on gold were closely related to those of the metal

salts. Based on IRAS measurements, it was proposed that the xanthate ions are coordinated to the gold surface through both sulfur atoms (Figure 4. 4). The XPS studies further confirmed a bridge-like coordination for the chemisorbed xanthates.

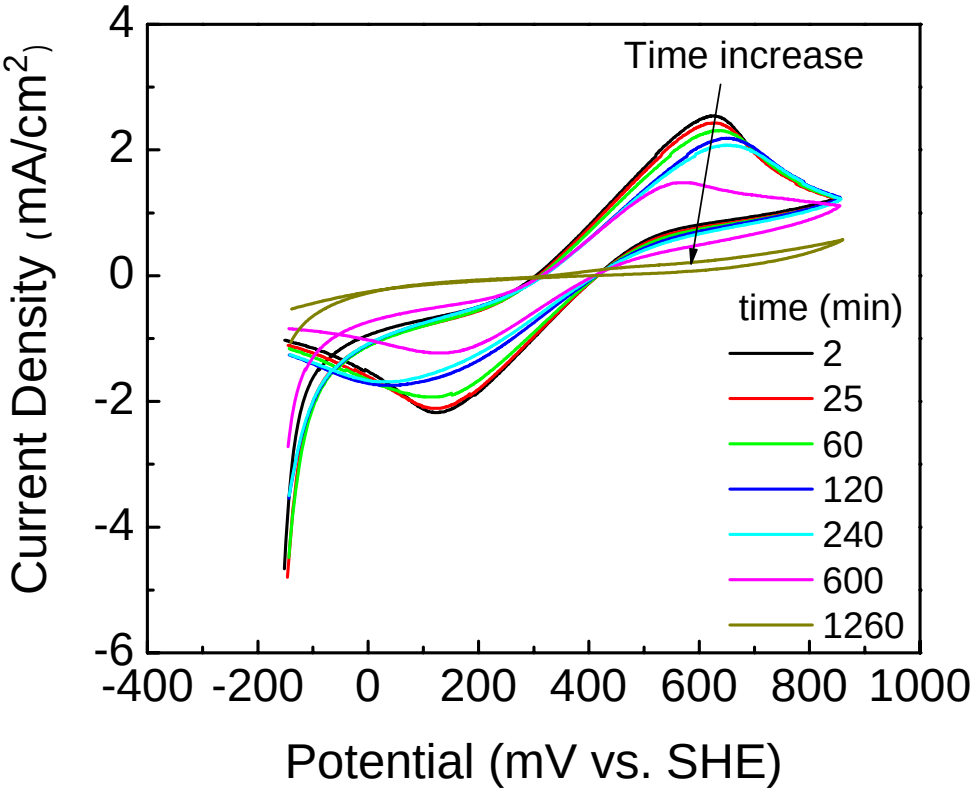

Figure 4.5. Cyclic voltammograms of a gold electrode recorded in 1×10^{-2} M $K_3Fe(CN)_6/K_4Fe(CN)_6$, 1×10^{-1} M $NaClO_4$ and 1×10^{-5} M KAX aqueous solutions at different adsorption times, with scan rate of 200 mV/s *versus* an SHE reference electrode.

Figure 4.5 shows cyclic voltammograms of gold in the presence of 1×10^{-5} M PAX in 1×10^{-2} M $K_3Fe(CN)_6/K_4Fe(CN)_6$ and 1×10^{-1} M $NaClO_4$. The scan rate was at 200 mV/s in both directions. The blocking capability of the amyl xanthate layers on gold formed in 1×10^{-5} M amyl xanthate aqueous solution at different immersion times towards the ferri/ferro redox couples was investigated. A cleaned bare gold electrode gave the expected cyclic

voltammograms of $K_3Fe(CN)_6/K_4Fe(CN)_6$. The anodic current peak shows the oxidation of $Fe(CN)_6^{-4}$ to $Fe(CN)_6^{-3}$ on gold; and the cathodic sweep shows the reduction of $Fe(CN)_6^{-3}$ to $Fe(CN)_6^{-4}$. There are no current peaks assigned to the oxidation or desorption of amyl xanthate ions observed. It is known that the electron transfer reaction might be occurring at pinhole sites.[22] With the immersion time extending from 2 to 1,260 minutes, noticeable decreases in the peak current were observed in the cyclic voltammograms. It appears that the amyl xanthate layer's ability to block the transfer of electrons to the gold electrode surfaces increased with time. After 1,260 minutes of immersion time, the voltammogram was of a sigmoidal line shape, which indicates that the layers had the least pinholes and defects. Thus, the layer was, from an electrochemical point of view, well packed. It is suggested that the organic hydrocarbon part of the xanthate molecule first lies down on the gold surfaces, and erects itself, approaching a conformation normal to the surface with the packing density increasing with reaction time.[20] It also indirectly indicates that the formation of a close-packed monolayer of amyl xanthate onto gold surface was a rather slow process, which required at least 20 hours.

4.4.2 Contact Angle Study

Equilibrium contact angle measurement would be another way to examine the adsorption process of amyl xanthate ions onto gold surfaces. The result of *in-situ* contact angle measurements on gold in amyl xanthate solutions with the captive bubble technique is shown in Fig. 4.6. The gold-coated glass plates were hydrophobized by *in-situ* adsorption using a range of aqueous concentration (1×10^{-6}, 5×10^{-6} and 1×10^{-5} M) of amyl xanthate

surfactants. Generally, the contact angle of gold dramatically changed upon contact with the xanthate solution, reaching peak values faster for higher concentrations of amyl xanthate. In 1 × 10^{-6} M solution, the contact angle of bare gold (62º) reached a maximum value of 87º after 180 minutes immersion time. In a higher concentration of 5 × 10^{-6} M, a peak value of 94º was obtained after 120 minutes. When the concentration was further increased to 1 × 10^{-5} M, a peak value of 94º was obtained after 57 minutes. As discussed before, according to the cyclic voltammetry experiments and literature reports,[20, 21] the xanthate readily adsorb on the gold by chemical reaction just like thiol. The adsorption rate of thiol on gold is influenced by many factors, such as temperature, solvent, concentration, and chain length of the

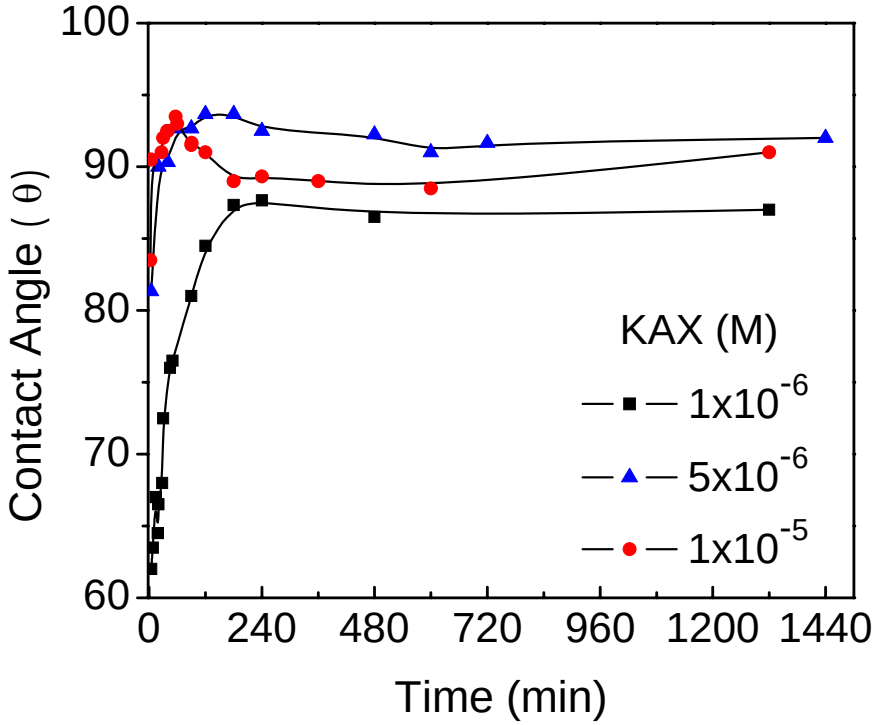

Figure 4.6. Contact angles of amyl xanthate layers on gold surface formed in different xanthate aqueous solutions with varying immersion time.

adsorbate.[23, 24] A xanthate monolayer forms with the polar head group in contact with gold,[17] and the methyl group (-CH_3) extends toward the aqueous phase, rendering the gold surface hydrophobic.

At higher concentrations (5×10^{-6} M and 1×10^{-5} M), the adsorption process was characterized by two distinct phases: a rapid adsorption followed by slower process. Within 5 minutes, the contact angles were close to the peak values. This initial, rapid adsorption was followed by a slower period lasting 1 hour at 1×10^{-5} M PAX and 2 hours at 5×10^{-6} M PAX. The maximum values (94º) were the same for 5×10^{-6} M and 1×10^{-5} M, indicating that the a full monolayer of xanthate formed on gold when the contact angle reached the peak value. The contact angles of gold decreased after reaching the maximum values. It is supposed that a physisorbed adlayer of xanthate, which reversely oriented with polar group toward the aqueous phase, was formed on top of a chemisorbed monolayer. According to the CV experiment conducted in a solution containing 1×10^{-5} M PAX and ferrocyanide/ferricyanide mixture solutions, the blocking capability reached the highest level after an immersion time of 21 hours. While the contact angle measurements show that the hydrophobicity reached maximum value after 1 hour in 1×10^{-5} M xanthate solution. It suggests that after the xanthate completely covered the gold surface, the monolayer took a much longer time (21 hours) to reorganize itself and formed a close-packed monolayer. In a very dilute solution of 1×10^{-6} M, the contact angle reached maximum value of 87º and stayed constant as time elapsed. The maximum contact angle on xanthate-coated gold was, however, less than the contact angle of 94º for the full coverage of xanthate. This indicates that at low concentrations, the entirety of xanthate molecules from the bulk solution migrated to the gold

surface without completely covering the gold surfaces. As suggested by Persson *et al*.,[20] the hydrocarbon chain lay down on the gold surface at low coverage densities, but erected itself with a conformation normal to the surface when the coverage densities increased.

According to the Young's equation, the changes of contact angle θ for gold surface can be affected by changes in the surface tension γ_{lv} of a xanthate solution, the surface tension γ_{sv} of gold, and the tension γ_{sl} of gold/liquid. The Young's equation is shown below:

$$\cos\theta = \frac{\gamma_{sv} - \gamma_{sl}}{\gamma_{lv}} \qquad (4.2)$$

When a gold plate was placed in an amyl xanthate solution (*e.g.*, 5×10^{-6} M), the amyl xanthate ions from the aqueous solution migrated and adsorbed on gold, making the gold surface hydrophobic. Under such conditions, the surface tension γ_{lv} of a xanthate liquid did not change with time. (Xanthate has no surface activity at the air/water interface due to short hydrocarbon chain.) Compared to the surface tension γ_{sv} of xanthate-coated gold, the interfacial tension γ_{sl} at the xanthate-coated gold/liquid interface changed much more with immersion time. The interfacial tension γ_{sl} increased as more amyl xanthate ions adsorbed onto the gold surface with the non-polar methyl group exposed to water, increasing contact angles. After a monolayer was formed on gold, the additional xanthate molecules started to adsorb on the monolayer with inverse orientation, causing a decrease for the interfacial tension γ_{sl}, thereby decreasing the hydrophobicity.

4.4.3 Surface Force Measurement

Figure 4.7 shows the surface forces measured as a function of immersion time between a flat gold-coated glass slide and a gold microsphere in a 1×10^{-6} M PAX solution.

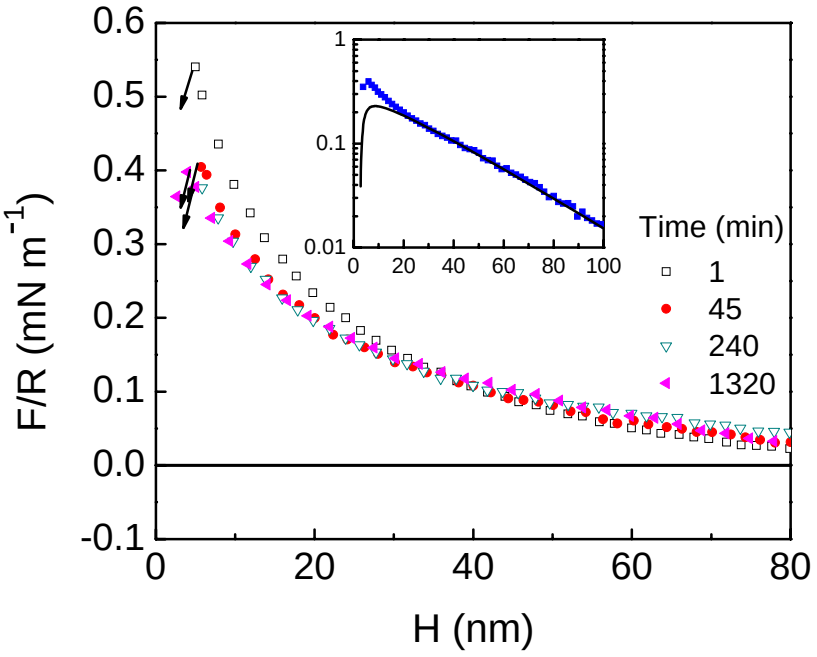

Figure 4.7. Surface forces measured between bare gold in 1 × 10^{-6} M PAX aqueous solution at different immersion times.

Fresh solutions were prepared before each set of experiments. The arrows represent the separation distance at which the two surfaces jumped into contact due to attractive forces. The jumps occur when the gradient of the surface force exceeds the spring constant and can be identified by the rapid acceleration of the sphere probe. As shown, there was no hydrophobic force observed for the immersion times investigated, and the surface forces measured in 1 × 10^{-6} M PAX were traditional DLVO forces, *i.e.*, a short-range van der Waals attractive force and a long-range electrostatic double-layer repulsive force. The repulsive double-layer forces dominated at separation distance H > 10 nm, and the repulsive forces decreased with time. The experimental force *versus* distance curves recorded for 1 × 10^{-6} M PAX solution at different immersion times were fitted using classical DLVO theory. To obtain the electrostatic component, the nonlinear Poisson-Boltzmann equation was solved using

constant potential boundary condition at the theoretical Debye length κ^{-1}. The van der Waals component of the interaction was calculated using an experimental Hamaker constant A_{131}= 1.2 × 10^{-20} J for gold-water-gold system.[24] The van der Waals force for the sphere-plate geometry is described as:

$$\frac{F}{R} = -\frac{A}{6H^2} \qquad (4.3)$$

where H is the closest distance separation the two microscopic surfaces. The inset shows the AFM force curve obtained for the immersion time of 45 minutes, and a calculated force curve using DLVO theory.

Table 4.1. The Contact Angles and Parameters (Surface Potentials, Debye Lengths) Obtained by Fitting the Surface Forces Measured in PAX Solutions after Different Immersion Times with DLVO Theory

C (M)	t (min)	θ (degree)	k^{-1} (nm)	ψ_0 (mV)
1×10^{-6}	1	65	25.4	-45.0
	45	81	28.6	-44.0
	240	87	37.8	-45.0
	1320	87	38.7	-46.0
5×10^{-6}	5	81	24.5	-48.0

The parameters extracted from these calculations are shown in Table 4.1. Also included in Table 4.1 are the contact angles measured for different immersion times. As shown in Figure 4.6, the contact angle increased with time and reached a limited value of 87º. At the same time, the surface potential ($\psi_0 \approx$ -45 mV) of gold did not change much, while the Debye length (κ^{-1}) increased from 25.4 to 38.7 nm. As discussed before, for 1 × 10^{-6} M PAX, the xanthate ions can not cover the entire gold surface. As the xanthate ions adsorbed onto the gold surfaces with time, the xanthate ions in the bulk solution were depleted, and the ionic strength decreased, increasing Debye length.

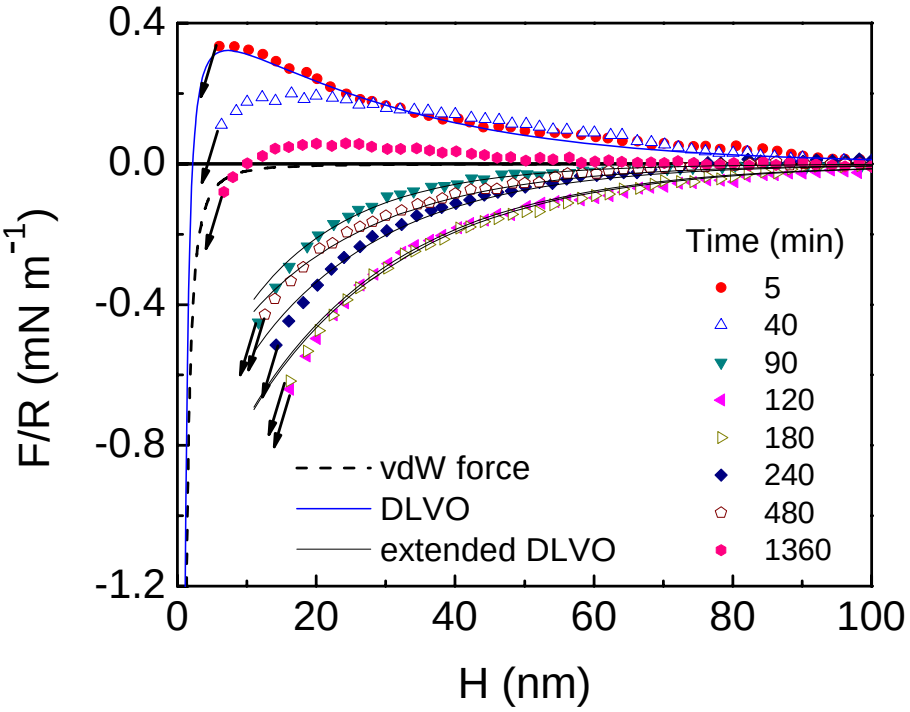

Figure 4.8. Surface forces measured between bare gold in a 5×10^{-6} M PAX aqueous solution at different immersion times.

The hydrophobic force measurements were also conducted at the higher concentrations of 5×10^{-6} and 1×10^{-5} M PAX. Figure 4.8 shows the surface forces measured at 5×10^{-6} M PAX. After the gold sphere and gold-coated glass plate were in contact with the surfactant solution for 5 minutes, the xanthate ions partially covered on gold, and a long-range repulsive force was observed. The repulsive force decreased with increased immersion time. At 90 minutes, a net-attractive force appeared which increased with further increase in immersion time. At 120 and 180 minutes, the measured force became most

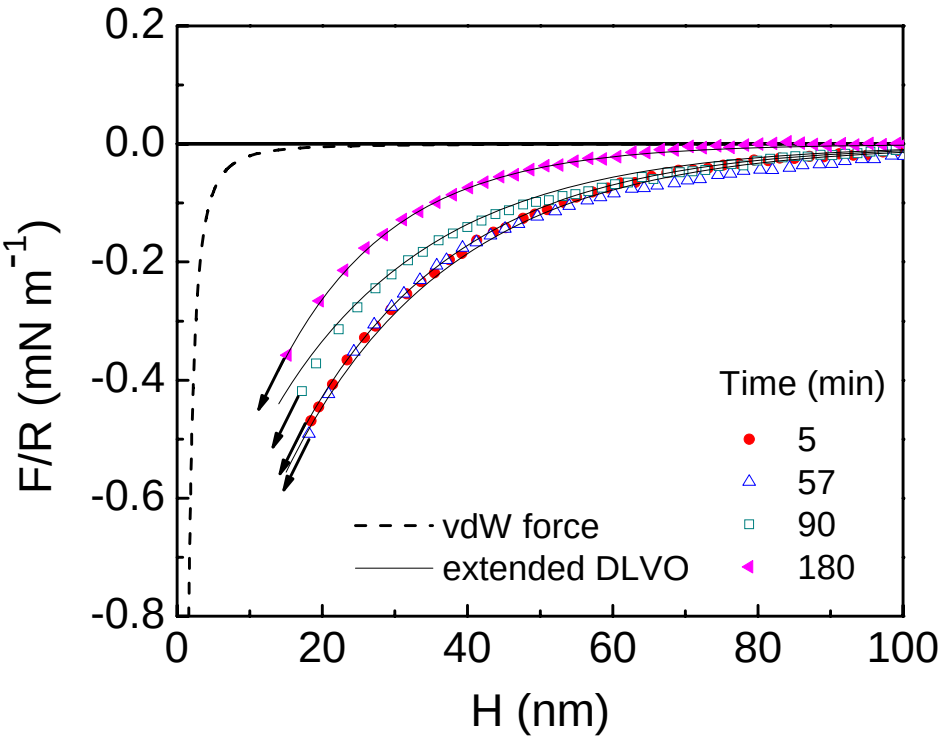

Figure 4.9. Surface forces measured between bare gold in a 1×10^{-5} M PAX aqueous solution at different immersion times.

attractive. Presumably, the gold surfaces were completely covered by monolayers of xanthate. After a 240 minutes immersion time, the attractive force decreased, probably due to the inverse orientation of the physisorbed xanthate adlayer.

The results obtained in a 1×10^{-5} M PAX solution are presented in Figure 4.9. At this high concentration, the gold surfaces were completely covered by xanthate after 5 and 57 minutes of immersion times, and gave rise to the strongest attraction. After the 90 minutes of immersion time, the additional xanthate ions adsorbed on the underlying chemisorbed monolayer with reverse orientation, which gave rise to a weaker attractive force. The attractive force appeared sooner in 5×10^{-6} M than in 1×10^{-5} M PAX solution. According to the contact angle measurements, the xanthate adsorption process is a concentration dependent

process. In summary, higher concentrations of PAX lead to faster adsorption rates on gold surfaces, creating a hydrophobic monolayer which in turn creates a long-range hydrophobic attractive force.

Table 4.2. Parameter *C* and Decay Length *D* Obtained by Fitting the Surface Forces Measured in PAX Solutions after Different Immersion Times with Extended DLVO Theory

C (M)	*t* (min)	θ (degree)	*C* (mN/m)	*D* (nm)
5×10^{-6}	90	93	-0.75	15.5
	120	94	-1.1	22.5
	180	94	-1.1	23
	240	93	-0.9	20
	480	92	-0.7	20
1×10^{-5}	5	91	-1.05	22
	57	94	-1.05	23
	90	92	-0.8	22.5
	180	89	-0.9	16

Previous studies[25-28] on the hydrophobic force, using the surfaces hydrophobized by chemical reaction with hydrophobizing agents, suggest that the long-range interaction originates from the gas bridges. The gas bridges are formed by coalescence between nanosize bubbles, which are captured on the surfaces upon immersing them into an aqueous solution. In the present work, gold surfaces were hydrophobized by *in-situ* adsorption of xanthate. The substrates were never exposed to air at any stage. As can be seen from Figure 4.8 and 4.9, strong attractive forces with an exceptional range, up to 100 nm, were observed. All of the force curves were smooth, without showing steps or kinks, indicating that the adsorption systems were relatively free of contamination or air bubbles. It further indicates that the hydrophobic forces measured in our study were not caused by bridging air bubbles as suggested by Parker *et al*.,[25] Higashitani *et al*.,[26, 27, 29] Attard *et al*.,[30-33] Ederth *et al*.,[34-37] and

Nguyen *et al*.[28]

Despite the extensive experimental evidence for the existence of the long-range hydrophobic force, no single theory can account for this interaction, and empirical equations were usually used to describe them.[24, 38-40] The long-range attractive force *versus* distance curves shown in Figure 4.8 and 4.9 were fitted to a single-exponential force law:

$$\frac{F}{R} = C\exp(-\frac{H}{D}) \qquad (4.4)$$

where F is the hydrophobic force, R is the radius of the gold microsphere, H is the surface separation distance of the gold microsphere and flat gold-coated glass plate, and C and D are the fitting parameters. C represents the magnitude of the attractive force and D, usually called decay length, represents the range of this interaction. Table 4.2 gives the values of C and decay length (D) as well as the contact angle (θ). From Figure 4.8 and 4.9, it is clearly seen that the hydrophobic force increased with increasing contact angle, which is in agreement with previous studies.[41] As shown in Table 4.2, the decay length (D) increased with the contact angle, ranging from 15.5 to 23 nm. For the same contact angle, the hydrophobic force was almost the same. The maximum contact angles measured in 5×10^{-6} M and 1×10^{-5} M PAX solutions were 94º. The fitting constants C and D were -1.1 mN/m and 23 nm in 5×10^{-6} M PAX and -1.05 mN/m and 23 nm in 1×10^{-5} M PAX solution. In view of the results of contact angle and surface force measurements, it is suggested that hydrophobic force increased with the surface coverage of xanthate ions on gold. The hydrophobic force was most attractive when xanthate ions covered the entire gold surface by forming a self-assembled monolayer. The relation between the surface adsorption of xanthate ions and the hydrophobic force was also found for alkyl thiol on gold.[24]

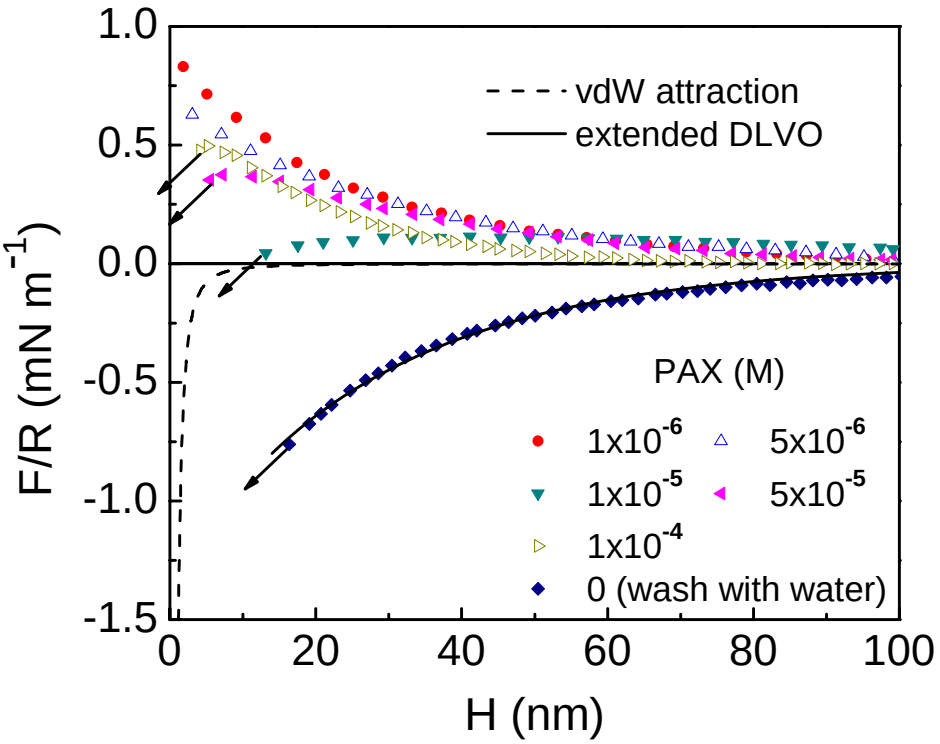

Figure 4.10. The surface forces measured between bare gold surfaces in PAX solutions as a function of concentration of PAX.

Figure 4.10 shows the results of the surface force measurements conducted as a function of the PAX concentration. The PAX solutions were injected into an AFM liquid glass cell starting from the lowest concentration (1×10^{-6} M) to the highest (1×10^{-4} M). For each new concentration, the gold microsphere and gold-coated glass plate were exposed to the surfactant solution for a period of 35 minutes before the force measurements were taken.

Figure 4.10 shows the same trend as the surface forces measured between a glass sphere and a silica plate in C_{18}TACl solution.[39] At 1×10^{-6} M, the xanthate ions were unable to cover the entire gold surfaces, allowing the surface charge on gold to give rise to a long-range electrostatic repulsive force. At 5×10^{-6} M, more xanthate ions adsorbed on gold, reducing the electrostatic force. While relatively short-ranged, the attractive force was longer

than the van der Waals force (represented as the dashed line), causing the gold sphere to jump to the gold-coated glass surface at a separation distance of 17 nm. This attraction was actually the hydrophobic force, and the repulsive force was the electrostatic force caused by the physisorbed xanthate layer with reverse orientation. At 5×10^{-5} M, the hydrophobic force decreased, represented by the decreased jump distance (H = 9 nm). When the concentration of PAX was increased to 1×10^{-4} M, an increase in surface charge and decrease in surface hydrophobicity were observed, caused by an adsorption of amyl xanthate ions on the chemisorbed monolayer. The repulsive electrostatic force increased and the hydrophobic force decreased with a jump distance of 5 nm. After the force measurement in 1×10^{-4} M PAX, the AFM liquid cell was flushed with nanopure water, replacing the xanthate solution. The force measurement revealed the existence of a strongly attractive hydrophobic force with a long range of up to 100 nm. This means that after water washing, the physisorbed adlayer of xanthate was removed, leaving the chemisorbed monolayer intact and giving rise to the long-range hydrophobic force.

The force measurement was also conducted after the gold sphere and gold-coated glass plate were immersed in 1×10^{-5} M potassium ethyl xanthate (KEX) solution for 6 hours. As shown in Figure 4.11, the red dotted line represents the force measured in KEX solution. The force was attractive and jumped at short separation distance. The thin dashed black line represents the van der Waals force calculated using an experimental Hamaker constant of 1.2×10^{-20} J. It is shown clearly that the measured attraction was smaller than the van der Waals force. It is speculated that the measured force was a combination of attractive hydrophobic force and a repulsive electrostatic force due to the physisorption of KEX. This physisorbed

KEX layer can be washed away using water. As shown, a long-range hydrophobic force appeared when the KEX solution was replaced with water.

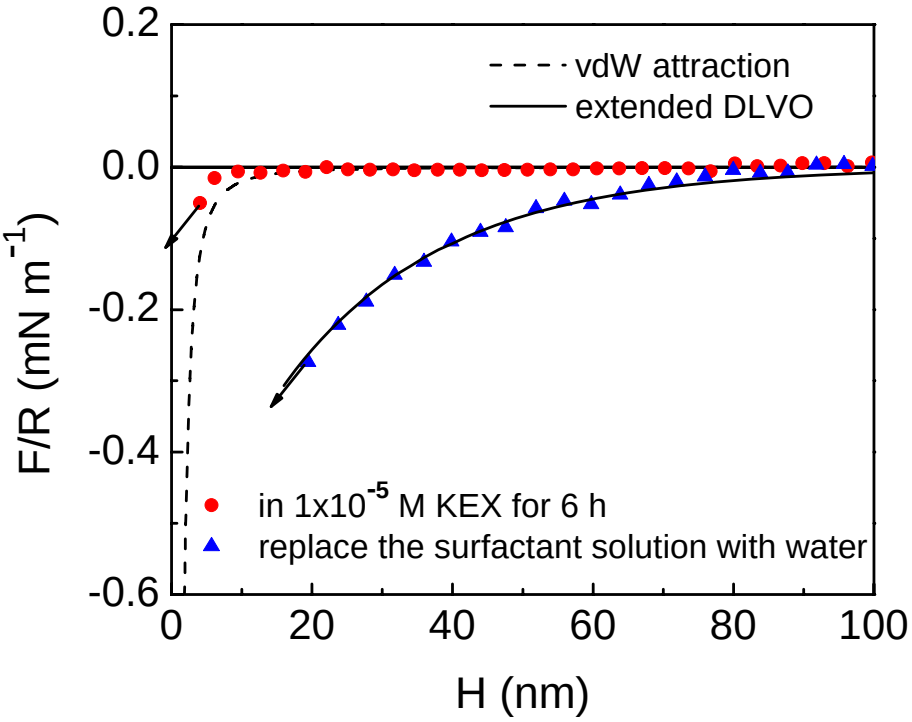

Figure 4.11. Surface forces measured between KEX adsorbed gold surfaces in 1 × 10^{-5} M KEX aqueous solution and in water.

Table 4.3. Effects of NaCl on Debye Length (κ^{-1}), *C* and Decay Length (*D*) for Gold Hydrophobized by *in-situ* Adsorption of PAX and KEX

	NaCl (M)	k^{-1} (nm)	*C* (mN/m)	*D* (nm)
PAX	0	94.5	-1.3	28
	1×10^{-4}	28.6	-1.4	14
	5×10^{-4}	13.3	-0.6	6
KEX	0	94.5	-0.6	22

The hydrophobic force curves shown in Figure 4.10 and 4.11 were fitted to a single exponential law, as described in Equation 4.3. The Debye length (κ^{-1}), *C* and decay length (*D*) in water as well as in NaCl solutions were given in Table 4.3. In water, the *C* and *D* values were much larger for PAX (*C* = -1.3; *D* = 28) than for KEX (*C* = -0.6; *D* = 22). Compared to

the most attractive hydrophobic forces measured in 5×10^{-6} M and 1×10^{-5} M of PAX, as shown in Figure 4.8 and 4.9, the hydrophobic force measured after water washing was larger and longer-ranged. According to the previous studies, the most attractive hydrophobic force appeared when the gold surfaces were covered by a monolayer of xanthate. In Figure 4.10, force measurements show that gold surfaces were fully covered in xanthate following an immersion in 1×10^{-4} PAX solution for 35 minutes. Thus, the measured force when 1×10^{-4} M PAX was replaced by water should be the same in terms of magnitude and range as the most attractive forces shown in Figure 4.8 and 4.9. However, data analysis shows that the *C* and decay length *D* for forces (*C* = -1.3 mN/m; *D* = 28 nm) as shown in Figure 4.10 were much larger than that (*C* = -1.1 mN/m; *D* = 23 nm) shown in Figure 4.8 and 4.9. Zhang *et al*.[40] had conducted surface force measurement using an AFM with a glass sphere and a silica plate immersed C_nTACl solutions. The C_nTACl represents the homologues of the surfactant with a carbon chain length from 12 to 18. They found the presence of the hydrocarbon chain ($-(CH_2)_nCH_3$) in water diminished the hydrophobic force. The decay length decreased linearly with the effective concentration of the CH_2/CH_3 groups of the C_nTACl homologues in water. In view of the hydrophobic force model derived using a mean-field approach by Eriksson *et al*.[42], they concluded that hydrophobic chains in solution disrupted the surface-induced water structure and thus, caused the hydrophobic force to decrease. When 1×10^{-4} M PAX was replaced by water, the increase of the attractive force measured suggests a decreased repulsive force and an increased hydrophobic force. The repulsive electrostatic force disappeared when the physisorbed xanthate layer was removed by water flushing, and the hydrophobic force increased because water also dispelled the "water destroying"

hydrocarbon chain.

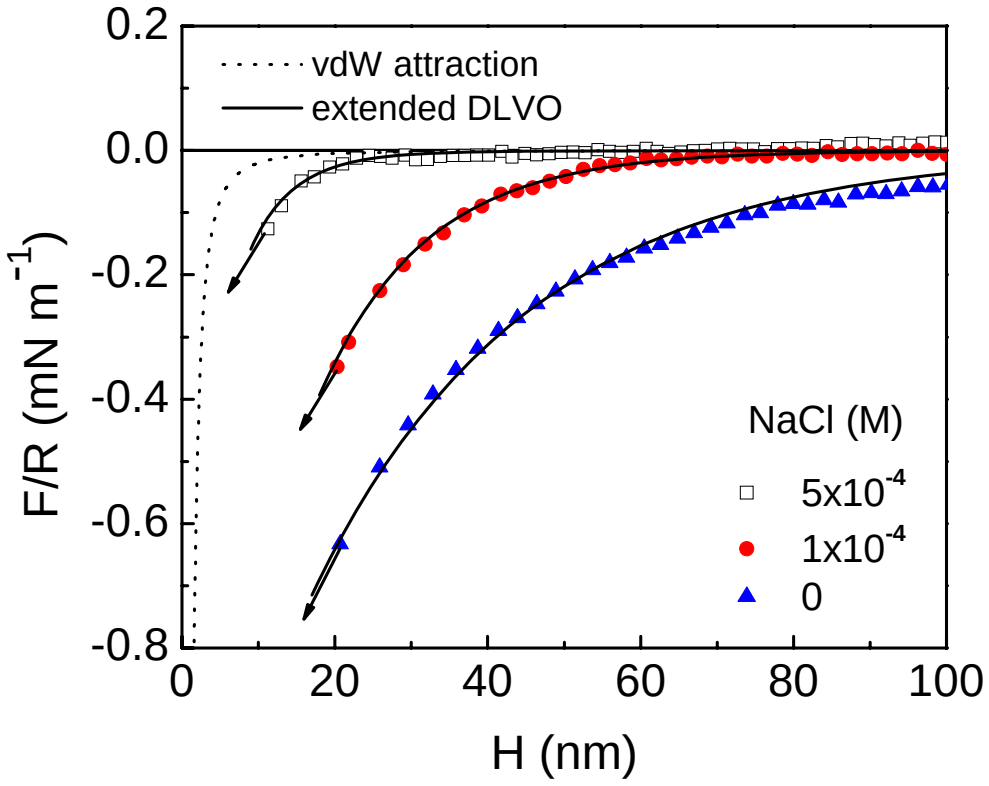

Figure 4.12. Surface force measured between PAX hydrophobic layers in different concentrations of NaCl aqueous solution.

After flushing with nanopure water, the liquid cell was filled by NaCl solutions with two different concentrations (5×10^{-4} M and 1×10^{-4} M). The effect of added salt on the hydrophobic force was investigated, and the experimental data are shown in Fig. 4.12 and the fitted parameters are given in Table 4.3. It is shown that the addition of NaCl decreased the magnitude and range of the attractive hydrophobic force, which is consistent with previous investigations.[39, 43-46] Because of its salt dependent character, the hydrophobic force was regarded as the attraction due to electrostatic correlations in an early study.[47] A charged-patch model developed by Miklavic *et al.*[48] predict that the attraction should be exponentially decaying at a rate equal to one half the Debye length (κ^{-1}), and data analysis shows that the

decay lengths in 1×10^{-4} M and 5×10^{-4} M are actually equal to one half of the corresponding Debye length. However, Miklavic's model presumes that the positive and negative surfactant patches on the two surfaces are free to migrate to lower the interaction. Because xanthate ions adsorbed on gold to form strong covalent bonding, it is not possible for them to migrate freely on gold. The "patchy bilayer" model developed by Meyer *et al*.[49] suggests that the long-range hydrophobic force measured between two surfactant-coated surfaces is a long-range electrostatic attraction, which results from the natural alignment of oppositely charged surfactant domain as two such surfaces approach. Neither the "charged patch" nor the "patchy bilayer" model can explain the long-range hydrophobic force in the present work. It is believed that the addition of NaCl disturbs the water structure between the hydrophobic surfaces.[40]

4.5 Conclusions

In the present work, cyclic voltammetry (CV), contact angle and surface force measurements were conducted to study the adsorption of amyl xanthate on gold and to measure the hydrophobic forces between xanthate-coated surfaces. The CV test verified the chemical adsorption of amyl xanthate ions on gold. The contact angle and surface force measurements revealed the reverse orientation of amyl xanthate on gold surfaces. According to the surface force measurement, the attractive hydrophobic force which was much greater in magnitude and range than expected for the van der Waals force has been detected at the high water contact angles. It has been found also that xanthate adsorption resulted in multi-layer formation. The molecules adsorbed in the second-layer adsorbed with inverse orientation,

which in turn caused a decrease in hydrophobic force. The molecules adsorbed in the second and subsequent layers can be readily washed by water, which gives rise to a strong hydrophobic force.

4.6 Acknowledgment

This work was funded by National Energy Technology Laboratory, U. S. Department of Energy (DE-FC26-02NT41607).

4.7 References

1. Yoon, R.-H.; Mao, L., *J. Colloid Interface Sci.* **1996,** 181, 613-626.

2. Derjaguin, B. V.; Dukhin, S. S., *Trans. Inst. Min. Metall.* **1961,** 70, 221-246.

3. Derjaguin, B. V.; Dukhin, S. S., In *Proceedings 13th Int. Miner. Process. Cong.*, Warszawa, 1979; Vol. 2, pp 1261-1287.

4. Laskowski, J.; Kitchener, J. A., *J. Colloid Interface Sci.* **1969,** 29, 670-679.

5. Blake, T. D.; Kitchener, J. A., *J. Chem. Soc., Faraday Trans. 1* **1972,** 68, 1435-1442.

6. Israelachvili, J.; Pashley, R., *Nature* **1982,** 300, 341-342.

7. Yoon, R.-H.; Aksoy, B. S., *J. Colloid Interface Sci.* **1999,** 211, 1-10.

8. Wang, L.; Yoon, R.-H., *Langmuir* **2004,** 20, 11457-11464.

9. Tzhayik, O.; Sawant, P.; Efrima, S.; Kovalev, E.; Klug, J. T., *Langmuir* **2002,** 18, 3364-3369.

10. Rao, S. R., Xanthates and Related Compounds. In Marcel Dekker, Inc.: New York, 1971; pp 15-18.

11. Ducker, W. A.; Senden, T. J.; Pashley, R. M., *Nature* **1991,** 353, 239-241.

12. Ducker, W. A.; Senden, T. J., *Langmuir* **1992,** 8, 1831-1836.

13. Cleveland, J. P.; Manne, S.; Bocek, D.; Hansma, P. K., *Rev. Sci. Instrum.* **1993,** 64, (2), 403-405.

14. Woods, R., *J. Phys. Chem.* **1971,** 75, 354-362.

15. Leppinen, J. O.; Yoon, R.-H.; Mielczarski, J. A., *Colloids Surf.* **1991,** 61, 189-203.

16. Talonen, P.; Sundholm, G.; Li, W.-H.; Floate, S.; Nichols, R. J., *Phys. Chem. Chem. Phys.* **1999,** 1, 3661-3666.

17. Gothelf, K. V., *J. Electroanal. Chem.* **2000,** 494, 147-150.

18. Sondag-Huethorst, J. A. M.; Fokkink, L. G. J., *Langmuir* **1992,** 8, 2560-2566.

19. Woods, R.; Hope, G. A.; Brown, G. M., *Colloids Surf., A* **1998,** 137, 339-344.

20. Persson, N. O.; Uvdal, K.; Liedberg, B.; Hellsten, M., *Progr Colloid Polym Sci* **1992,** 88, 100-109.

21. Ihs, A.; Uvdal, K.; Liedberg, B., *Langmuir* **1993,** 9, 733-739.

22. Finklea, H. O.; Snider, D. A.; Fedyk, J., *Langmuir* **1993,** 9, 3660-3667.

23. Bain, C. D.; Troughton, E. B.; Tao, Y.-T.; Evall, J.; Whitesides, G. M.; Nuzzo, R. G., *J. Am. Chem. Soc.* **1989,** 111, 321-335.

24. Wang, J.; Yoon, R.-H., *Langmuir* **2008,** 24, 7889-7896.

25. Parker, J. L.; Claesson, P. M.; Attard, P., *J. Phys. Chem.* **1994,** 98, 8468-8480.

26. Ishida, N.; Sakamoto, M.; Miyahara, M.; Higashitani, K., *Langmuir* **2000,** 16, (13), 5681-5687.

27. Ishida, N.; Sakamoto, M.; Miyahara, M.; Higashitani, K., *J. Colloid Interface Sci.* **2002,**

253, 112-116.

28. Nguyen, A. V.; Nalaskowski, J.; Miller, J. D.; Butt, H.-J., *Int. J. Miner. Process.* **2003,** 72, 215-225.

29. Sakamoto, M.; Kanda, Y.; Miyahara, M.; Higashitani, K., *Langmuir* **2002,** 18, 5713-5719.

30. Carambassis, A.; Jonker, L. C.; Attard, P.; Rutland, M. W., *Phys. Rev. Lett.* **1998,** 80, (24), 5357-5360.

31. Attard, P., *Langmuir* **2000,** 16, 4455-4466.

32. Tyrrell, J. W. G.; Attard, P., *Phys. Rev. Lett.* **2001,** 87, (17), 176104-1.

33. Attard, P.; Moody, M. P.; Tyrrell, J. W. G., *Physica A* **2002,** 314, 696-705.

34. Ederth, T.; Claesson, P.; Liedberg, B., *Langmuir* **1998,** 14, 4782-4789.

35. Ederth, T., *J. Phys. Chem. B* **2000,** 104, 9704-9712.

36. Ederth, T.; Liedberg, B., *Langmuir* **2000,** 16, 2177-2184.

37. Ederth, T.; Tamada, K.; Claesson, P. M.; Valiokas, R.; Colorado, R.; Graupe, M.; Shmakova, O. E.; Lee, T. R., *J. Colloid Interface Sci.* **2001,** 235, 391-397.

38. Rabinovich, Y. I.; Yoon, R.-H., *Langmuir* **1994,** 10, 1903-1909.

39. Zhang, J.; Yoon, R.-H.; Mao, M.; Ducker, W. A., *Langmuir* **2005,** 21, 5831-5841.

40. Zhang, J.; Yoon, R.-H.; Eriksson, J. C., *Colloids Surf., A* **2007,** 300, 335-345.

41. Yoon, R.-H.; Ravishankar, S. A. R., *J. Colloid Interface Sci.* **1996,** 179, 391-402.

42. Eriksson, J. C.; Ljunggren, S.; Claesson, P. M., *J. Chem. Soc., Faraday Trans. 2* **1989,** 85, (3), 163-176.

43. Claesson, P. M.; Christenson, H. K., *J. Phys. Chem* **1988,** 92, 1650-1655.

44. Christenson, H. K.; Claesson, P. M.; Berg, J.; Herder, P. C., *J. Phys. Chem.* **1989,** 93, 1472-1478.

45. Kekicheff, P.; Spalla, O., *Phys. Rev. Lett.* **1995,** 75, (9), 1851-1855.

46. Claesson, P. M.; Blom, C. E.; Herder, P. C.; Ninham, B. W., *J. Colloid Interface Sci.* **1986,** 114, (1), 234-242.

47. Attard, P., *J. Phys. Chem.* **1989,** 93, (17), 6441-6444.

48. Miklavic, S. J.; Chan, D. Y. C.; White, L. R.; Healy, T. W., *J. Phys. Chem.* **1994,** 98, 9022-9032.

49. Meyer, E. E.; Lin, Q.; Hassenkam, T.; Oroudjev, E.; Israelachvili, J. N., *Proc. Nat. Acad. Sci. U.S.A* **2005,** 102, 6839-6842.

Chapter 5

Surface Forces between Hydrophobized Gold Surfaces Submerged in Alcohols and in Water-Ethanol Mixtures

5.1 Abstract

Hydrophobic surfaces prepared by the adsorption of alkanethiols of different chain lengths onto a gold microsphere and a gold-coated flat glass plate were used to study the long-range hydrophobic force. Direct surface force measurements were conducted in air-equilibrated alcohols, water, and water/ethanol mixtures using an Atomic Force Microscope (AFM) at room temperature. The force measurements in alcohols showed that long range attractions existed in ethanol, 1-butanol and water between two C_4SH-coated gold surfaces. In methanol, the attractive force was slightly larger than the non-retarded van der Waals force.

The surface forces measured on C_4SH-, $C_{12}SH$- and $C_{16}SH$-coated gold surfaces in water/ethanol mixtures were purely attractive, and the surface force curves were all smooth, exhibiting no kinks or steps. With all of the three hydrophobic surfaces, the attraction was strongest in pure water and pure ethanol. The attraction decreased in the ethanol-water mixtures, its range and strength reaching a minimum at mole fractions in the range of 0.1 to 0.9, depending on the length of the hydrocarbon chain of the thiol used for hydrophobizing the gold surfaces. For all three cases, the decay length (D) and pre-exponential constant (C) passes through a minimum at the mole fraction of ethanol 0.2, indicating a transition from a water structure to an ethanol structure. Considerations of thin film thermodynamics suggests

that at low ethanol concentration more of the ethanol is expelled from the film while more of the water is expelled from the film at high ethanol concentration.

5.2 Background

For many years it has been recognized that both the water and ethanol surfaces exposed to air at room temperature are characterized by anomalously low surface entropies. Upon raising the temperature, however, the surface entropy increases. For a pure vapor-liquid system, it passes through a pronounced maximum before vanishing at the critical temperature.[1] This type of behavior is anticipated also for water or ethanol in contact with a (macroscopic) hydrophobic solid surface and can be explained, in a qualitative manner at least, by invoking the notion of a surface-induced, H-bond-dependent, dynamic structure that gradually becomes less extensive and less well-ordered at elevated temperatures.

Focusing on mixtures of water (1) and ethanol (2) in contact with air, we note that upon raising the ethanol concentration, the surface tension at first drops quite rapidly for alcohol mole fractions less than about 0.2 but only rather slowly, and almost linearly, in the range above $x_2 \approx 0.2$[2, 3]. From the surface tension curves and available vapor pressure data,[4] Butler and Wightman[5] showed that the Gibbs surface excess of ethanol, $\Gamma_{2(1)}$, passes through a pronounced maximum at $x_2 = 0.17$ (Figure 5.1). This maximum can be rationalized by invoking that above $x_2 = 0.17$, the interfacial structure and composition vary at a considerably slower rate than the bulk composition, whereas the reverse holds true below this particular mole fraction.

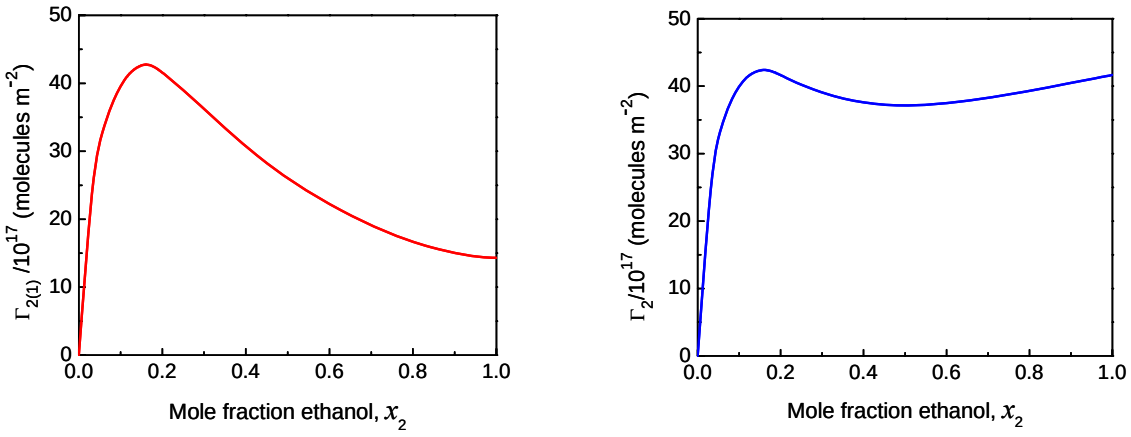

Figure 5.1. The Gibbs surface excess of ethanol, $\Gamma_{2(1)}$, in the water (1)-ethanol (2) mixture/air interface plotted *versus* the mole fraction of ethanol, x_2. Note the pronounced maximum for $x_2 \approx 0.17$. For comparison, the superficial density of ethanol, Γ_2, as obtained on the basis of Equations 5.1 and 5.2 are also shown. Temperature is 25ºC.

A more transparent estimate of the ethanol adsorption is obtained by assuming a mixed monolayer surface phase and introducing the condition

$$\Gamma_1 a_1 + \Gamma_2 a_2 = 1 \qquad (5.1)$$

to be used in conjunction with the expression for the Gibbs surface excess of ethanol, $\Gamma_{2(1)}$, viz.,

$$\Gamma_{2(1)} = \Gamma_2 - \Gamma_1 x_2 / x_1 \qquad (5.2)$$

where Γ_1 and Γ_2 stand for the (monolayer) superficial densities of water and ethanol, respectively, and a_1 and a_2 denote the corresponding molecular areas that are assumed to be constant. As above, x_1 and x_2 are the bulk mole fractions. In Figure 5.1, we show the (room temperature) ethanol adsorption isotherm obtained in this manner by relying on the $\Gamma_{2(1)}$ data obtained from Butler and Wightman,[5] and putting water molecular area a_1 equal to 10 Å^2 and ethanol molecular area a_2 equal to 24 Å^2 that are believed to be reasonable estimates of the molecular areas.[6] This isotherm exhibits, however, the unexpected features of a maximum at

x_2 = 0.13 and a faint minimum at x_2 = 0.40, indicating a rather complex, non-ideal interfacial behavior which the simplistic *ansatz* expressed by Equation 5.1 (in effect determining the surface phase considered) is unable to cover in a proper manner. Nevertheless, there is no question about the existence of a transition occurring between about x_2 = 0.1 and x_2 = 0.3, from a laterally mixed to a layer-wise arranged, alcohol-rich interface.

By the same token, the solubility of *e.g.*, oxygen in water-ethanol mixtures, studied long ago by Shchukarev and Tolmacheva,[7] was found to depend strongly on the structural features of water for mole fractions less than $x_2 \approx 0.2$, whereas for higher mole fractions, the formation of clusters of aggregated ethyl groups appear to be decisive for the oxygen solubility. This is in line with more recent IR, x-ray and neutron diffraction results.[8, 9]

From sum-frequency vibration spectroscopy (SFVS), studies of water-alcohol (methanol[10] and ethanol[11, 12]) mixtures, it has been clarified that in the low concentration range, the main event occurring is that dangling -OH groups (about one per 30 Å^2) which belong to the top layer of water molecules, successively become replaced by methyl (water-methanol) or ethyl (water-ethanol) groups. At high alcohol mole fractions, a hydrogen-bonded bilayer of alcohol molecules is present as the uppermost layer which includes about twice as many alkyl groups as the number of dangling -OH groups originally present in the case of a pure water surface. The purpose of our investigation, to be presented below, was to investigate to what extent the structural changes occurring for alcohol-water mixtures are reflected in the surface forces operating between hydrophobic solid surfaces submerged in such mixtures. To this end, we have employed an AFM set-up and made use of the colloidal probe technique.[13, 14]

5.3 Methods and Materials

5.3.1 Surface Force Measurements by Means of AFM

Surface force measurements were conducted at room temperature (22±1° C) using a Digital Instruments Nanoscope Ⅲ (Veeco Instruments, Inc., Santa Barbara, CA) atomic force microscope (AFM). The AFM instrument was equipped with a contact mode fluid cell and a scanner "E". All AFM force measurements were carried out in a manner described earlier by Zhang and Yoon.[14] Triangular silicon nitride (Si_3N_4) cantilevers (Model: NP-20, Veeco probes) were used for force measurement. The spring constant was calibrated according to the Cleveland method.[15] The force measurements were carried out without delay after thiol monolayers had been generated on the gold substrates.

5.3.2 Reagents

A Nanopure Ⅲ (Barnstead, IA) water purification system was employed to obtain double-distilled, deionized water with a resistivity of 18.2 MΩ/cm at 25ºC. To remove the particulates in water, a submicron postfilter (0.2 μm in pore size, Fisher Scientific) was integrated with the water purification unit. 1-butanethiol (C_4SH, 97%, TCI America), 1-dodecanethiol ($C_{12}SH$, 98%, Aldrich) and 1-hexadecanethiol ($C_{16}SH$, ≧ 97%, TCI America) were used to hydrophobize the gold substrates. Ethanol was obtained from AAPER alcohol, KY; methanol (99.8%) from Fluka; and 1-butanol from Fisher Scientific. Other liquid reagents, such as H_2SO_4 (98%, VMR International) and H_2O_2 (29.0-32.0%, Alfa Aesar), were used to clean the gold plates. All reagents listed were used as received.

5.3.3 Gold Plates

The surface force measurements were carried out using gold micro-spheres and gold-coated glass slides. Gold-coated glass slides were obtained by depositing gold onto glass using a vacuum evaporator. A 50 Å chromium layer was first deposited, followed by coating a 500 Å thick layer of gold. The chromium layer was necessary to ensure a strong adhesive bonding between gold and glass.

5.3.4 Gold Probes

Gold spheres with suitable diameters were produced following the procedure devised by Raiteri *et al*.[16] A gold wire (0.0127 mm dia, 99.9%, Alfa Aesar) was connected to a power supply (120V, AC), briefly creating a short circuit. This was done in a glass tray. A small aerosol cloud of gold particles was produced in the spark. In this way, gold spheres with a wide size distribution in the micrometer range were produced. Spheres with diameters 10~20 μm were chosen for the experiments. In each experiment, a gold sphere was glued onto a cantilever with EPON 1004 resin (Shell Chemical Co) using a homemade three-dimensional micromanipulator under an Olympus BH-2 light microscope.

5.3.5 Preparation of Hydrophobic Surfaces

To generate high-quality self-assembled thiol monolayer coatings, the gold substrates were thoroughly cleaned prior to hydrophobizing them by thiol coating.[17, 18] There are several cleaning procedures available for gold that are based on "piranha" solution,[19-21] chromic acid[22, 23] or UV/ozone treatment.[18, 24] For the present investigation, a flat gold plate was first

cleaned by immersion into a boiling "piranha solution" (30:70 H_2O_2/H_2SO_4) for 20 minutes. (WARNING: *piranha solution reacts violently with organic matter, especially when hot, and is extremely corrosive*). The surface was then flushed with nano-pure water for 1 minute to remove the residual acid, rinsed in pure ethanol for 2 minutes, and blow-dried with N_2 gas. The cleaned gold substrates were immediately contacted by a thiol solution.

A hot H_2O_2-H_2SO_4 mixture is an extremely strong oxidizing agent. It is not only efficient in removing organic contaminants but also tends to oxidize the gold surface itself.[17] The cleaning procedure results in a surface with zero water contact angle, which is due to formation of gold oxide (Au_2O_3). The gold oxide is thermodynamically unstable in the ambient and tends to decompose. It has been reported that ethanol reduces Au_2O_3 to gold.[17, 18] In the present work, a gold plate rinsed in ethanol for 2 minutes gave a contact angle of 65^o, indicating that the solvent washing substantially removed the oxidation product.

As for cleaning the gold sphere, a given sphere was glued onto an AFM cantilever and then cleaned by UV irradiation rather than being cleaned in the corrosive piranha solution. This was adopted to avoid the possibility of destroying the glue holding the sphere onto the cantilever. Typically, a gold sphere was flushed with ethanol, illuminated by a UV light (254 nm) for 2 hours, and then rinsed again with ethanol before being contacted in a thiol solution for hydrophobization.

Hydrophobization of the gold surfaces was achieved by immersing the spheres and plates in i) a 1×10^{-2} mM C_4SH-in-ethanol (absolute) solution for 5 hours, ii) a 1×10^{-2} mM $C_{12}SH$-in-ethanol solution for 2 hours, and iii) a 1×10^{-2} mM $C_{16}SH$-in-ethanol solution for 10 minutes. The strong chemical bonding between the -SH group and the gold surface

coupled with assembly causes the thiols adsorb spontaneously from solution.[19] The adsorption rate depends on critically the thiol concentration.[25] Dilution to 1×10^{-2} mM or less can be applied to form smooth monolayers, given sufficient time for the adsorption to reach a completion.[19] After the hydrophobization, the gold substrates were washed with ethanol and dried under a nitrogen gas stream. In a given force measurement, we used the same immersion time for gold plate and sphere. It was very important that the gold sphere was glued onto the cantilever prior to the hydrophobization procedure due to the poor adhesion between the glue and a hydrophobic gold sphere.

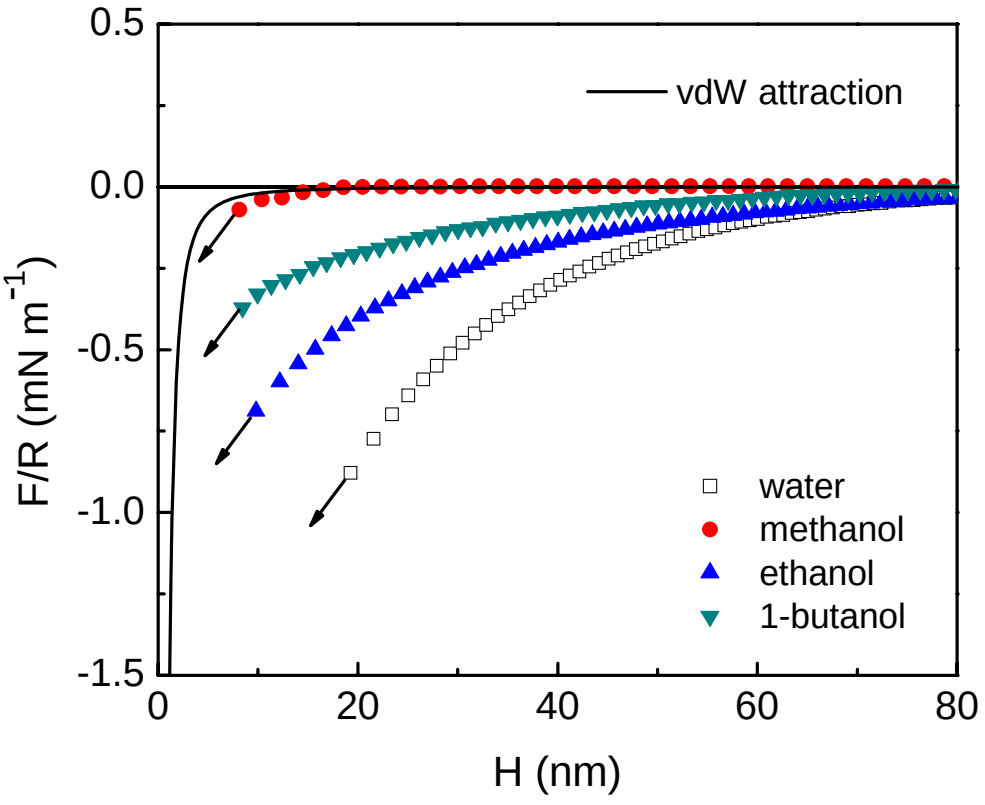

Figure 5.2. Surface force curves obtained for pure water, methanol, ethanol and 1-butanol at room temperature (22±1ºC) using C_4SH-coated gold surfaces, which were prepared by immersing gold surfaces in a 1×10^{-2} mM C_4SH-in-ethanol (absolute) solution for 5 hours.

5.4 Results and Discussion

Figure 5.2 shows the surface force curves recorded for the C_4SH-coated gold surfaces at room temperature in pure water, methanol, ethanol and 1-butanol, respectively. As shown, the strongest attraction was observed in pure water, but long-range attractions were also observed in ethanol and 1-butanol. With methanol, however, the attraction was almost as weak as the non-retarded van der Waals force. A commonality of these liquids is that all of them are H-bonding liquids.

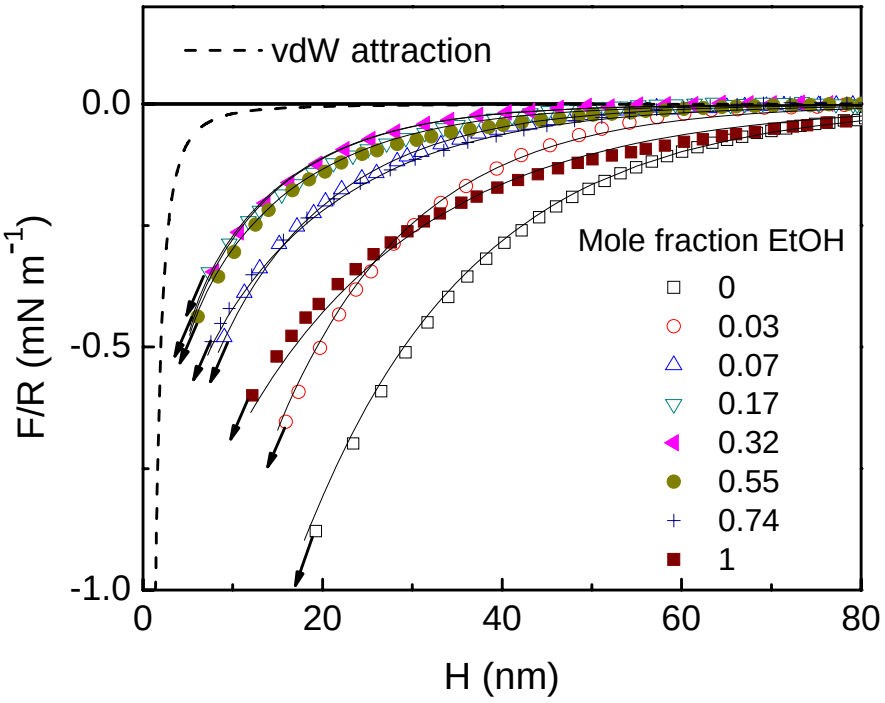

Figure 5.3. Surface force curves obtained at room temperature (22±1ºC) for water-ethanol mixtures using C_4SH-coated gold surfaces, which were prepared by immersing gold surfaces in a 1×10^{-2} mM C_4SH-in-ethanol (absolute) solution for 5 hours.

Boinovich and Emelyanenko[26] conducted the FTIR studies for the thin films of ethanol, butanol and pentanol sandwiched between fluorite (CaF_2) surfaces, and observed

changes in the stretching vibrations of the -OH and -CH groups at thicknesses below about 5 nm. This finding suggests that the structure of these H-bonded liquids in the vicinity of the solids is different from that of the bulk liquid. Although fluorite is hydrophilic, structural changes may also be expected when an H-bonded liquid is confined between hydrophobic surfaces such as thiol-coated gold. In this regard, the results presented in Figure 5.3 suggest that long-range attractions originate from increased structuring of liquids in the vicinity of hydrophobic surfaces.

Figure 5.3 shows the results of the surface force measurements conducted with C_4SH-coated gold substrates in varying concentrations of ethanol solutions. The water contact angle of the thiol-coated gold was 95^o. As shown, the long-range attraction was the strongest in pure water, and diminished with increasing ethanol concentrations. It reached a minimum at mole fractions in the range of 0.17−0.55, and began to increase as the ethanol concentration was further increased. A strong long-range attraction was observed in pure ethanol, but it was still weaker than in pure water.

Figure 5.4 shows a similar set of measurements conducted with C_{12}SH-coated gold substrates in varying mole fractions of ethanol. The water contact angle of the thiolated gold was 105^o. The trend was the same as obtained with the C_4SH-coated gold in that the long-range attraction decreased with increasing ethanol concentration reaching a minimum at mole fractions of 0.17−0.32, which was narrower in range than with the C_4SH-coated gold substrates. Also, the long-range attraction observed in pure ethanol was about the same as with pure water.

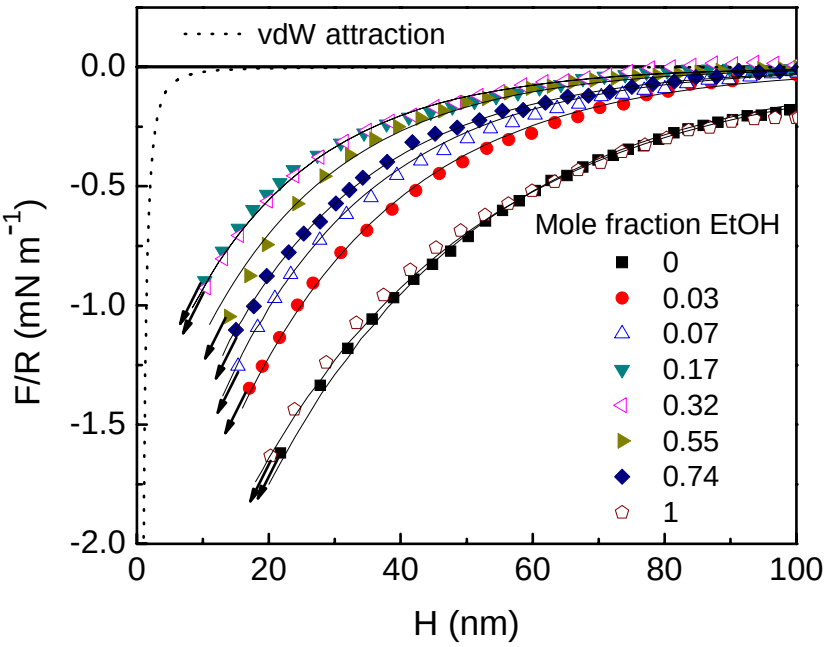

Figure 5.4. Surface force curves obtained at room temperature (22±1ºC) for water-ethanol mixtures using $C_{12}SH$-coated gold surfaces, which were prepared by immersing gold surfaces in a 1×10^{-2} mM $C_{12}SH$-in-ethanol (absolute) solution for 2 hours.

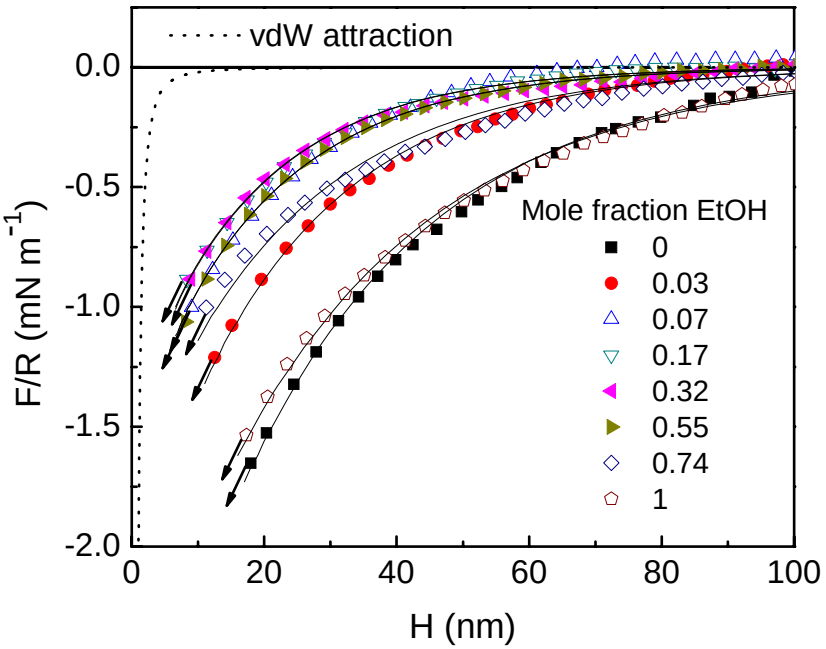

Figure 5.5. Surface force curves obtained at room temperature (22±1ºC) for water-ethanol mixtures using $C_{16}SH$-coated gold surfaces, which were prepared by immersing gold surfaces in a 1×10^{-2} mM $C_{16}SH$-in-ethanol (absolute) solution for 10 minutes.

A similar set of experiments was also conducted with $C_{16}SH$-coated gold substrates, and the results are presented in Figure 5.5. The weakest attractions were obtained in the mole fractions of 0.17−0.55, and the result obtained in pure ethanol was about the same as in pure water.

The attractive surface forces for ethanol-water mixtures were first seen by Ederth *et al*.[27] who, however, made just a couple of runs on solutions of ethanol in water (12.5 and 20% by weight). The forces he recorded are about an order of magnitude weaker than those we have obtained. However, the trend toward a rapidly diminishing surface force as a result of ethanol addition was also evident in his measurements.

It is noteworthy that all the surface forces recorded were purely attractive, and the force curves were all smooth without kinks or steps. Thus, these results do not support the charged-patch[28] or bridging nano-bubble[29] mechanism.

The results presented in Figures 5.3-5.6 have been fitted to single-exponential force law:

$$\frac{F}{R} = C\exp\left(-\frac{H}{D}\right) \tag{5.3}$$

where F denotes the measured surface force, R the radius of the gold sphere, C a pre-exponential constant, and D is the decay length. The C and D parameters obtained from the curve-fitting exercise are plotted in Figures 5.6-5.8 *versus* the ethanol mole fraction (x_2). In all three cases, both C and D parameters pass through minima at $x_2 = 0.2$. As discussed above, earlier investigations showed that a transition from a water-structure related to an ethanol-cluster related behavior takes place at this mole fraction[2, 3, 7]. At the same time, the top layer of ethanol molecules become more or less fully developed by changing from a truly

mixed water-ethanol monolayer to an ethanol surface layer devoid of dangling -OH groups.

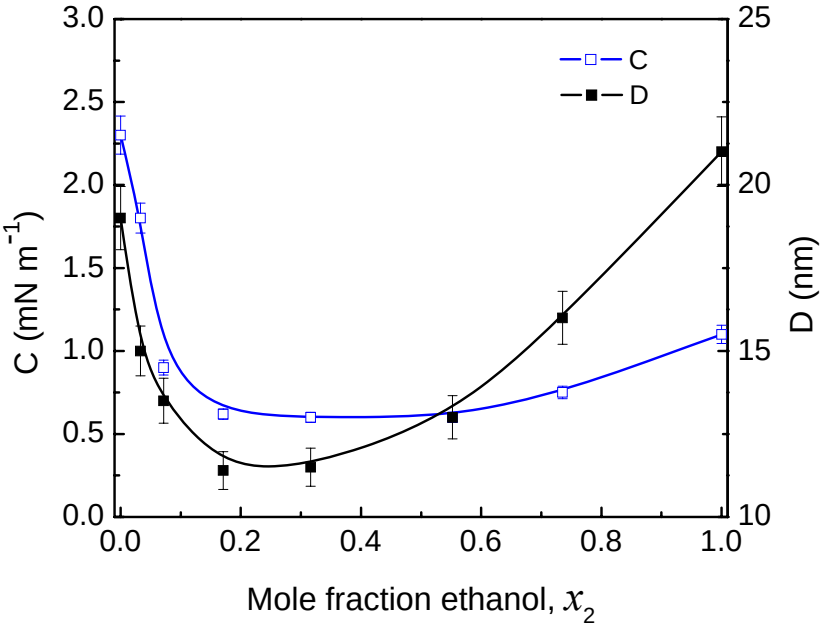

Figure 5.6. The parameters *C* and *D* in Equation 5.3 plotted versus the mole fraction of ethanol (x_2) for the case of C_4SH-coated gold surfaces.

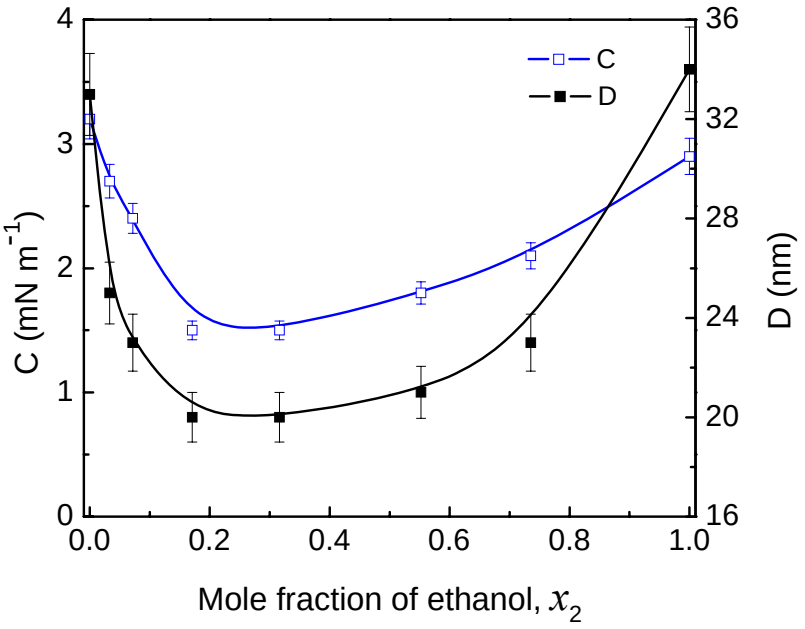

Figure 5.7. The parameters *C* and *D* in Equation 5.3 plotted versus the mole fraction of ethanol (x_2) for the case of C_{12}SH-coated gold surfaces.

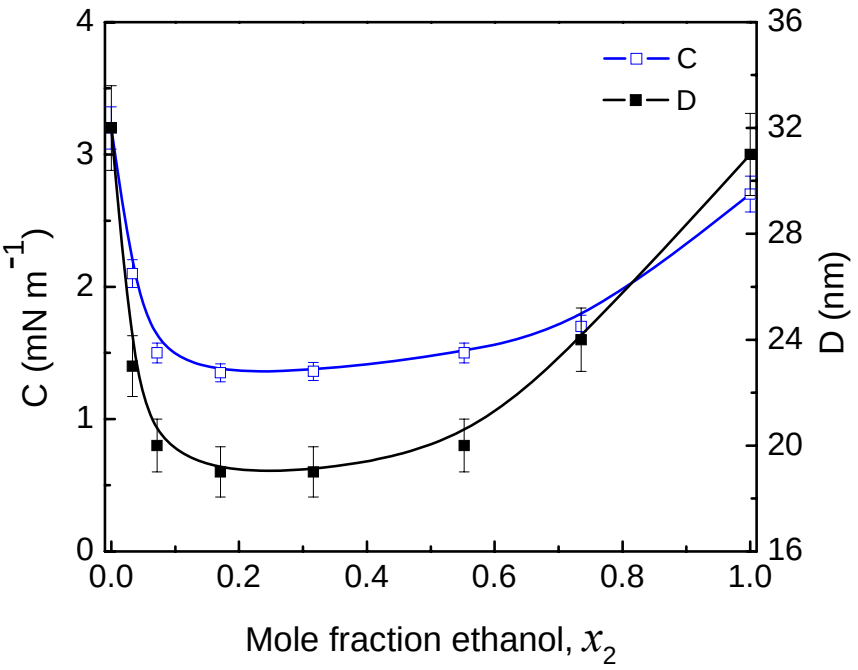

Figure 5.8. The parameters C and D in Equation 5.3 plotted versus the mole fraction of ethanol (x_2) for the case of $C_{16}SH$-coated gold surfaces.

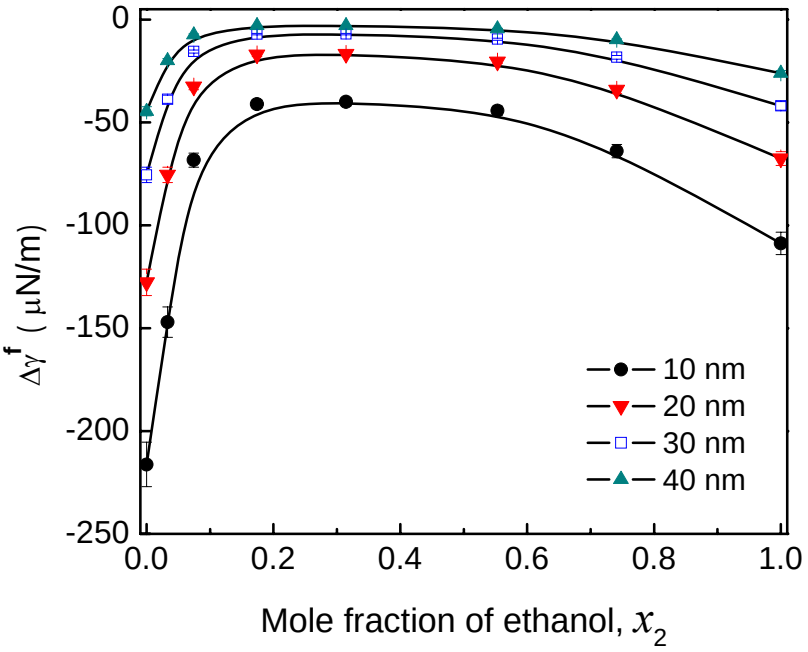

Figure 5.9. The $\Delta\gamma^f$ *versus* x_2 functions derived for the film thickness H = 10, 20, 30 and 40 nm by using the surface force data obtained for C_4SH-coated gold surfaces (Figure 5.3).

The exponential force law obtained (Equation 5.3) from the experimental data obtained with the C_4SH-coated gold (Figure 5.3) were employed to derive the $\Delta\gamma^f$-functions:

$$F / 2\pi R = \gamma^f - \gamma^{f,\infty} = \Delta\gamma^f \tag{5.4}$$

where γ^f represents the tension of the planar film of water with a thickness H, and $\gamma^{f,\infty}$ is the same at an infinite separation. Thus, $\Delta\gamma^f$ represents the change in film tension (or Gibbs free energy) as two surfaces approach each other from an infinitely large distance to H and can be related to the surface force measured at a given film thickness. Figure 5.9 shows the changes in $\Delta\gamma^f$ as a function of the mole fraction of ethanol at different separations, H. Invoking the ethanol partial vapor pressure determined by Dobson[4] (which was critically examined by Butler and Wightman[5]), it is then an easy matter to make use of the Gibbs surface tension equation analogue for a thin liquid film, viz.,

$$\left(\frac{\partial\Delta\gamma^f}{\partial\ln p_2}\right)_{T,H} = -\Delta\Gamma_2^{f,ex} \tag{5.5}$$

to derive the changes arising in the thin film of its ethanol content as a result of the attractive interaction between the two hydrophobic surfaces.

The results of such exercises are shown in Figure 5.10. It appears that at low ethanol concentrations in the bulk, the ethanol excess of a thin film is less than for a very thick film. In other words, upon letting the two hydrophobic surfaces approach each other, more ethanol than might be expected on a regular basis, is being expelled from the film. Conversely, for mole fractions approaching unity, upon thinning the water component is preferably being expelled from the film and we are left with a positive excess of ethanol. Recall that diminishing the absolute value of the hydrophobic attraction force means that the film tension increases. As a consequence, according to Equation 5.5, $\Delta\Gamma_2^{f,ex}$ must be negative.

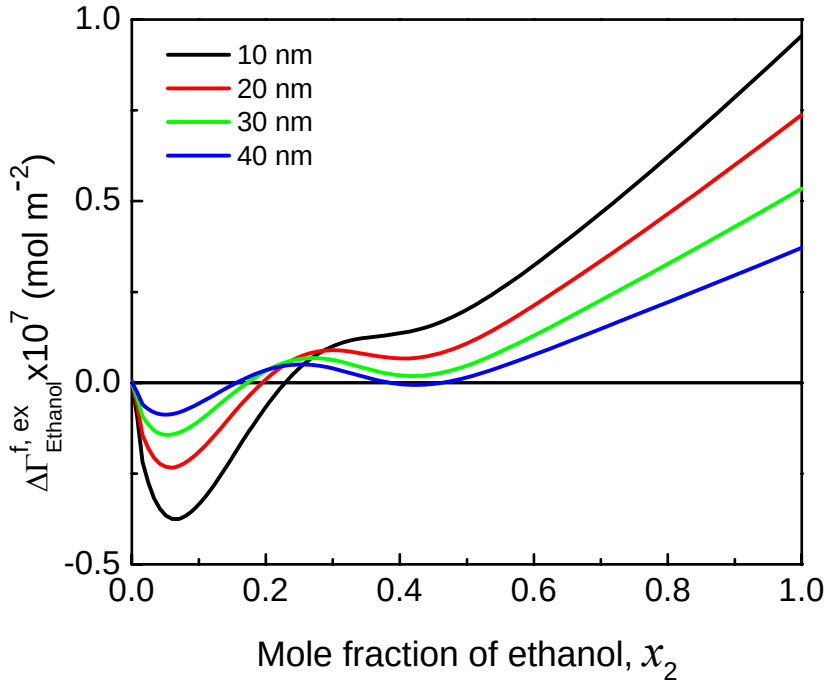

Figure 5.10. The film excess of ethanol, $\Delta\Gamma_2^{f,ex}$, derived from the $\Delta\gamma^f$-functions in Figure 5.9 by applying Equation 5.4.

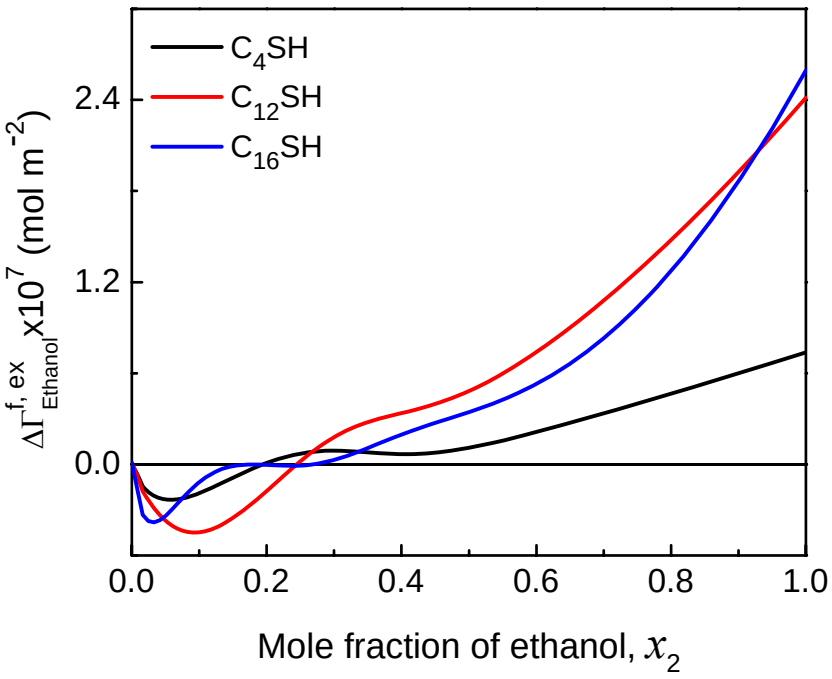

Figure 5.11. The film excess of ethanol, $\Delta\Gamma_2^{f,ex}$ for H = 20 nm obtained for C_4SH-, $C_{12}SH$- and $C_{16}SH$-coated gold surfaces.

Figure 5.11 shows the ethanol film excess functions, $\Delta\Gamma_2^{f,ex}$ (x_2) for H = 20 nm generated by employing the surface force data recorded for C_4SH-, $C_{12}SH$- and $C_{16}SH$-coated gold surfaces. A semi-quantitative agreement is noted. For all three cases $\Delta\Gamma_2^{f,ex}$ is negative for low and positive for high ethanol mole fractions.

5.5 Model Considerations

In terms of the recently presented bridging-cluster theory[30] of hydrophobic attraction that might apply for dilute solutions of alcohol in water, the pre-exponential constant C is given by the expression:

$$C = \left(\frac{2\pi k_B T}{a_2} \right) \times \exp\left(- \frac{2a_2 \Delta\gamma_{eff}}{k_B T} \right) \qquad (5.6)$$

where a_2 is the (mean) cross-sectional area of a cluster and $\Delta\gamma_{eff}$ stands for the effective change in interfacial free energy per unit area, arising due to attaching the cluster ends to the hydrophobic surface. Assuming the latter to be a positive quantity, approximately independent of the cluster cross section, one can anticipate C to diminish when the cross section area a_2 becomes larger. Moreover, the inverse of the decay length D is simply to be regarded as the work per unit length to form the middle part of a long bridging cluster. It should increase with a_2, and upon raising the ethanol concentration. In this way, we can tentatively account for the rapidly decreasing decay length D upon adding alcohol to water, at least in a preliminary way.

As to the other end of the concentration scale, *i.e.*, x_2 is high, the ethyl groups and the H-bonded -OH groups plus water molecules may form alternating layers that are parallel to the hydrophobic surface. The structure may gradually become less and less well ordered with

distance away from the surface. In this concentration range, our original order-parameter-based theory[31] might apply, in which case the decay length would be given by the simple expression:

$$D = \left(c_3 / 2c_2\right)^{1/2} \tag{5.7}$$

where the cooperative constant c_3 represents a tendency to avoid gradients in the order parameter, s, inside the thin film. A comparatively large value of c_3 means that the layered structure arrangement will prevail for some distance toward the core of the thin film, giving rise to an attractive surface force. Adding more water should cause a reduced cooperatively (*i.e.,* a smaller c_3) and increase the free energy of forming an ordered alcohol-water (*i.e.*, a larger c_2), both contributing to decreasing the decay length D.

5.6 Conclusions

AFM surface force measurements were conducted between hydrophobized gold surfaces in water, C-1 to C-4 alcohols, and ethanol-water mixtures. Long-range attractions were observed in all of these H-bonding liquids, the range and strength of the attractions decreasing in the order of water, ethanol, butanol, and methanol. In the ethanol-water mixtures, the attractions were the maximum when the ethanol mole fraction was zero and unity, and the strength and range of the attractions varied with composition. At the higher mole fractions, the long-range attraction increased, most probably due to the increased structuring of ethanol. Since each ethanol molecule forms two H-bonds, it is likely that layered, laterally homogenous ethanol structures are formed at higher mole fractions. At lower mole fractions, three-dimensional water structure may be formed in view of the fact

that each water molecule forms four H-bonds of equal strength.

The results obtained in the present work may thus indicate that the long-range attraction (or hydrophobic force) originates from the liquid structure. The structure of water or ethanol is disturbed in the presence of the other, causing a decrease in the hydrophobic force. That the hydrophobic force increases with decreasing separation between hydrophobic surfaces suggests that the structuring is induced by the hydrophobic surface.

5.7 Acknowledgment

This work was funded by National Energy Technology Laboratory, U. S. Department of Energy (DE-FC26-02NT41607).

5.8 References

1. Eriksson, J. C., *Arkiv Kemi* **1966,** 26, (2), 49-72.

2. Butler, J. A. V.; Wightman, A., *J. Chem. Soc. (London)* **1932**, 2089-2097.

3. Teitelbaum, B. Y.; Gortalova, T. A.; Sidorova, E. E., *Doklady Acad. Nauk S. S. S. R* **1951**, (25), 911.

4. Dobson, H. J. E., *J. Chem. Soc., Trans.,* **1925,** 127, 2866-2873.

5. Butler, J. A. V.; Wightman, A., *J. Chem. Soc.* **1932**, 2089-2097.

6. Li, Z. X.; Lu, J. R.; Styrkas, D. A.; Thomas, R. K.; Rennie, A. R.; Penfold, J., *Mol. Phys.* **1993,** 80, (4), 925-939.

7. Shchukarev, S. A.; Tolmacheva, T. A., *ZhurnalStrukt. Khim* **1968,** 9, 21-28.

8. Nishi, N.; Takahashi, S.; Matsumoto, M.; Tanaka, A.; Muraya, K.; Takamuku, T.;

Yamaguchi, T., *J. Phys. Chem.* **1995,** 99, 462-468.

9. Dixit, S.; Crain, J.; Poon, W. C. K.; Finney, J. L.; Soper, A. K., *Nature* **2002,** 416, 829-832.

10. Liu, W.-T.; Zhang, L.; Shen, Y. R., *J. Chem. Phys.* **2006,** 125, 144711-1 -6.

11. Sung, J.; Park, K.; Kim, D., *J. Korean. Phys. Soc.* **1989,** 44, 1394.

12. Sung, J.; Park, K.; Kim, D., *J. Am. Chem. Soc* **1989,** 111, 321-335.

13. Ducker, W. A.; Senden, T. J.; Pashley, R. M., *Nature* **1991**, (353), 239-241.

14. Zhang, J.; Yoon, R.-H.; Mao, M.; Ducker, W. A., *Langmuir* **2005,** 21, 5831-5841.

15. Cleveland, J. P.; Manne, S.; Bocek, D.; Hansma, P. K., *Rev. Sci. Instrum.* **1993,** 64, (2), 403-405.

16. Raiteri, R.; Preuss, M.; Grattarola, M.; Butt, H.-J., *Colloids Surf., A* **1998,** 136, 191-197.

17. Ron, H.; Rubinstein, I., *Langmuir* **1994,** 10, 4566-4573.

18. Ron, H.; Rubinstein, I., *J. Am. Chem. Soc.* **1998,** 120, 13444-13452.

19. Bain, C. D.; Troughton, E. B.; Tao, Y.-T.; Evall, J.; Whitesides, G. M.; Nuzzo, R. G., *J. Am. Chem. Soc* **1989,** 111, 321-335.

20. Kane, V.; Mulvaney, P., *Langmuir* **1998,** 14, 3303-3311.

21. Giesbers, M.; Kleijn, J. M.; Stuart, M. A. C., *J. Colloid Interface Sci.* **2002,** 252, 138-148.

22. Hillier, A. C.; Kim, S.; Bard, A. J., *J. Phys. Chem.* **1996,** 100, 18808-18817.

23. Biggs, S.; Mulvaney, P., *J. Chem. Phys.* **1994,** 100, (11), 8501-8505.

24. Sondag-Huethorst, J. A. M.; Fokkink, L. G. J., *Langmuir* **1992,** 8, 2560-2566.

25. Karpovich, D. S.; Blanchard, G. J., *Langmuir* **1994,** 10, 3315-3322.

26. Boinovich, L. B.; Emelyanenko, A. M., *Adv. Colloid Interface Sci.* **2002,** 96, 37-58.

27. Ederth, T., *J. Phys. Chem. B* **2000,** 104, 9704-9712.

28. Miklavic, S. J.; Chan, D. Y. C.; White, L. R.; Healy, T. W., *J. Phys. Chem.* **1994,** 98, 9022-9032.

29. Parker, J. L.; Claesson, P. M.; Attard, P., *J. Phys. Chem.* **1994,** 98, 8468-8480.

30. Eriksson, J. C.; Henriksson, U., *Langmuir* **2007,** 23, 10026-10033.

31. Eriksson, J. C.; Ljunggren, S.; Claesson, P. M., *J. Chem. Soc. Faraday Trans. 2* **1989,** 85, (3), 163-176.

Chapter 6

Hydrophobic attraction originates from changes in water structure: thermodynamic evidence

6.1 Abstract

In 1982, Israelachvili and Pashley[1] reported the first measurements of a hitherto unknown attractive force between two mica surfaces hydrophobized in cetyltrimethylammonium bromide (CTAB) solutions. Follow-up experiments conducted by many investigators confirmed their results, while others suggested that the "hydrophobic force" is an artifact due to nanobubbles or cavities.[2-4] Evidences for the latter included the discontinuities (or steps) in the force *versus* distance curves[5] and the pancake-shaped nano-bubbles seen in atomic force microscopic (AFM) images.[3] Recent measurements[6-8] conducted in degassed water showed, however, smooth force *versus* distance curves, indicating that the hydrophobic force is not an artifact due to nanobubbles. In the present work, we have conducted AFM force measurements with gold substrates hydrophobized by self-assembly of alkanethiols with different chain lengths. The measurements carried out at 10-40ºC show that the hydrophobic force decreases with temperature for all cases. Thermodynamically, these results imply that as two hydrophobic surfaces approach each other the excess film entropy per unit area (S^f) decreases, which suggests that the hydrophobic force is due to the structuring of water in the thin film confined by two hydrophobic surfaces rather than from an artifact. Our analysis also shows that the hydrophobic interaction entails a reduction in the excess film enthalpy per unit area (H^f), with the change in excess film enthalpy (ΔH^f) being slightly more negative than the corresponding entropy term ($T\Delta S^f$). The difference between these two quantities gives the change in film tension ($\Delta\gamma^f$) or in Gibbs (free) energy per unit area. By multiplying this difference with 2π,

in accordance with the Derjaguin approximation,[9] one obtains the surface force (F) normalized by the radius (R) of the gold sphere used in the force measurement. The nearly parallel enthalpy and entropy changes observed may be associated with the formation of clathrate cages at the hydrophobic surface/water interfaces of the thin water film by virtue of cooperative hydrogen bonding. The presence of the clathrate cages at the hydrocarbon-water interface is supported by the decrease in water density observed by recent neutron reflectivity measurements.[10] Surface force measurements conducted in ethanol-water mixtures also show that the long-range attractions are due to the structuring of the liquids in the thin liquid films between hydrophobic surfaces.

6.2 Introduction

There have been intense debates in the scientific community as to the existence of a long-range hydrophobic force between hydrophobic solid surfaces in water and its possible origin. After the observations of such a non-DLVO force firstly made by Israelachvili and Pashley[1] for in situ hydrophobized mica using a surface force apparatus (SFA) in the early 1980s, the scientific community had been divided into different camps. One argues that the long-range hydrophobic force is actually the capillary force in view of the "discontinuities" (or steps) characteristic, attributed to nano-bubble bridging, for the force curves recorded[2, 11, 12]. Another one claims that the additional attractive force is related to the structuring of confined water induced by the hydrophobic solid surface.[13, 14] And the third one insists that, however, the hydrophobic force is an electrostatic correlation force of charged patches on the hydrophobic surfaces.[15, 16] Addressing the controversy should help us better understand a variety of important issues ranging from self-assembly, protein folding and stability, molecular origin of life, enzyme-coenzyme interactions, recovery of energy minerals (oil, coal, bitumen, kerogen, methane hydrates), *etc.*

A large part of the debate is due to the difficulty in preparing molecularly smooth and stable hydrophobic surfaces for surface force measurements. For unstable hydrophobic surfaces, indicated by contact angle hysteresis, the long-range attractions measured are usually believed to be ascribed to significant molecular rearrangement,[17] local charge fluctuations[18] when two hydrophobic surfaces come into contact in water, or patchy bilayer formation when the surfaces were immersed in water.[16] Preparation of ideal hydrophobic surfaces is thus of importance to decide whether there is actually a true long-range hydrophobic force arising from thin water film between hydrophobic solid surfaces. Some of the supposedly most reliable surface force data were produced by Claesson and Christenson[19] and, more recently, by Lin *et al*.[20] using Langmuir-Blodgett deposited monolayers of a double chain surfactant dioctadecyldimethylammonium bromide (DODAB) on mica. Unfortunately, these surfaces lack full stability, especially when exposed to salt solutions. More recently, self-assembly of long single-chain thiols on gold from alcohol solution has been used to generate robust hydrophobic surfaces. Ederth *et al*.[21] hydrophobized gold substrates in 1 mM C_{16}SH-in-ethanol solutions and used them for surface force measurements in pure water. However, their force curves exhibited steps, indicating coalescence of pre-existing gas bubbles on the two hydrophobic surfaces during the measurements. Under the conditions employed by these investigators, we obtained essentially the same results.[22] But it was found that the steps disappeared when the thiol-coated gold surfaces were rinsed with appropriate organic solvents after hydrophobizing them in 1 mM solutions for long periods of time (> 6 hours), or when they were hydrophobized in a dilute (1×10^{-2} mM) solution for short periods of time (< 10 minutes). Thus, one has to apply appropriate treatment times and concentrations to ensure that the hydrophobic surfaces generated by chemisorbing an alkanethiol entail little else but full monolayers of thiols firmly bonded by their -SH end groups to the gold substrate. Otherwise, too small surface forces may be measured or nano bubbles will nucleate on

surfaces causing steps in the force curves.

In the present work, gold spheres and gold-coated glass plates were hydrophobized using appropriate treating procedure. The gold surfaces, treated with alkanethiols with different chain lengths (n = 2−16), were used to measure the surface forces using the AFM colloidal probe technique.[23, 24] A Veeco Multimode AFM equipped with a temperature controller was used to record the forces in pure water at different temperatures.

6.3 Materials and Methods

6.3.1 Chemicals

The alkanethiols used to hydrophobize the gold surfaces in this work are H-$(CH_2)_n$-SH, denoted briefly as C_nSH, where n = 2, 4, 12, 16. They are all liquid at room temperature. Ethanethiol (C_2SH; 98%), 1-butanethiol (C_4SH; 97%) and 1-hexadecanethiol ($C_{16}SH$; ≥ 97%) were purchased from TCI America (Portland, USA). 1-dodecanethiol ($C_{12}SH$; 98%) was obtained from Aldrich. They were stored in the refrigerator and used without further purification. The alkanethiol solutions were prepared in pure ethanol (Decon Laboratories, Inc). H_2SO_4 (98%, VMR International) and H_2O_2 (29.0 – 32.0%, Alfa Aesar) were used as received to clean the gold plates. Ultrapure water (18.2 MΩ • cm^{-1}, 25ºC) was obtained using a Millipore direct-Q3 ultrapure (Millipore, MA) water system.

6.3.2 Gold Surfaces Preparation

The flat gold surfaces (0.5 × 0.5 sq inch) were produced by coating smooth glass substrates with a thermally evaporated 500 angstrom thick Au (99.9%) in a vacuum evaporator. A 50 angstrom Cr interlayer was used to promote Au adhesion. The maximum peak-to-valley distance was 3.3 nm and a typical root mean square (rms) roughness of the gold-coated glass over a surface area of 1 × 1 μm^2 was 0.8 nm, as measured by AFM.

Gold spheres with suitable size were produced following the procedure devised by Raiteri *et al*.[25] Gold wire (0.0127 mm dia, 99.9%), purchased from Alfa Aesar, was connected to a power supply (120V, AC), briefly creating a short circuit. This was done in a glass tray. A small aerosol cloud of gold micro particles was produced in the electric spark. In this way, gold spheres with a wide size distribution in the micrometer range were produced. Spheres with radius of 3~7 μm were chosen for the surface force measurements.

6.3.3 Colloidal Probe Preparation

In order to measure the force between surfaces of a gold microsphere and gold-coated flat glass, a gold probe was made by gluing a gold sphere onto to the end of a AFM cantilever with Epon 1004 (Shell Chemical Co) using a homemade 3-dimensional (X, Y, Z) translation stage under a high-resolution optical microscope (BH2, Olympus). The polymer glue which melts at about 105ºC, is insoluble in water. The translation stage is equipped with a hot plate, which sits under the microscope and was used to melt the polymer glue. A clean glass plate with gold microspheres and tiny particles of glue spreading on it was placed on the hot plate. An AFM cantilever, gripped by a clump, was attached to the 3-dimensional translation stage. The AFM cantilever was cleaned by soaking in pure ethanol and followed by irradiating using a UV lamp (Model ENF-240 C, Spectronics Corporation; $\lambda = 254$ nm) for 10 minutes before use. Firstly, the cantilever approached to a tiny glue drop and the cantilever tip dipped into it. Then the glue-laden tip came close to a desired gold sphere. The radius of sphere R was determined under the microscope. When the sphere was touched by the glue, it spontaneously transfered to the cantilever tip due the capillary force.

6.3.4 Hydrophobization of Gold

To obtain high-quality thiol monolayers, the carbonaceous impurities on gold have to

be removed first. The gold plates were cleaned by soaking in a boiling piranha etch solution (a mixture of 10 ml H_2O_2 and 20 ml H_2SO_4) for 20 minutes and then washed by rinsing with nanopure water for 1 minute, followed by an ethanol wash for 2 minutes. This was done in a fume hood. (**Caution**: *piranha solution reacts violently with many organic materials and should be used with extreme care*). For the cases of gold spheres, they were cleaned after they had been glued onto AFM cantilever springs. To prevent the glue from being destroyed by the piranha solution, each gold sphere was flushed with ethanol, exposed in a short-wave UV light (λ = 254 nm) for 2 hours, and then rinsed with ethanol again. The high energy UV radiation can decompose and remove the organic compounds on gold.

All glassware such as volumetric flasks and pyrex dishes, used to prepare and contain thiol solutions, were left overnight in sulfuric acid bath and cleaned by rinsing in ultrapure water. Gold surfaces were hydrophobized with alkanethiols by soaking in ethanolic solution of the alkanethiol for a desired period of time. After self-assembly, the surfaces were thoroughly rinsed with pure ethanol and water and then dried in a nitrogen gas stream. For a given force measurement, a gold sphere and a gold-coated glass were soaked in the same solution at the same time, so that the hydrophobicity of the two microscopic surfaces would be the same.

In the present study, gold surfaces were hydrophobized using short and long-chain alkanethiols. The monolayers with different hydrocarbon chain lengths were obtained by placing gold substrates in 1 mM solution of ethanethiol in ethanol for 6 hours, 1×10^{-2} mM ethanolic solution of butanethiol for 5 hours, 1×10^{-2} mM dodecanethiol for 3 hours and in 1×10^{-2} mM hexadecanethiol for 10 minutes, respectively. Previous contact angle and force measurement studies established that these procedures produce monolayers that can cover the entire gold surface. To ensure the accuracy of the experiment, for every set of experiment, fresh thiol surfactant solutions were used to prepare the hydrophobic coatings, because the

ethanolic thiol solutions degrade with time.

6.3.5 AFM Force Measurement

Surface force measurements with temperature control were carried out using a Nanoscope IVa (Digital Instruments, Inc.) in Nanoscale Characterization and Fabrication Laboratory (NCFL) at Virginia Tech. The MultiMode AFM was equipped with a heater/cooler accessory, which enables force measurement at both reduced and elevated temperatures. Primary components of the equipment include a heater/cooler Peltier element, a specialized scanner "J", a scanner cooling system which is comprised of a peristaltic pump and an ice bucket, and a Digital Instruments Thermal Applications Controller (TAC) which set and control the liquid temperature by regulating the Peltier element. The Peltier element was plugged into the connector on top of the scanner. The coated flat gold sample was mounted onto a sample puck and placed under the glass fluid cell sealed with a silicone O-ring. The metallic sample puck was placed on top of the Peltier element. Triangular silicon nitride cantilevers (NP-20, Veeco Probes, Inc.) bearing the gold microspheres were used for the force measurements. The spring constant (k) were determined using the resonant frequency technique.[26] The unloaded and loaded resonant frequencies were obtained using Tapping mode AFM. In each experiment, the liquid cell, used to hold the sphere probe, was cleaned in an ultrasonic water bath. Ultrapure water was injected into liquid cell for force measurement using a Norm-Ject syringe. All of the measurements were conducted in air-equilibrated solution. The separation distance (H) between the gold sphere and the flat-gold coated glass plate was measured by monitoring the deflection of the cantilever on which the gold sphere was attached. Measured forces (F) were normalized with respect to the radii (R) of the gold spheres.

The initial measurements were conducted in water at 10ºC and subsequently at 20, 30,

and 40ºC. It usually takes 15 minutes for water temperature to increase 10ºC. Because the reflective index of water changes with temperature, the deflection voltage signal of AFM changes with temperature as well. The stabilization of deflection voltage signal indicates the water temperature reaches the target temperature. After the measurement at 40ºC, the temperature was tentatively brought back to 20ºC and the experiment repeated to check the reproducibility and the stability of the hydrophobic surfaces at the higher temperatures. The force measurements were reproducible, and the data presented here represent the results of 2-3 repeat experiments at a given temperature.

The force measurements were also carried out using a Nanoscope Ⅲ (Digital Instruments, Inc.) atomic force microscope in ethanol-water mixtures at the room temperature (22±1ºC) in our lab. The MultiMode AFM was equipped with a standard fluid cell and a scanner "E". The water used in the present work was purified using the Millipore Direct Q-3 water purification system. No efforts were made to conduct the measurements in degassed water or ethanol-water mixtures.

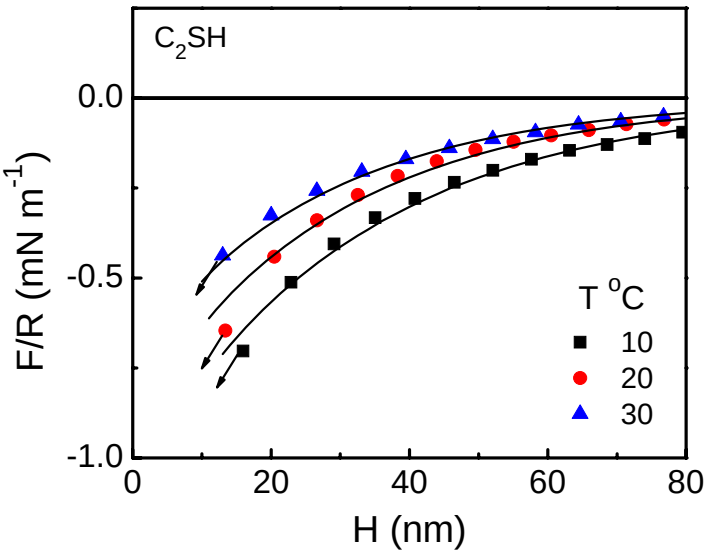

Figure 6.1. The long-range attractive forces between C_2SH-hydrophobized gold sphere and gold-coated glass plates as measured in air-equilibrated water at different temperatures. The solid lines represent fits of the data using a single-exponential force function of Equation 6.1, with D = 32, 29, 28 nm and C = 1.05, 0.87 and 0.7 mN/m at 10, 20, and 30, respectively.

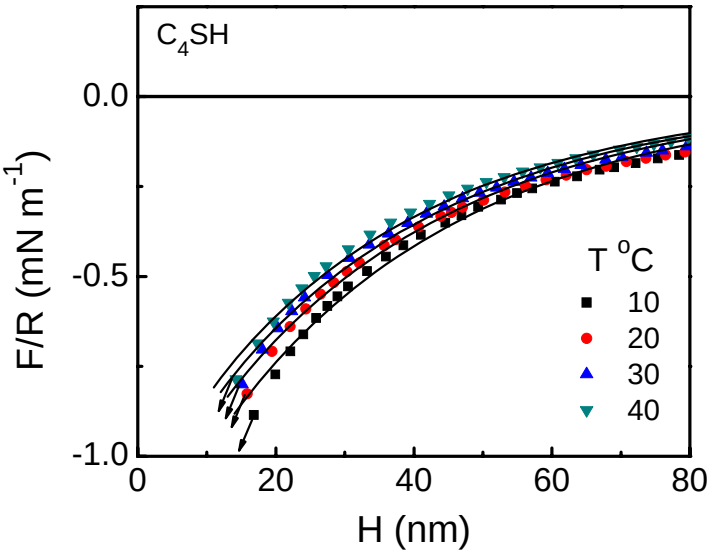

Figure 6.2. The long-range attractive forces between C_4SH-hydrophobized gold sphere and gold-coated glass plates as measured in air-equilibrated water at different temperatures. The solid lines represent fits of the data using a single-exponential force function of Equation 6.1, with D = 35, 34.5, 34.0, 33.5 nm and C = 1.3, 1.2, 1.15, and 1.1 mN/m at 10, 20, 30, and 40ºC, respectively.

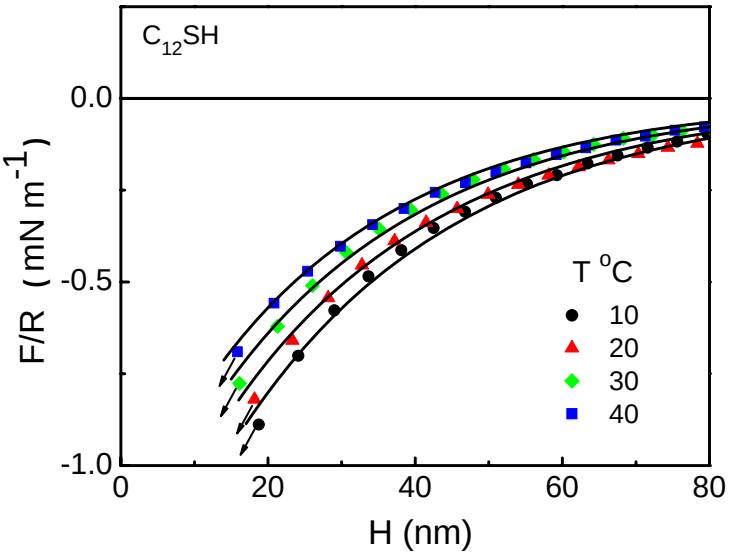

Figure 6.3. The long-range attractive forces between $C_{12}SH$-hydrophobized gold sphere and gold-coated glass plates as measured in air-equilibrated water at different temperatures. The solid lines represent fits of the data using a single-exponential force function of Equation 6.1, with D = 30, 29.5, 28.5, 27.5 nm and C = 1.55, 1.4, 1.28, and 1.17 mN/m at 10, 20, 30, and 40ºC, respectively.

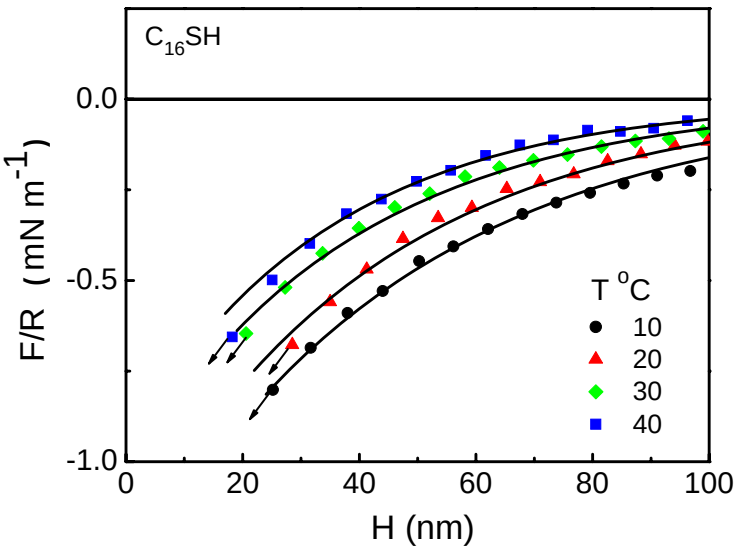

Figure 6.4. The long-range attractive forces between $C_{16}SH$-hydrophobized gold sphere and gold-coated glass plates as measured in air-equilibrated water at different temperatures. The solid lines represent fits of the data using a single-exponential force function of Equation 6.1, with D = 47.7, 42.4, 39.0, 35.0 nm and C = 1.37, 1.25, 1.03, and 0.95 mN/m at 10, 20, 30, and 40ºC, respectively.

6.4 Results and Discussion

6.4.1 Effect of Temperature

The interaction forces (F) measured between two hydrophobized gold surfaces as a function of separation distance (H) in air-equilibrated water over a range of temperatures are presented here. Figure 6.1, 6.2, 6.3 and 6.4 shows the force *versus* distance curves obtained at 10, 20, 30 and 40ºC for gold surfaces coated with C_2SH, C_4SH, $C_{12}SH$ and $C_{16}SH$, respectively. All of the curves are smooth without steps as shown, indicating that the surface forces measured are not due to the coalescence of pre-existing gas bubbles during the measurements. The isotherms recorded can be represented by a single-exponential expression:

$$F/R = -C\exp(-H/D) \qquad (6.1)$$

where F denotes the measured surface force, normalized by the radius of the gold sphere, R, and H is the closest separation distance between the gold sphere and plate. The solid lines in Figure 6.1, 6.2, 6.3 and 6.4 represent Equation 6.1 with appropriate C and D values that best fit the experimental data. Figure 6.5 shows the same data as shown in Figure 6.4 for $C_{16}SH$-coated gold which was plotted on a log-linear scale. The measured forces can be converted to film tension changes by means of the Derjaguin approximation:[9, 13]

$$F/2\pi R = \gamma^f - \gamma^{f,\infty} = \Delta\gamma^f = \Delta G^f \qquad (6.2)$$

where γ^f represents the tension of the planar film of water with a thickness H, and $\gamma^{f,\infty}$ is the same at an infinite separation. Thus, $\Delta\gamma^f$ represents the change in film tension (or Gibbs free energy ΔG^f) as two surfaces approach each other from an infinitely large distance to a given separation distance H. The value of $2\pi\Delta\gamma^f$ is the surface force actually measured for sphere-plate geometry.

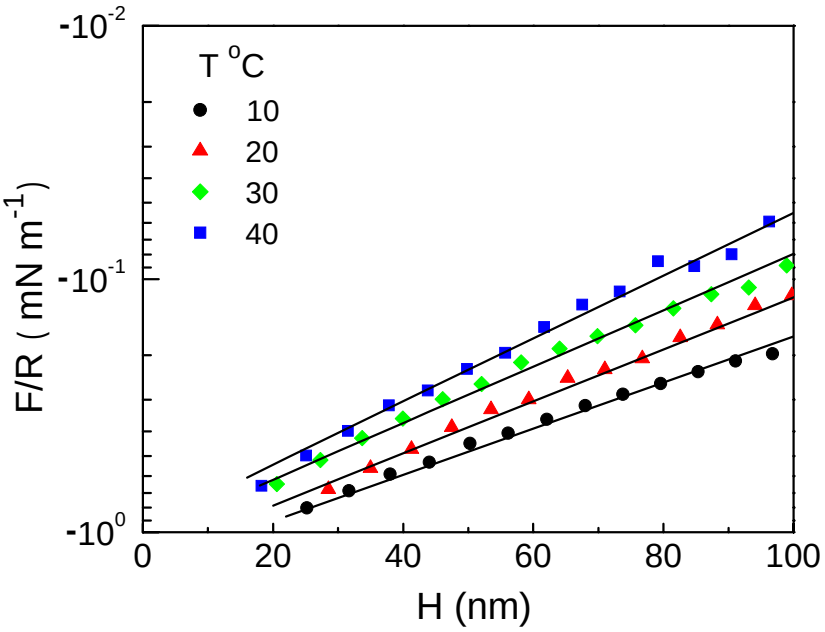

Figure 6.5. Same data as shown in Figure 6.4 for C_{16}SH-coated gold was plotted on a log-linear scale.

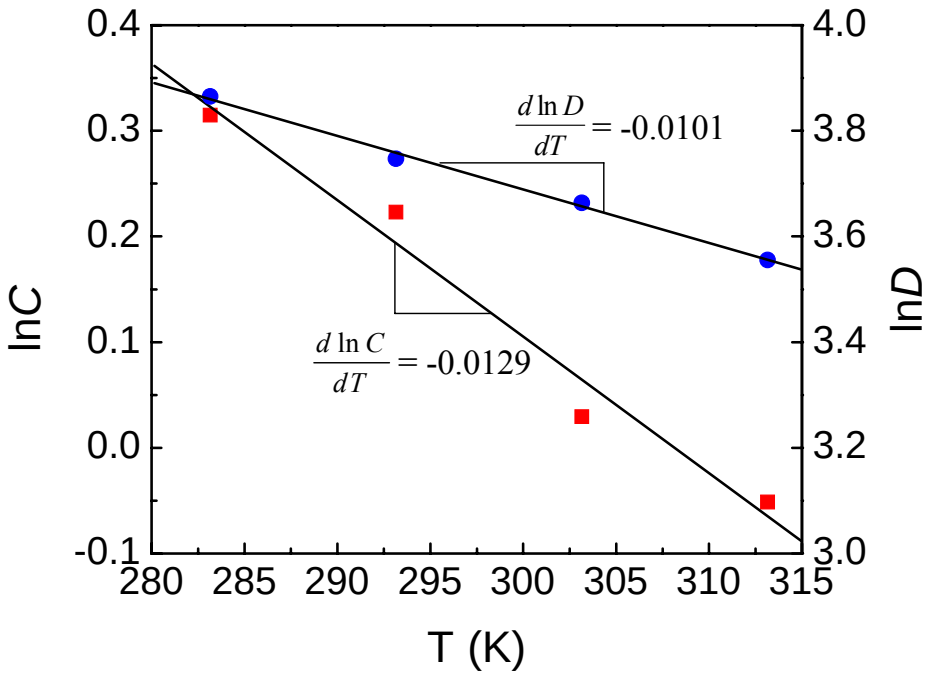

Figure 6.6. ln$C$ and ln$D$ obtained for C_{16}SH-coated gold as functions of absolute temperature. The temperature derivatives of ln$C$ and ln$D$ are -0.0129, and -0.0101, respectively.

From the force *versus* distance curves recorded for C_2, C_4, C_{12} and $C_{16}SH$-coated gold at different temperature, we find that in all cases the temperature coefficients of the hydrophobic surface force for a fixed surface separation H are positive. In other word, upon raising the temperature, the magnitudes of the hydrophobic attraction diminish. In principle, this temperature effect was first documented by Tsao *et al*.[27] on mica surfaces hydrophobized by the adsorption of cationic surfactants of different chain lengths from cyclohexane solutions. From film thermodynamics, we have the following relationship for a planar (pure) water film at constant pressure P and separation distance H:

$$\left(\frac{\partial \Delta\gamma^{f}}{\partial T}\right)_{p,H} = -\Delta S^{f} \qquad (6.3)$$

in which $\Delta S^{f}\left(\equiv S^{f} - S^{f,\infty}\right)$ is the change in excess film entropy per unit area, and T is the absolute temperature. From Equations 6.1-6.3, one obtains the following relation:

$$\Delta S^{f} = -\Delta\gamma^{f}\left(\frac{d\ln C}{dT} + \frac{H}{D}\frac{d\ln D}{dT}\right) \qquad (6.4)$$

which was used to determine the entropy changes from the values of $\Delta\gamma^{f}$ and the temperature coefficients of the C and D parameters. Since $\Delta\gamma^{f}$ is a negative quantity and the temperature derivatives of ln*C* and ln*D* are negative (Figure 6.6), the excess entropy ΔS^{f} of a thin water film between thiol-coated gold surfaces is thus a negative quantity. The excess entropy of the film is equal to the entropy per m^2 of the actual thin film minus the entropy of a hypothetical thin film per m^2 that entails the same number of water molecules per m^2 but is lacking face-to face interactions. Accordingly, the real film has somewhat lower entropy than the corresponding hypothetical film.

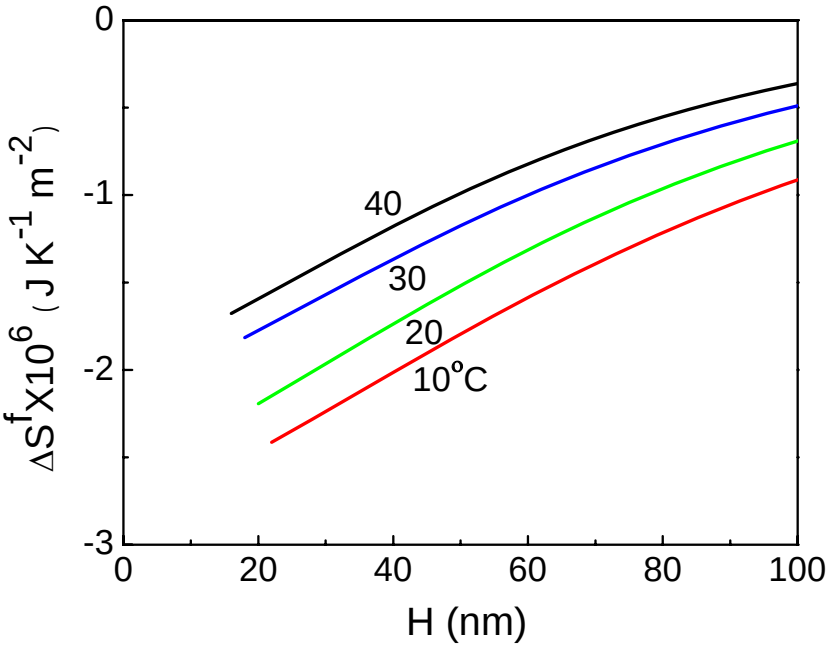

Figure 6.7. The changes in excess film entropy (ΔS^f) per m^2 in the thin films of water between two $C_{16}SH$-coated gold surfaces as the film thickness (H) decreases, or as the temperature increases.

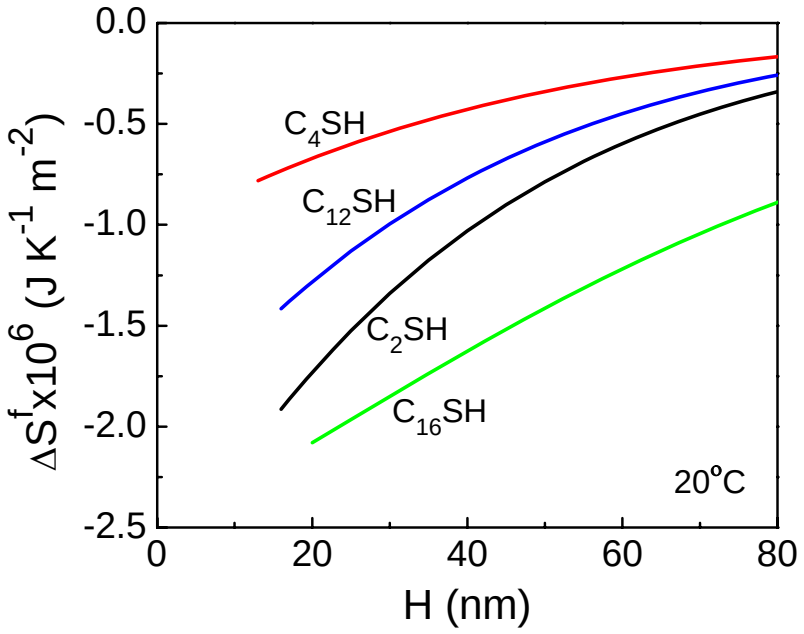

Figure 6.8. Changes in excess film entropy (ΔS^f) per m^2 in the thin films of water between two gold surfaces hydrophobized by alkanethiols with different chain lengths at 20ºC.

As shown in Figure 6.7 and 6.8, the change in excess film entropy (ΔS^f) becomes more negative when the thickness of the film (H) confined between two hydrophobic surfaces is reduced. A typical value of ΔS^f for a plane-parallel film of thickness 20 nm between two $C_{16}SH$-coated surfaces turns out to be -0.0022 $mJm^{-2}K^{-1}$, which is about 0.008% of the entropy change associated with the liquid water-to-ice phase transition. Although the effect dealt with here is an exceedingly minute one, the decrease in excess film entropy indicates that the thin film of water becomes increasingly structured as two hydrophobic surfaces approach each other. Note also that at a given film thickness H, ΔS^f becomes more negative at lower temperatures, which is akin to the anomalous behavior of supercooled water. As is well known, the density of water decreases below its maximum at 4ºC, which has invoked the presence of various low-density species (*e.g.*, "ice-like" species,[28] pentagonal dodecahedra,[29] clathrate cages,[30] *etc*.) in pure water. All of these species represent highly ordered structure of water; therefore, their formation in colder water entails entropy decrease. Likewise, the results presented in Figure 6.7 may indicate the formation of low-density species at the hydrophobic surface/water interface. Figure 6.8 shows changes in excess film entropy (ΔS^f) per m^2 in the thin films of water as functions of separation distance between two gold surfaces hydrophobized by C_2SH, C_4SH, $C_{12}SH$ and $C_{16}SH$ at 20ºC. As the chain length decreases from 16 to 4, the change in excess film entropy decreases. The difference between changes in excess film entropy obtained from different surfaces may due to different states of the hydrophobic carbon chains on the surface (*e.g.* crystalline order of hydrocarbon chain)[27]. For C_2SH, the obtained change in excess film entropy is comparable to that for $C_{16}SH$, and larger than that for C_4SH and $C_{12}SH$, probably due to the experimental uncertainty.

Thermodynamically, the change in film tension ($\Delta\gamma^f$) is composed of enthalpic (ΔH^f) and entropic ($T\Delta S^f$) parts. Using Equation 6.5, one can obtain the excess enthalpy per unit

area (ΔH^f) for fixed surface separation distance H:

$$\Delta H^f = \Delta\gamma^f + T\Delta S^f \qquad (6.5)$$

As shown in Figure 6.9, the slope of a ΔH^f *versus* T plot at a given separation distance is positive, meaning that the constant-pressure heat capacity (C_p) of the thin film between two hydrophobic surfaces is a little larger than that of the corresponding hypothetical water film without film face-face interactions, which is another indication that the film of water is more structured.

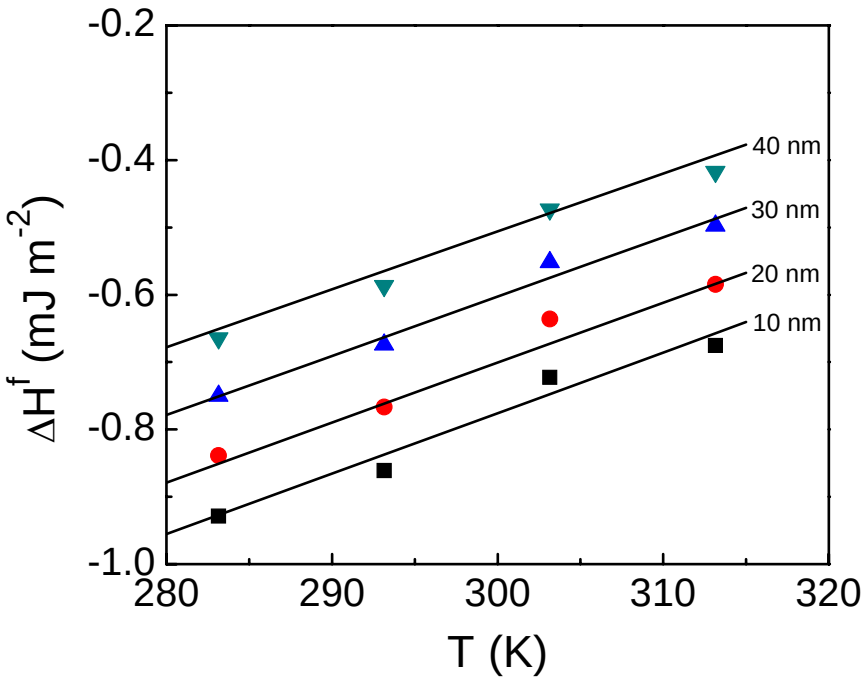

Figure 6.9. A plot of ΔH *versus* T at surface separation distance of 10, 20, 30 and 40 nm for C_{16}SH-coated gold surfaces.

Figure 6.10 shows the changes in these thermodynamic functions (*i.e.* $\Delta\gamma^f$, ΔS^f and ΔH^f) for the interaction between the C_{16}SH-coated gold surfaces at 20ºC. It is seen that the enthalpic part is a little larger than the entropic part. This finding contradicts the general perception that the hydrophobic interaction is entropic in nature,[31] that is, the interaction is

driven by a positive entropy change, in which case the attractive force at a fixed film thickness should increase as temperature rises. However, our results show the opposite; ΔS^f is negative and the hydrophobic force decreases with temperature, as shown in Figures 6.1-6.5, 6.7 and 6.8, respectively. Israelachvili and Pashley[32] and Tsao *et al*.[27] also found that the hydrophobic force decreases with temperature. Since both ΔH^f and ΔS^f are negative, the Gibbs free energy change ($\Delta\gamma^f$) becomes negative or an attractive hydrophobic force appears when $|\Delta H^f|>|T\Delta S^f|$, as shown in Figure 6.10. Thus, hydrophobic force originates from the thermodynamic properties of water rather than an artifact created by nanobubbles or cavitation[2, 3] The negative enthalpy change may be due to the formation of the low-density species such as clathrate cages[30] at the hydrocarbon/water interfaces. The negative enthalpy change associated with the clathrate formation exceeds the corresponding entropy cost.

Recent investigations have clarified that the nature of a hydrophobic interaction depends critically on the length scale of the hydrophobic species involved[33,34]. For small hydrophobic solutes, such as noble gases and hydrocarbons (*e.g.*, methane), water molecules can go around the hydrophobic species and form H-bonded network without compromising the number and strengths of the H-bonds. Each water molecule can "straddle" the small hydrophobic species due to its high curvature,[30] which will allow them to maintain four, highly directional H-bonds. As H-bonding is cooperative,[35] *i.e.*, a pair of adjacent H-bonds are more stable than two isolated bonds, the water molecules surrounding a hydrophobic solute can reinforce each other and form a concave clathrate structure with the mean bond energy stronger than that of a simple dimer.[30] Monte Carlo simulations showed indeed that the mean H-bond length of water around an apolar solute is shorter, while they are longer around a polar group.[36] Further, the extended x-ray absorption fine structure (EXAFS) spectrum of the solid krypton (Kr) clathrate is the same as that of Kr in cold water, which confirmed the formation of clathrate (or "iceberg") structures around hydrophobic solutes.[37]

The thermodynamic cost of forming the clathrate structure will for the most part be a decrease in entropy. However, the entropy cost is less than the cost of breaking some H-bonds to accommodate a hydrophobic solute in water and not forming the clathrate structure around it.

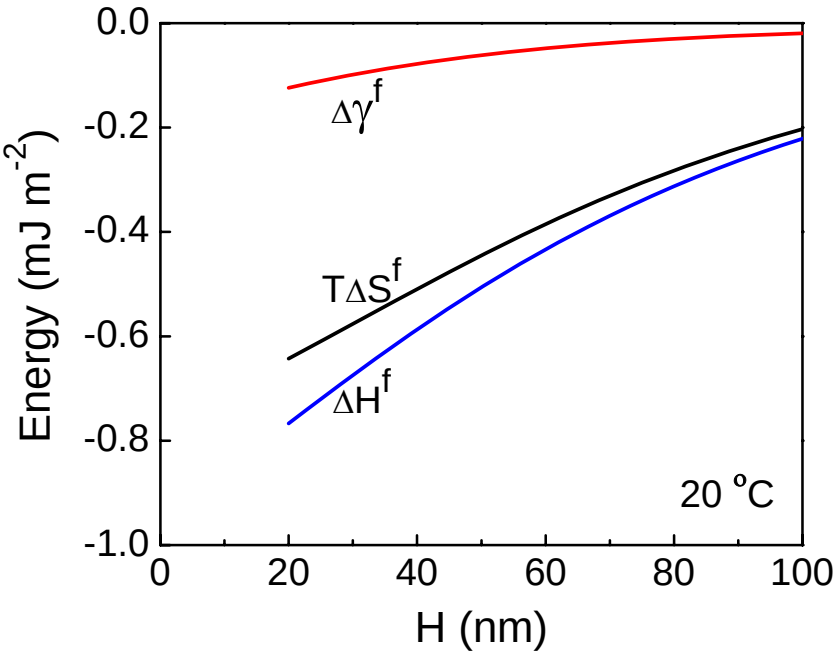

Figure 6.10. Changes in the excess thermodynamic functions for the hydrophobic interaction between $C_{16}SH$-coated gold macroscopic surfaces in air-equilibrated water at 20ºC. The enthalpy (ΔH^f) of interaction is slightly more negative than the corresponding entropic term ($T\Delta S^f$), and the difference between the two represents the change in the Gibbs free energy ($\Delta\gamma^f$). Since both ΔH^f and ΔS^f are negative, attractive hydrophobic force is observed only when $|\Delta H^f|>|T\Delta S^f|$.

When a larger hydrophobic species is placed in water, the water molecules in the immediate vicinity will lose some of the H-bonds as a consequence of the low curvature of the extended surface, resulting in a significant enthalpy increase. According to Chandler[34], the crossover from an entropic to an enthalpic hydration occurs at about 1 nm. For *n*-alkanes of 20 or fewer carbons, entropic hydration is still possible due to the high curvatures of the CH_2 and CH_3 groups, which serves as the basis for the well-known entropic self-assembly of

n-alkanes in water at room temperature.[31]

Recognizing the importance of the length scale in hydrophobic interaction, Lum *et al.*[38] suggested that the water molecules in the vicinity of the extended hydrophobic surfaces tend to move away from the surface, leading to drying and large forces of attraction. Many investigators followed this theory and determined the density of the vicinal water by the neutron reflectivity (NR) measurements. The results showed that preexisting nanobubbles are excluded[10, 39, 40] and the density of the vicinal water is lower than in the bulk, which has lead to a suggestion that hydrophobic force is a "depletion force"[10] caused by the drying effect. The NR studies showed also that the depletion length (D), a measure of density decrease, increases with increasing temperature[41, 42] and electrolyte concentration[42]. Maccarini *et al.*[42] suggested that these results corroborate with the AFM surface force measurements reported in the literature.[43] The results presented in Figure 6.1-6.5 show, on the contrary, that hydrophobic forces decrease with increasing temperature. Moreover, it is well documented that hydrophobic forces decrease with increasing electrolyte concentration[7, 44]. In addition, high-resolution in situ x-ray study shows that the hydrophobic water gas was not affected by dissolving gases[39] (*e.g.*, Ar, Xe, Kr, N_2, O_2, CO, and CO_2), which should enhance the hydrophobic force[8].

According to the clathrate cage model of Stillinger[30], the clathrates formed in water can join together by sharing the edges and faces of polyhedrons, which entails less overall order than when they are dispersed. Clumping (or clustering) of clathrates is, therefore, a way to minimize the entropy cost associated with structuring water. Since clathrates represent the low-density species present in water, the results of the NR measurements[10] may be considered to support the presence of clathrates in the thin films bounded by hydrophobic surfaces. The number and size of the clathrates may increase with decreasing film thickness, which may account for the corresponding decrease in water density, decrease in excess

entropy (S^f), and hence increase in hydrophobic force. Eriksson *et al.*[14] assumed that the clusters are of quasi-cylindrical shape, and derived a surface-thermodynamic model for the long-range attractive forces observed between charge-free hydrophobic surfaces.[14] The possibility of forming linear clusters is to some extent supported by the recent spectroscopic evidence that a water molecule is bonded to its neighbors by two strong and two weak H-bonds rather than four bonds of equal strength.[45]

6.4.2 Effect of Solutes

It has been shown that the long-range attractions between hydrophobic surfaces decrease considerably in degassed solutions.[6, 8] This important observation can be analyzed by means of the Gibbs surface tension equation adapted for thin planar films at constant temperature, pressure, and film thickness:

$$\left(\frac{\partial \Delta\gamma^f}{\partial \mu_S}\right)_{T,p,H} = -\Delta\Gamma_S^f \qquad (6.5)$$

in which μ_S is the chemical potential of a solute (dissolved air) and $\Delta\Gamma_S^f$ is its excess quantity per m^2 in the thin film of thickness H. Since the attractive force increases (*i.e.*, $\Delta\gamma^f$ becomes more negative) in the presence of dissolved air, $\Delta\Gamma_S^f$ must be positive in the thin film, that is, the amount of a dissolved gas in a thin film between two hydrophobic surfaces is higher than in a thick film. The excess dissolved gas in a thin film should promote the clathrate structure by the hydrophobic hydration mechanism described above and, hence, should give rise to a stronger hydrophobic force. The van der Waals attraction between the guest (gas) and host (water) molecules should also contribute to the stabilization of clathrate structure. Meagher *et al.*[6] and Meyer *et al.*[8] showed that hydrophobic force becomes shorter ranged in degassed water, which may be attributed to the weakening of the clathrate structure and, hence, smaller number and size of the clathrates.

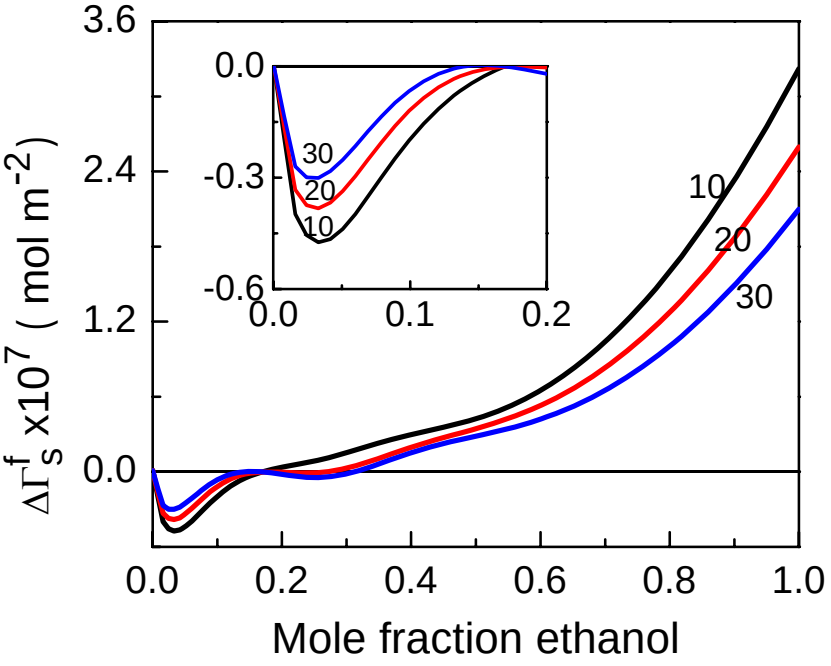

Figure 6.11. The excess quantities of ethanol ($\Delta\Gamma_s^f$) per m^2 in the thin films of water-ethanol mixtures between two $C_{16}SH$-hydrophobized surfaces plotted versus ethanol mole fraction.

Thermodynamically, clathrate structures are more readily formed at colder temperatures and higher pressures. However, remnants of the clathrates may also be found at ambient conditions. Evidence for this is that the solubilities of gases[46] (*e.g.*, O_2, N_2 and Ar) and hydrocarbons[47] in water at ambient conditions are substantially higher than predicted by the ordinary solution theory based on entropy of mixing. Shinoda[47] attributed the deviation to the "iceberg" formation.

We have also conducted surface force measurements in ethanol-water mixtures between two $C_{16}SH$-coated gold surfaces and the work was reported in Chapter 5. The hydrophobic surfaces were prepared by immersing a gold microsphere and a gold-coated glass in 1×10^{-5} M thiol in ethanol for 10 minutes. It is found that the long-range attraction in water changes significantly with adding ethanol. Figure 5.8 shows the changes in the C and D constants of Equation 6.1. The attraction is the lowest at about 0.2 mole fraction of ethanol

and increases on either side, and both C and D have minimum values at about the ethanol mole fraction 0.2. This finding mirrors other properties of ethanol-water mixtures regarding oxygen solubility[48] and the surface excess of ethanol at the air-solution interface.[49]

The data presented in Figure 5.8 have been used to calculate the film excess of ethanol ($\Delta\Gamma_S^f$) using Equation 6.5. By invoking vapor pressure data of Butler and Wightman[49] that yield the changes in ethanol with the chemical potential changes of ethanol, we can thus compute the excess of ethanol in the film as a function of composition for different film thickness. The results presented in Figure 6.11 show that at low ethanol concentrations $\Delta\Gamma_S^f$ is negative, indicating that some of the ethanol is excluded from the thin film. This is most probably because ethanol disrupts the water structure in the vicinity of hydrophobic surfaces. As the ethanol concentration is increased, the strong, long-range attraction reappears, and $\Delta\Gamma_S^f$ becomes positive, which means that water molecules are to some extent expelled from the thin films between the hydrophobic surfaces. Both water and ethanol are H-bonding liquids. It appears, however, that the H-bonding of one becomes less extensive in the presence of the other, and causes the long-range attraction to diminish.

Neto[50] also observed strong long-range attractions between hydrophobic surfaces in pure ethanol, and Boinovich and Emelyanenko[51] detected structural changes in the thin ethanol films (<5 nm) formed between fluorite surfaces using an infrared spectroscopic technique. In all likelihood, a layer-wise molecular arrangement that extends toward the core of the thin film is generated.

6.5 Summary and Conclusions

Our new thermodynamic data lend support for the hydrophobic force originating from the structural differences between water in the thin and thick films bounded by hydrophobic surfaces. This conclusion is the same as originally suggested by Rabinovich and Derjaguin[52]

and Eriksson *et al*[13]. The water molecules in the vicinity of hydrophobic surfaces reorganize themselves to form clathrates and clusters thereof, and cause hydrophobic attractions to appear. In the presence of dissolved gases, the clathrate structure becomes stronger, which gives rise to long-range hydrophobic forces. In degassed solutions, the clathrate structure becomes weaker, which in turn causes the hydrophobic force to become short-ranged[8] and oil-in-water emulsions to become stabilized without surfactant[53]. Unlike the dissolved inert gases, ethanol disrupts the water structure and, hence, diminishes the long-range attractions. Further studies in the thermodynamics of hydrophobic interactions should lead to a better understanding of the origin of hydrophobic force, which plays an important role in a variety of scientific and technological fields.

6.6 Acknowledgement

The authors are grateful for the financial assistance from the National Energy Technology Laboratory, the U.S. Department of Energy (DE-FC26-02NT41607).

6.7 References

1. Israelachvili, J.; Pashley, R., *Nature* **1982,** 300, 341-342.
2. Parker, J. L.; Claesson, P. M.; Attard, P., *J. Phys. Chem.* **1994,** 98, 8468-8480.
3. Tyrrell, J. W. G.; Attard, P., *Phys. Rev. Lett.* **2001,** 87, (17), 176104-1.
4. Seo, H.; Yoo, M.; Jeon, S., *Langmuir* **2007,** 23, 1623-1625.
5. Sakamoto, M.; Kanda, Y.; Miyahara, M.; Higashitani, K., *Langmuir* **2002,** 18, 5713-5719.
6. Meagher, L.; Craig, V. S. J., *Langmuir* **1994,** 10, 2736-2742.
7. Zhang, J.; Yoon, R.-H.; Mao, M.; Ducker, W. A., *Langmuir* **2005,** 21, 5831-5841.

8. Meyer, E. E.; Lin, Q.; Israelachvili, J. N., *Langmuir* **2005,** 21, 256-259.

9. Derjaguin, B. V., *Kolloid Zeits* **1934,** 69, 155-164.

10. Doshi, D. A.; Watkins, E. B.; Israelachvili, J. N.; Majewski, J., *Proc. Nat. Acad. Sci. U.S.A* **2005,** 102, 9458-9462.

11. Nguyen, A. V.; Nalaskowski, J.; Miller, J. D.; Butt, H.-J., *Int. J. Miner. Process.* **2003,** 72, 215-225.

12. Ederth, T., *J. Phys. Chem. B* **2000,** 104, 9704-9712.

13. Eriksson, J. C.; Ljunggren, S.; Claesson, P. M., *J. Chem. Soc., Faraday Trans. 2* **1989,** 85, (3), 163-176.

14. Eriksson, J. C.; Henriksson, U., *Langmuir* **2007,** 23, 10026-10033.

15. Miklavic, S. J.; Chan, D. Y. C.; White, L. R.; Healy, T. W., *J. Phys. Chem.* **1994,** 98, 9022-9032.

16. Meyer, E. E.; Lin, Q.; Hassenkam, T.; Oroudjev, E.; Israelachvili, J., *Proc. Nat. Acad. Sci. U.S.A* **2005,** 102, (19), 6839-6842.

17. Christenson, H. K.; Yaminsky, V. V., *Colloids Surf., A* **1997,** 129-130, 67-74.

18. Podgornik, R., *J. Chem. Phys* **1989,** 91, (9), 5840-5849.

19. Claesson, P. M.; Christenson, H. K., *J. Phys. Chem* **1988,** 92, 1650-1655.

20. Lin, Q.; Meyer, E. E.; Tadmor, M.; Israelachvili, J. N.; Kuhl, T. L., *Langmuir* **2005,** 21, 251-255.

21. Ederth, T.; Claesson, P.; Liedberg, B., *Langmuir* **1998,** 14, 4782-4789.

22. Wang, J.; Yoon, R.-H., *Langmuir* **2008,** 24, 7889-7896.

23. Ducker, W. A.; Senden, T. J.; Pashley, R. M., *Nature* **1991,** 353, 239-241.

24. Rabinovich, Y. I.; Yoon, R.-H., *Langmuir* **1994,** 10, 1903-1909.

25. Raiteri, R.; Preuss, M.; Grattarola, M.; Butt, H.-J., *Colloids Surf., A* **1998,** 136, 191-197.

26. Cleveland, J. P.; Manne, S.; Bocek, D.; Hansma, P. K., *Rev. Sci. Instrum.* **1993,** 64, (2), 403-405.

27. Tsao, Y.-H.; Yang, S. X.; Evans, D. F.; Wennerstrom, H., *Langmuir* **1991,** 7, 3154-3159.

28. Roentgen, W. C., *Ann. Phys.* **1892,** 281, 91-97.

29. Pauling, L., *Science* **1961,** 134, 15-21.

30. Stillinger, F. H., *Science* **1980,** 209, 451-457.

31. Tanford, C., *The Hydrophobic Effect*. 2 ed.; Wiley: New York, 1980.

32. Israelachvili, J. N.; Pashley, R. M., *J. Colloid Interface Sci.* **1984,** 98, (2), 500-514.

33. Chandler, D., *Nature* **2002,** 417, 491.

34. Chandler, D., *Nature* **2005,** 437, 640-647.

35. Frank, H. S.; Wen, W.-Y., *Discuss. Faraday Soc.* **1957,** 24, 133-140.

36. Sharp, K. A.; Madan, B., *J. Phys. Chem. B* **1997,** 101, 4343-4348.

37. Kauzmann, W., *Nature* **1987,** 325, 763-764.

38. Lum, K.; Chandler, D.; Weeks, J. D., *J. Phys. Chem. B* **1999,** 103, 4570-4577.

39. Mezger, M.; Reichert, H.; Schoder, S.; Okasinski, J.; Schroder, H.; Dosch, H.; Palms, D.; Ralston, J.; Honkimaki, V., *Proc. Nat. Acad. Sci. U.S.A* **2006,** 103, (49), 18401-18404.

40. Poynor, A.; Hong, L.; Robinson, I. K.; Granick, S., *Phys. Rev. Lett.* **2006,** 97, 266101.

41. Jensen, T. R.; Jensen, M. Q.; Reitzel, N.; Balashev, K.; Peters, G. H.; Kjaer, K.; Bjqrnholm, T., *Phys. Rev. Lett.* **2003,** 90, (8), 086101-1.

42. Maccarini, M.; Steitz, R.; Himmelhaus, M.; Fick, J.; Tatur, S.; Wolff, M.; Grunze, M.;

Janecek, J.; Netz, R. R., *Langmuir* **2007,** 23, 598-608.

43. Kokkoli, E.; Zukoski, C. F., *Langmuir* **1998,** 14, 1189-1195.

44. Christenson, H. K.; Claesson, P. M.; Berg, J.; Herder, P. C., *J. Phys. Chem.* **1989,** 93, 1472-1478.

45. Wernet, P.; Nordlund, D.; Bergmann, U.; Cavalleri, M.; Odelius, M.; Ogasawara, H.; Naslund, L. A.; Kirsch, T. K.; Ojamae, L.; Glatzel, P.; Pettersson, L. G. M.; Nilsson, A., *Science* **2004,** 304, 995-999.

46. Battino, R.; Clever, H. L., *Chem. Rev.* **1966,** 66, (4), 395-463.

47. Shinoda, K., *J. Phys. Chem.* **1977,** 81, (13), 1300-1302.

48. Shchukarev, S. A.; Tolmacheva, T. A., *ZhurnalStrukt. Khim* **1968,** 9, 21-28.

49. Butler, J. A. V.; Wightman, A., *J. Chem. Soc. (London)* **1932**, 2089-2097.

50. Neto, C. Universita degli Studi di Firenze, Firenze, 2001.

51. Boinovich, L. B.; Emelyanenko, A. M., *Adv. Colloid Interface Sci.* **2002,** 96, 37-58.

52. Rabinovich, Y. I.; Derjaguin, B. V., *Colloids Surf.* **1988,** 30, 243-251.

53. Maeda, N.; Rosenberg, K. J.; Israelachvili, J. N.; Pashley, R. M., *Langmuir* **2004,** 20, 3129-3137.

Chapter 7

Conclusions and Recommendations

7.1 Conclusions

In this work, the force measurements were conducted with gold surfaces pretreated by *ex-situ* adsorption of alkanethiols and *in-situ* adsorption of water-soluble xanthates of different chain lengths, concentrations, and immersion times. Further, the force measurements were conducted in the presence of various solutes such as inorganic electrolytes, ionic surfactants, and alcohols that can affect the properties (*e.g.*, structure) of the thin water films between two hydrophobic surfaces. To gain an understanding of the water structure, the changes in the excess film entropies and enthalpies across the film thickness were determined by measuring the surface forces at different temperatures.

Based on the findings of the present study, conclusions can be drawn as follows:

1. I observed long-range attractions between gold surfaces pretreated by *ex-situ* adsorption of alkanethiols (n = 2-16) and *in-situ* adsorption of water-soluble xanthate surfactants (*i.e.*, PAX, KEX). The long-range attractive forces decayed exponentially, and were detected at the separation distance of up to 120 nm. The force curves exhibited no steps, indicating that the long-range attraction was not due to bridging bubbles.
2. The surface forces measured between hydrophobized-gold surfaces depend on surface treatment conditions such as surfactant concentration and immersion time. When the surfaces were hydrophobized in 1 mM 1-hexadecanethiol of ethanol

solution longer than 6 hours, the measured forces were net-attractive and long-ranged. However, the force curves exhibited steps, indicating that the measured forces were due to bridging bubbles. It is possible that the thiol monolayer can have defects (or pits) in which air bubbles can nucleate. When the gold substrates were hydrophobized in a dilute (1×10^{-2} mM) thiol solution at relatively short contact time (10 minutes), a long-range attractive force which decayed exponentially with a decay length of 35 nm was obtained, and the force curve exhibited no steps. It is possible that at lower concentrations and shorter contact times smoother coatings are formed, which are less likely to trap nanobubbles and hence give rise to smooth force curves.

When the gold substrates were immersed in the 1×10^{-2} mM $C_{16}SH$- and $C_{12}SH$-in-ethanol solutions for different periods of time, the attractive forces increased with immersion time, and then decreased. All the forces measured were stronger and longer-ranged than the van der Waals force. The contact angles on these surfaces were greater than 90º. When the force measurements were conducted after washing the substrates with appropriate solvents, strong long-range hydrophobic forces appeared. The same behavior was also found for gold in PAX solutions after different immersion times. It is suggested that the decrease of hydrophobic force is caused by the formation of the bilayers of thiol or xanthate, which can be washed away by using appropriate solvents.

3. The long-range attractions were observed between thiol-coated gold surfaces regardless of weather the contact angles were greater or smaller than 90º. When

gold surfaces were hydrophobized with C_2SH, the contact angle was less than 90º. In this case, no cavitation is possible. Yet, the AFM force measurement gave a long-range attraction. It is suggested that hydrophobic force is not due to the bubbles present on hydrophobic surfaces or to the cavitation (or drying).

4. The long-range hydrophobic attraction increases with increasing chain length of alkanethiol, decreases in the presence of salt (*e.g.*, NaCl) and surfactant (*e.g.*, $C_{12}TACl$, PAX), and changes with ethanol concentration. The strongest hydrophobic attraction measured on the C_4SH-coated gold was weaker than those measured on $C_{12}SH$- and $C_{16}SH$-coated gold surfaces. The latter two surfaces had the same water contact angles and were indistinguishable with respect to the hydrophobic attractions measured. It was also found that the hydrophobic force measured with PAX was much larger than that with KEX.

   The attractive forces measured on $C_{12}SH$-, $C_{16}SH$- and PAX-coated gold surfaces were effectively reduced by electrolyte (NaCl), indicating that they may be of electrostatic origin. For this mechanism to work, it is necessary that the charged patches be mobile when two surfaces approach each other to maximize the correlation and give rise to a long-range attraction. However, the strong covalent Au-S bonding provides robust and immobile hydrophobic monolayers, which precludes the possibility of charged patches being mobile. Further, there is no reason that thiol or xanthate adsorption produced charged patches as they chemisorbs on gold. For the case of xanthate adsorption, both the adsorbate and adsorbent are negatively charged. Our work leaves the possibility that the

long-range attraction is caused by the changes in water structure near hydrophobic surfaces. It is possible that the electrolyte (NaCl), ionic surfactant (C_{12}TACl) and residual xanthate (PAX) in solution break the H-bonded water structure and, hence, reduce the hydrophobic force.

The surface force data obtained in water-ethanol mixtures showed that the attractions were strong and long-ranged in pure water and pure ethanol, whereas they were weaker and of shorter range in water-ethanol mixtures with mole fraction of ethanol from 0.1 to 0.9. The data have been analyzed by using thin film thermodynamics. The results mirror the well-known, rather special bulk properties of water-ethanol mixtures. At mole fractions below about 0.2, a breakdown of the water structure due to introducing ethanol molecules was a predominant feature, explaining the reduction of hydrophobic attraction in both strength and range. For high ethanol mole fractions, we can assume that a layered, laterally homogenous surface structure was formed that stretches some distance away from the hydrophobic surfaces, likewise giving rise to a long-range attraction that was readily disturbed, however, by adding more water.

5. Hydrophobic force may be a structural force. The measurements carried out at 10−40ºC show that the hydrophobic force decreased with increasing temperature. Thermodynamically, these results imply that as two hydrophobic surfaces approach each other the changes in excess film entropy (S^f) and enthalpy (H^f) per unit area decrease, which suggests that the hydrophobic force is due to the structuring of water in the thin film confined by two hydrophobic surfaces rather

than from an artifact.

7.2 Recommendations for Future Work

Based on the results obtained in this work, the following areas of research are recommended:

1. It has been suggested that the hydrophobic force may be related to the structure of water confined between hydrophobic surfaces. Direct evidence for the structure change of water is needed. Therefore, systematic neutron reflectivity (NR) measurement, *in-situ* x-ray or nuclear magnetic resonance (NMR) studies on water between two hydrophobic surfaces which are close to each other are highly recommended.
2. Based on the surface force measurements at different temperatures, it was speculated that water molecules form partial or full clathrates in the vicinity of hydrophobic surfaces and the presence of gases facilitates the clathrate hydrate formation. In the future work, the AFM force measurements are recommended to be conducted in the presence of different gases (*e.g.*, CO_2, CH_4, H_2, He, N_2) dissolved in water to investigate the gas effect. Molecular dynamic simulation of water in the vicinity of hydrophobic surfaces is recommended to pursue the molecular origin of the hydrophobic force.